NUCLEAR INSTRUMENTS & METHODS

A JOURNAL ON ACCELERATORS, INSTRUMENTATION AND TECHNIQUES IN NUCLEAR PHYSICS

EDITOR: K. SIEGBAHN - UPPSALA

VOLUME 5

JULY 1959 — NOVEMBER 1959

NORTH-HOLLAND PUBLISHING COMPANY — AMSTERDAM

PRINTED IN THE NETHERLANDS
DRUKKERIJ MEIJER N.V. – WORMERVEER AND AMSTERDAM

NUCLEAR INSTRUMENTS AND METHODS

EDITORIAL BOARD:

J. B. ADAMS (CERN)
F. A. ALSINA (Buenos Aires)
E. AMALDI (Rome)
H. L. ANDERSON (Chicago)
K. T. BAINBRIDGE (Cambridge, Mass.)
C. J. BAKKER (CERN)
P. R. BELL (Oak Ridge)
R. E. BELL (Montreal)
A. BERTHELOT (Saclay)
H. BRINKMAN (Groningen)
E. H. COOKE–YARBOROUGH (Harwell)
S. DE BENEDETTI (Pittsburgh)
M. DE HEMPTINNE (Louvain)
A. DE-SHALIT (Rehovoth)
M DEUTSCH (Cambridge, Mass.)
S. DU TOIT (Pretoria)
B. S. DŽELEPOV (Leningrad)
W. GENTNER (CERN)
P. C. GUGELOT (Amsterdam)
H. HALBAN (Paris)
O. HAXEL (Heidelberg)
P. HUBER (Basel)
D. J. HUGHES (Brookhaven)
S. KIKUCHI (Tokyo)
J. KOCH (Copenhagen)
M. S. KOZODAEV (Moscow)
S. LIVINGSTON (Cambridge, Mass.)
E. M. MCMILLAN (Berkeley)
M. G. MEŠČERJAKOV (Moscow)
P. B. MOON (Birmingham)
M. L. OLIPHANT (Canberra)
W. PAUL (Bonn)
A. S. RAO (Bombay)
G. SALVINI (Rome)
P. SAVIĆ (Belgrade)
P. SCHERRER (Zürich)
CH. SCHMELZER (CERN)
H. W. B. SKINNER (Liverpool)
R. TANGEN (Oslo)
D. TAYLOR (Northampton)
V. I. VEKSLER (Moscow)
O. WERNHOLM (Stockholm)
G. VON DARDEL (CERN)
R. R. WILSON (Cornell)
S. D. WINTER (Saclay)

JULY 1959 VOLUME 5 (1959) No. 1

GREGG M. SINCLAIR LIBR.
UNIVERSITY OF HAWAII
8-7-63

NUCLEAR INSTRUMENTS & METHODS

A JOURNAL ON ACCELERATORS, INSTRUMENTATION AND TECHNIQUES IN NUCLEAR PHYSICS

EDITOR: K. SIEGBAHN - UPPSALA

CONTENTS

HILDING SLÄTIS, On bubble chambers (survey article) 1
P. C. MARIN, An accurate photo-neutron standard 26
J. KOCKUM and N. STARFELT, Measurement of photonuclear absorption cross sections 37
A. SARAZIN, J. SAMUELI et G. DUCROS, Mesure de temps de montée d'impulsions électriques inférieures à la millimicroseconde 44
F. J. LOEFFLER, T. R. PALFREY and G. W. TAUTFEST, The energy dependence of the Cornell thick-walled ionization chamber 50
ARIEH FISCHMANN-ARBEL, Precision Schmitt trigger 56

NORTH-HOLLAND PUBLISHING COMPANY - AMSTERDAM

NUCLEAR INSTRUMENTS AND METHODS

A journal on accelerators, instrumentation and techniques in nuclear physics

EDITOR: K. SIEGBAHN, UPPSALA

EDITORIAL BOARD:

J. B. ADAMS (CERN)
F. A. ALSINA (Buenos Aires)
E. AMALDI (Rome)
H. L. ANDERSON (Chicago)
K. T. BAINBRIDGE (Cambridge, Mass.)
C. J. BAKKER (CERN)
P. R. BELL (Oak Ridge)
R. E. BELL (Montreal)
A. BERTHELOT (Saclay)
H. BRINKMAN (Groningen)
E. H. COOKE–YARBOROUGH (Harwell)
S. DE BENEDETTI (Pittsburgh)
M. DE HEMPTINNE (Louvain)
A. DE-SHALIT (Rehovoth)
M. DEUTSCH (Cambridge, Mass.)
S. DU TOIT (Pretoria)
B. S. DŽELEPOV (Leningrad)
W. GENTNER (CERN)
P. C. GUGELOT (Amsterdam)
H. HALBAN (Paris)
O. HAXEL (Heidelberg)
P. HUBER (Basel)
D. J. HUGHES (Brookhaven)
S. KIKUCHI (Tokyo)
J. KOCH (Copenhagen)
M. S. KOZODAEV (Moscow)
S. LIVINGSTON (Cambridge, Mass.)
E. M. MCMILLAN (Berkeley)
M. G. MEŠČERJAKOV (Moscow)
P. B. MOON (Birmingham)
M. L. OLIPHANT (Canberra)
W. PAUL (Bonn)
A. S. RAO (Bombay)
G. SALVINI (Rome)
P. SAVIĆ (Belgrade)
P. SCHERRER (Zürich)
CH. SCHMELZER (CERN)
H. W. B. SKINNER (Liverpool)
R. TANGEN (Oslo)
D. TAYLOR (Northhampton)
V. I. VEKSLER (Moscow)
O. WERNHOLM (Stockholm)
G. VON DARDEL (CERN)
R. R. WILSON (Cornell)
S. D. WINTER (Saclay)

INSTRUCTIONS FOR CONTRIBUTORS

Contributions may be sent to the Editor, Professor K. Siegbahn, Institute of Physics, University of Uppsala, Sweden, either directly or through the intermediation of one of the members of the Editorial Board. Contributions may be written in English, French or German but should always, except for very short papers, be supplied with a brief abstract in English. Figures should be in inked original drawings or glossy prints and they should be sufficiently large. Contributors should make sure that important details in drawings and photographs will show up clearly in the diminished copy used by the publisher.

Books for review should be sent to Professor Siegbahn.

Objective and descriptive material on endeavours and product developments from the industry for the section "Spotlight on Industry" should be sent directly to the publishers, North-Holland Publishing Company, P.O. Box 103, Amsterdam.

Nuclear Instruments and Methods is published monthly. The subscription price of a volume of 360 pages is $ 17.00 (130 s), postage free.

Subscriptions should be sent to the publishers, North-Holland Publishing Company, P.O.Box 103, Amsterdam or to any subscription-agent.

No part of this issue may be reproduced in any form, by print, photoprint, microfilm or any other means without written permission from the publisher. Reprints, photoprints or microfilms are obtainable at cost from the publisher.

PHILIPS

equipment for

Nuclear Physics and

Atomic Energy

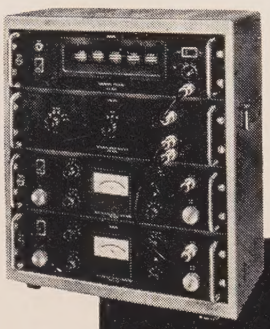

- Synchro-cyclotrons for various final energies.
- Cockcroft-Walton accelerators.
- Generators for very high d.c. voltages.
- Linear electron accelerators.
- Reactor control instrumentation.
- Radiation measuring and detection equipment.
- Civil defence instruments.
- Area monitoring instrumentation.
- Geiger counter tubes.
- Photomultipliers.
- Radio-active isotopes.
- Air & gas liquefiers.
- Vacuum measuring equipment.

Generally low-level beta-counting involves the use of relatively cumbersome and heavy equipment, which occupies quite a lot of laboratory space. Thanks to the introduction of a new type of guard counter, an invention of the Philips Research Laboratories, it was found possible to solve space and weight problems in a neat way. Shown here is the Low-Level Beta-Counting Arrangement, type PW 4127, and its corresponding measuring equipment. Background-reduction to less than 1.3 c.p.m. is obtained with a thin end-window counter used for measuring low-energy betas, and to less than 1.5 c.p.m. with an end-window counter for general low-intensity work.
The shielding comprises 30 mm of special lead, some 250 years old, with an extremely low specific activity, and 100 mm of iron.

PHILIPS

PHILIPS

Nuclear Equipment

For further information please apply to one of the following addresses:

N.V. PHILIPS' GLOEILAMPENFABRIEKEN, Scientific Equipment Department, Eindhoven-Holland
RESEARCH & CONTROL INSTRUMENTS LTD., Instrument House, 207/215, King's Cross Road, London WC1
PHILIPS ELECTRONICS INC., Instruments Division, 750, South Fulton Avenue, Mount Vernon N.Y. U.S.A.

Four Simultaneous 100 Channel Spectra Without Any Loss In Resolution

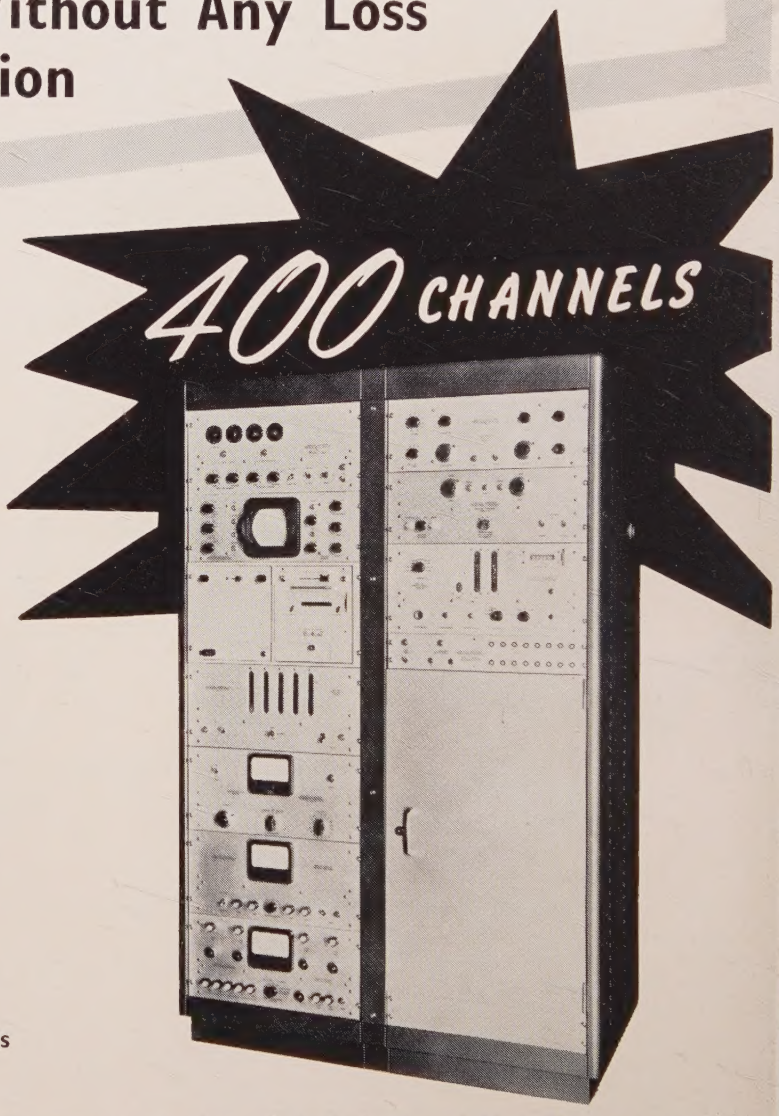

- Ferrite Core Memory
- 400 Channels
- 0.5% Linearity
- Memory Subgrouping
- External Programming
- Auto-Print Operation
- Spectrum Transfer Circuit
- 2^{16} Count Capacity
- Coincidence Features
- Dead Time Meter
- Elapsed Timer
- Free Installation
- Free Course of Instruction
- Clear Anodized Front Panels

RIDL is proud to present the newest member of their family of Multi-Channel Analyzers – the Model 34-9 400 Channel Analyzer – incorporating all RIDL standard features. This unit may be used as two 200 Channel Analyzers or four 100 Channel Analyzers, with no sacrifice in resolution. For automatic operation, high resolution, extreme reliability and adaptability, the 34-9 is unmatched by any Multi-Channel Analyzer on the market today. Write today to Department MC for complete specifications.

RIDL INC.

Radiation Instrument Development Laboratory, Inc.

5737 South Halsted Street, Chicago 21, Illinois USA TRiangle 3-2345

Representatives in major cities

NOW

GREATER ACCURACY and EFFICIENCY IN PULSE HEIGHT ANALYSIS WITH 3 COUNTING MODES

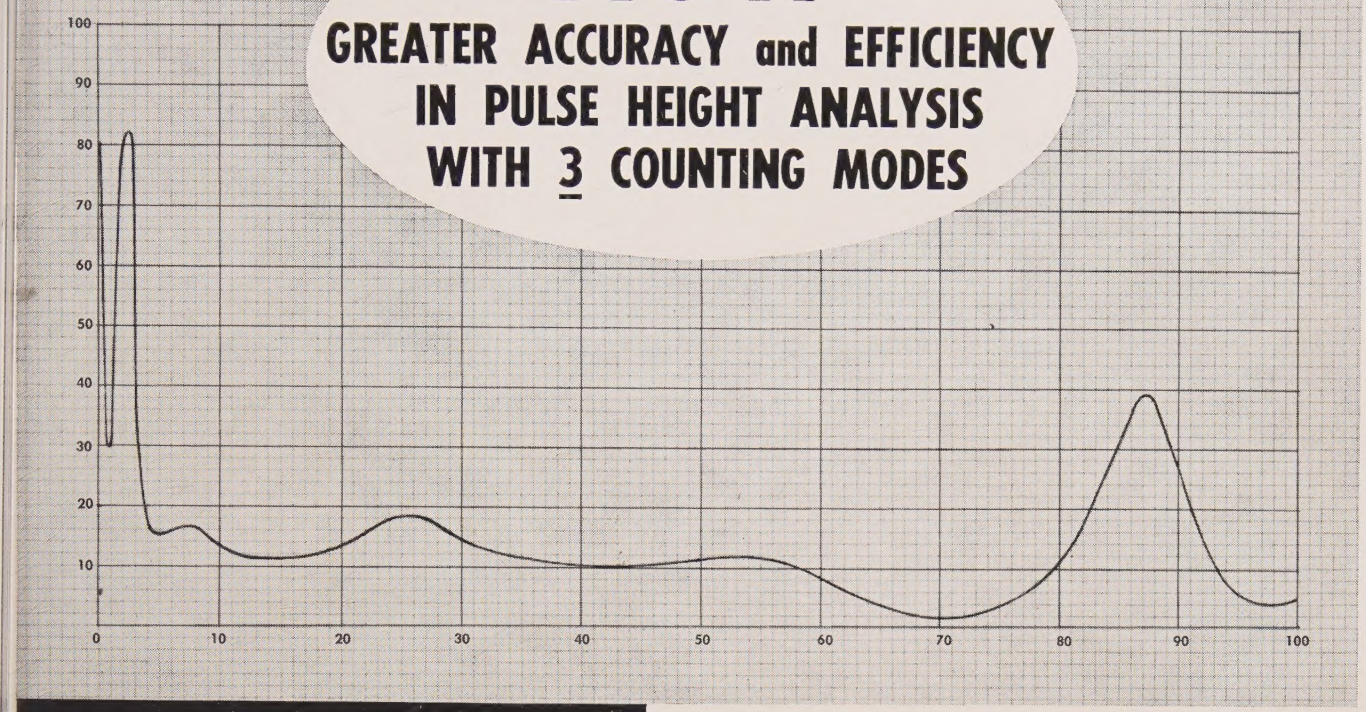

A C_s 137 spectrum taken in a standard 0-10 volt window mode. The *upper limit mode* of the PA-3B would count pulses between the limits of the photo peak.

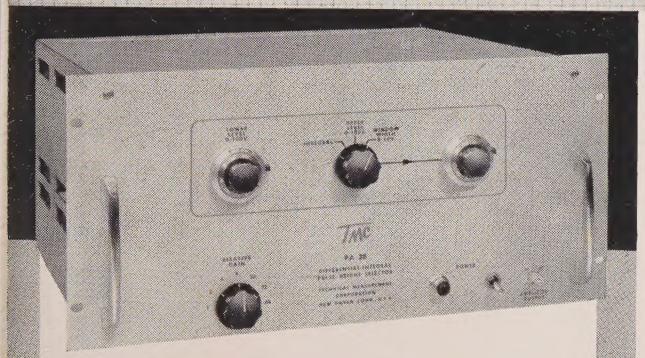

TMC PA-3B AMPLISORTER counting modes:

1 **INTEGRAL MODE** — for counting all pulses above base line

2 **WINDOW MODE** — for standard window counting as in conventional analyzers — window variable 0-10 volts

3 **UPPER LIMIT MODE** — for wider differential range counting — upper and lower limits each variable 0-100 volts

The TMC Model PA-3B combination single-channel pulse height analyzer and linear amplifier attains a new degree of efficiency and accuracy through an added *third* counting mode. Where other analyzers can go no further than counting in a window mode, the PA-3B provides an *upper limit* mode to count between any desired lower and upper limits on the spectrum. This gives the PA-3B an extremely wide differential range and makes it the most capable instrument for such precise operations as isotope monitoring, x-ray diffraction measurement and other experimental set-ups where extreme instrument efficiency is essential.

The linear amplifier section is a non-blocking Chase Higinbotham long-tail-pair type. It features binary gain control from 1 to 64, maximum gain of 8000, and fixed RC clipping. (Negative input and 1.5 us. clipping are standard, but positive input and other clipping times may be specified.) Price of Model PA-3B, $700.

Where *two-channel analysis* is desired, the Model PA-4A Dual-Channel Analyzer provides all the features of the PA-3B, but has a second analyzer unit in place of the linear amplifier. Price of the PA-4A is $900.

Complete data and specifications on the PA-3B, PA-4A, or any of a variety of TMC radiation measurement instruments are available on request.

TMC

TECHNICAL MEASUREMENT CORPORATION

441 WASHINGTON AVE., NORTH HAVEN, CONNECTICUT

Model SC 700

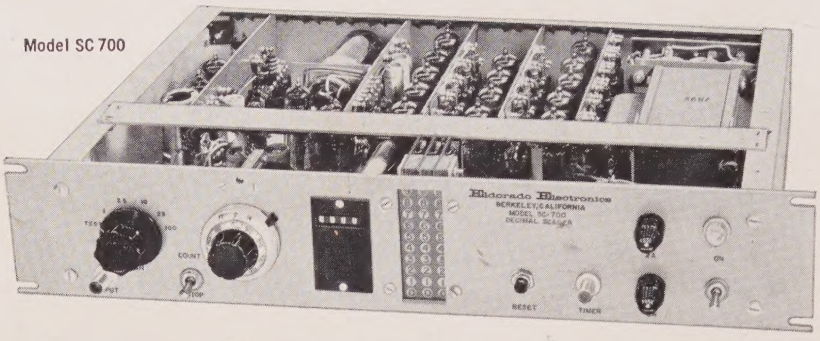

New Eldorado SC 700 Decimal Scaler with

better than 1 microsecond resolution

Designed for general radiation counting, Eldorado's compact new SC700 Decimal Scaler provides high performance at a budget price, $595.

FEATURES

- Small Size – 3½" panel height, weighs only 16 pounds.
- 25 Millivolt Sensitivity
- Seven Decades of Count Storage
- Calibrated Input Amplifier
- Precision Integral Discriminator
- Building Block Construction
- Built-in Test Circuit
- Provision for External Timer

For complete technical information, please address Dept.____.

Eldorado Electronics

2821 TENTH ST. • BERKELEY 10, CALIF.
Phone THornwall 1-4613

13

SENIOR PHYSICIST-ENGINEER

Leading American Company in the nuclear field has an opening for a

SENIOR GEIGER TUBE SPECIALIST

Applicant should have had a minimum of 5 years' experience with halogen nuclear counters. While halogen tube experience is preferred, consideration will also be given to applicants having comparable experience with organic quench nuclear counters, high vacuum tubes or gas discharge tubes.

Applicant should have had intimate design experience with all aspects of counting tubes and should be familiar with all pertinent physical phenomena governing the behavior of nuclear counters. He should be able to utilize this theoretical knowledge in conjunction with a thorough understanding of materials, vacuum technology and specialized fabrication techniques to conceive, design and construct prototype counters with outstanding characteristics. He would be expected to be able to recommend the optimum facilities for producing these tubes as well as specifying in detail the necessary manufacturing instructions.

Applicants who should have a reading and speaking knowledge of English and who should be willing to immigrate to the U.S. are invited to write to

DEPT. NI-5
NORTH-HOLLAND PUBLISHING COMPANY
POST OFFICE BOX 103
AMSTERDAM, THE NETHERLANDS

EKAF

type 30301

non overloading Linear Amplifier

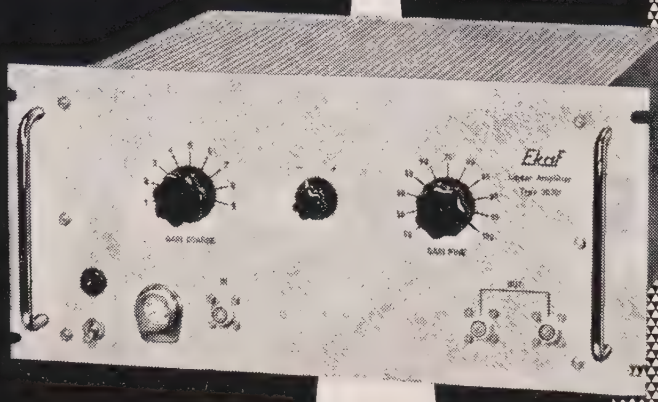

The EKAF type 30301 non overloading Linear Amplifier has been designed for spectrum analysis. Amplifier has ultra short dead time through special clipping circuit, even in case of pulses of long decay. Non overloading circuit limits sharply at 130 V.

Brief specifications:

Gain	**: 6400 (with clipping filter) 12800 (without clipping filter)**
Risetime	**: < 0,3 μ sec**
Input polarity:	**positive and negative (polarity switch)**
Output:	**: Linear positive pulses 0-110 V limits sharply at 130 V**
Linearity	**: < 1 % for outputs 0-110V**
Stability	**: built in power supply, stabilization ratio > 2000**

ELEKTRONISCH-KERNFYSISCHE APPARATENFABRIEK N.V.

Sales Office:
74, Laan Copes van Cattenburch,
The Hague, Holland.
Tel. 630977

INSULATED WIRE
that will withstand
2000°F

AERO PAK
Insulated Wires
will last forever in service eliminating costly replacement

- Available in outside diameters of .04 to .32.
- One or more wires insulated with a pure mineral swaged into a metal tube.
- Can be sharply bent.
- Sheath can be welded without loss of insulation.
- Available in a variety of sheath metals with thermocouples and other wire materials.
- Complete thermocouple probes available using this material made to your requirements.

Write for Bulletin M–I

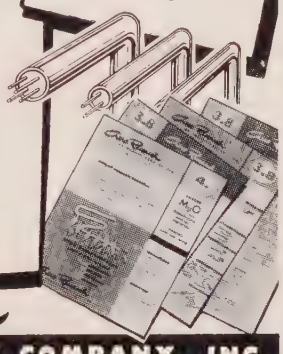

Aero Research
INSTRUMENT COMPANY, INC.
315 NO. ABERDEEN STRFET, CHICAGO 7, ILLINOIS

FOR SCINTILLATION & PROPORTIONAL COUNTING
Non-overloading Linear Amplifiers
MODELS 108 and 108 p

* GAIN–40,000, continuously variable
* RISE TIME–0.2 microsecond
* ACCEPTS + AND — PULSES

Tremendous Dynamic Range
EXCEEDS 1,000,000 (0.1 mV to 100 V)

Excellent linearity for small pulses in the presence of tremendous overloads that paralyze other amplifiers.
Model 108 P includes precision trigger type Pulse-Height Selector.

Model 413 Mercury relay precision sliding Pulser

The one pulser that fills every need of the Nuclear Physics Laboratory
0 to 100 Volts

10 full scale ranges from 1 mV to 100 volts
Fast rise and exponential decay of 1, 3, 10. 30, and 100 microsec simulate pulses from scintillation, proportional and Geiger counters.
Incorporates both manual control and precision motor drive.
The ideal instrument for precise calibration and test of pulse-height analyzers and other nuclear instrumentation.

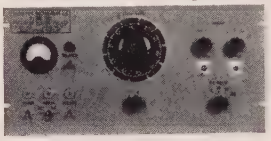

Window widths are determined AUTOMATICALLY, 10 × more ACCURATELY, 40 × FASTER than with conventional pulsers.

Model 108 Amplifier . . . . . $ 545.00
Model 108 P Amplifier (includes pulse-height selector) $ 595.00
Model 413 Precision Sliding Pulser . . . . . $ 630.00
Prices f.o.b. Silver Spring. Md.

RADIATION INSTRUMENT CO.
P.O. BOX 733 SILVERSPRING, MARYLAND, U.S.A.

NORTH-HOLLAND BOOKS

Analytical and Canonical Formalism in Physics

by

ANDRÉ MERCIER

Head of the Department of Theoretical Physics, University of Berne

6 × 9″ VIII + 222 pages Guilders 20.00 (40 s.)

THE CONTENTS

i LAGRANGIAN FORMALISM
ii LAGRANGIAN DENSITY
iii CANONICAL FORMALISM
iv CANONICAL FORM OF ELECTRODYNAMICS
v HAMILTONIAN DENSITIES
vi TRANSFORMATIONS
vii CANONICAL FORMALISM WITH VANISHING JACOBIAN DETERMINANT

Sole Agency for U.S.A.: Interscience Publishers Inc. – New York

NORTH-HOLLAND PUBLISHING COMPANY — AMSTERDAM

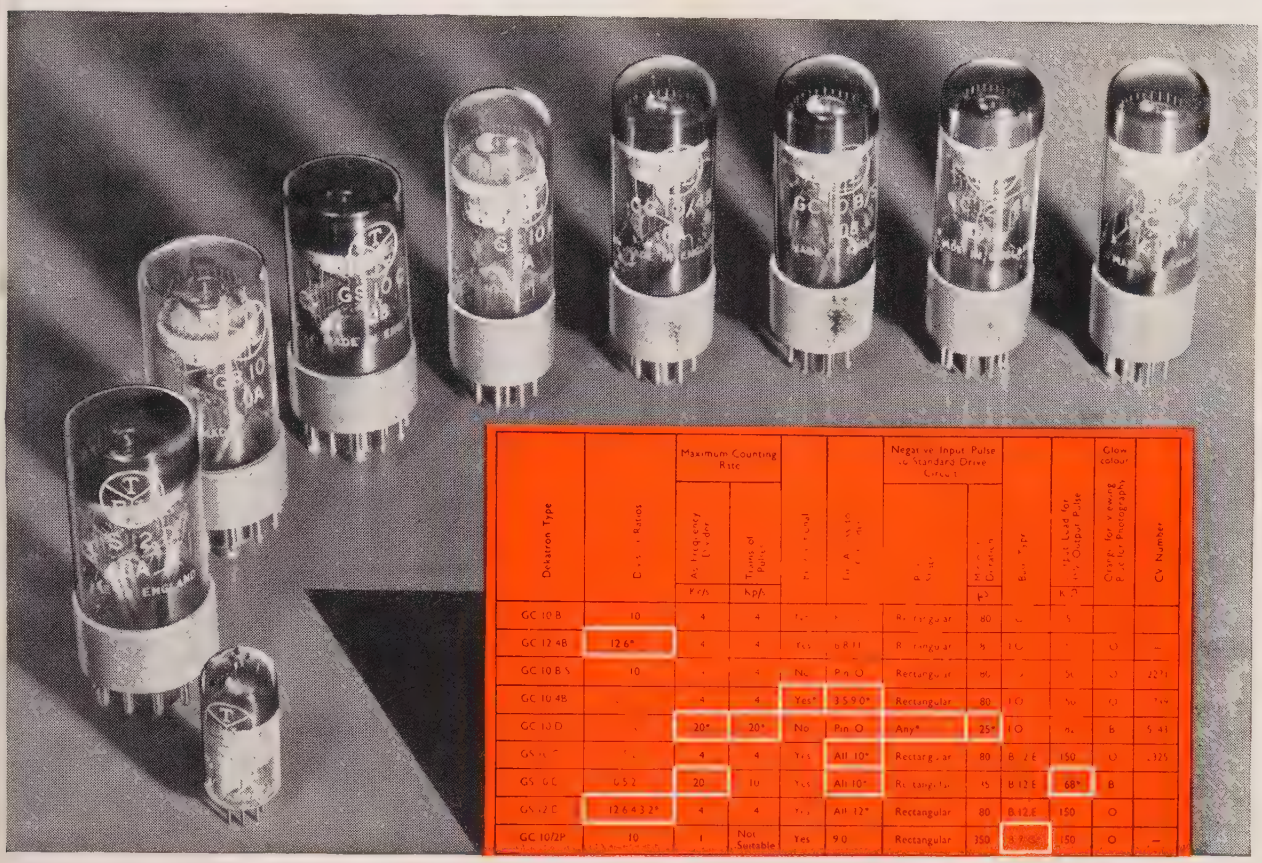

Dekatron Type	Division Ratios	Maximum Counting Rate: Asymmetry (Decades) c/s	Maximum Counting Rate: Trains of Pulses kp/s	Negative Input Pulse for Standard Drive Circuit: Polarity	Negative Input Pulse for Standard Drive Circuit: Amplitude	Negative Input Pulse for Standard Drive Circuit: Pin Order	Negative Input Pulse for Standard Drive Circuit: Minimum Duration μs	Base Type	Load for 150V Output Pulse kΩ	Glow colour	CV Number
GC 10 B	10	4	4	Yes	90	Rectangular	80	B 12 E	150	O	—
GC 17 4B	12.6*	4	4	Yes	0.8	Rectangular	80	B 12 E	150	O	—
GC 10 B 5	10	4	4	No	Pin O	Rectangular	80	B 12 E	150	O	2275
GC 10 4B	10	4	4	Yes*	35-90*	Rectangular	80	B 12 E	150	O	2276
GC 10 D	10	20*	20*	No	Pin O	Any*	25*	B 12 E	150	B	5 43
GS 10 C	10	4	4	Yes	All 10*	Rectangular	80	B 12 E	150	O	2275
GS 10 E	5 2	20	10	Yes	All 10*	Rectangular	15	B 12 E	68*	B	
GS 12 C	12 6 4 3 2*	4	4	Yes	All 12*	Rectangular	80	B 12 E	150	O	
GC 10/2P	10	1	Not Suitable	Yes	90	Rectangular	350	B 7 G	150	O	—

Table showing comparative characteristics and special features.*

DEKATRONS

The most comprehensive range of glow-transfer scaling tubes in the world

Described as the most significant advance in the technique of slow and medium speed counting during the last decade, Dekatron scaling tubes have logged hundreds of thousands of unfailing working hours. Leading manufacturers of counting, timing and measuring instruments prefer these reliable tubes because they allow simplified circuitry, replace a number of thermionic tubes, operate at low current, dissipate negligible heat and are moderately priced.
Available in decade and duo-decade types, the Dekatron is the original and the leading counting tube for superior performance.
Are *you* taking full advantage of the economy, long life and versatility of these cold-cathode scaling tubes?

If you would like more information please write to:—

THE TECHNICAL SERVICES DEPT.,
TUBE DIVISION
BEESTON · NOTTINGHAM · ENGLAND

FEATURES INCLUDED IN THIS RANGE

- BI-DIRECTIONAL COUNTING
- SPEEDS UP TO 20,000 COUNTS PER SEC.
- ONLY RANGE TO INCLUDE 10 OR 12 CATHODE TUBES
- ACCESS TO ONE, FOUR OR ALL CATHODES
- NO SHAPING OF INPUT WAVEFORM NECESSARY

ETELCO

DEKATRON IS AN ETELCO TRADE MARK

ETELCO LIMITED, HEAD OFFICE: 22 LINCOLNS INN FIELDS LONDON, W.C.2. Telephone: HOLborn 6935

E115AR/93AR

ORIGINATORS AND SOLE MANUFACTURERS OF DEKATRON SCALING TUBES

INTERNATIONAL

advertise

YOUR NUCLEAR PRODUCTS IN

sell

YOUR NUCLEAR PRODUCTS

reap

YOUR NUCLEAR SALES REWARDS

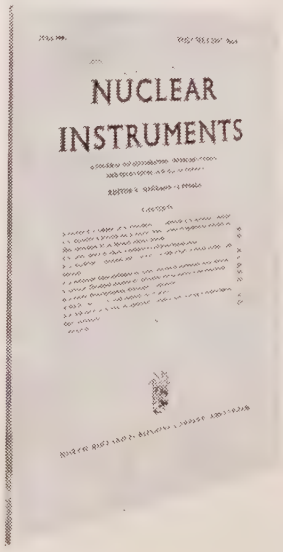

world wide

KEY NUCLEAR MANAGEMENT
NUCLEAR SCIENTISTS
NUCLEAR ENGINEERS
NUCLEAR PRODUCTION PERSONNEL

SUBSCRIBE TO

you reach

THE WHOLE NUCLEAR SALES WORLD IN

Entirely international in scope Nuclear Instruments and Methods is the one nuclear scientific journal that has an established subscription clientele throughout the whole world-where-ever nuclear men are at work—they want your nuclear products—they need your nuclear products—advertise in Nuclear Instruments and tell them WHAT – HOW – WHERE they can get your nuclear products

GO INTERNATIONAL WITH YOUR SALES PROGRAM TODAY WRITE

WILLIAM F. BAARS - ADVERTISING MANAGER NORTH-HOLLAND PUBLISHING COMPANY

P.O. BOX 103 – AMSTERDAM, HOLLAND

INTERNATIONAL

Economical Nuclear Power

Will Come Only Through Experience

HERE'S A SINGLE EXPERIENCED SOURCE FOR:

STATIONARY STEAM GENERATING SYSTEMS

Example · Indian Point, Pressurized Water, Thorium Converter: Design and manufacture of nuclear system

MARINE PROPULSION SYSTEMS

Example · N. S. Savannah: Design and manufacture of nuclear system

MAJOR DEVELOPMENT PROJECTS

Examples · Liquid Metal Fuel Reactor Experiment, Gas Suspension Study

RESEARCH REACTORS

Examples · Hamburg, Germany; Sao Paulo, Brazil

MAJOR NUCLEAR COMPONENTS

Reactor Vessels · ***Examples*** · **BR-3 Yankee EBWR U.S. Navy**

Heat Exchangers · ***Examples*** · **Shippingport SRE U.S. Navy**

Pressurizers · ***Examples*** · **Yankee U.S. Navy**

FUEL ELEMENTS AND CORES

Examples · Materials Testing Reactor, Engineering Test Reactor, Research Reactors, U.S. Navy

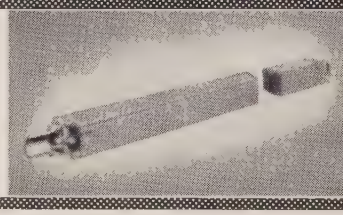

These are but a few examples of the work done by B&W to help release the energy of the atom for useful power. For more information, please write for AEB-8, "B&W and Nuclear Power Development." The Babcock & Wilcox Company, Atomic Energy Division, 161 East 42nd Street, New York 17, N. Y. The Babcock & Wilcox Company, 343 Avenue Louise, Brussels 5, Belgium.

B&W

THE BABCOCK & WILCOX COMPANY

AE-68-E

NUCLEAR ENERGY EQUIPMENT

Complete nuclear systems, cores, components, fuel elements, nuclear research and developmen

The place of the Particle Accelerator in Basic Research...

Pulsed Neutrons for Reactor Research and Teaching - II

A source of pulsed neutrons allows the scientist to conduct many important experiments in nuclear-pile technology and neutron physics. These experiments are designed to measure important parameters of a particular moderator or subcritical assembly or to demonstrate some aspect of neutron physics.

Subcritical Assemblies

Campbell[1], using a pulsed deuteron beam from a Van de Graaff® accelerator, has investigated the multiplicative properties of a water-U^{235} assembly. The dependence of thermal neutron lifetime on physical dimensions was measured and was found to agree with theory, with a reasonable allowance being made for the age to reach thermal energies.

Borst[2], using a 2-Mev Van de Graaff with the Be^{9} (d, n) reaction, obtained an output of about 5×10^{10} neutrons per second and a neutron multiplication of 6.7 in a water-moderated "pickle barrel". The assembly had a criticality factor of 0.85. With the high neutron output from the Van de Graaff, it is possible to carry out lifetime studies of prompt and delayed neutrons, measurements of the effect of impurity in the water moderator and the effect of control rods on the criticality factor, measurements of cross-sections, and many other experiments concerned with neutron physics.

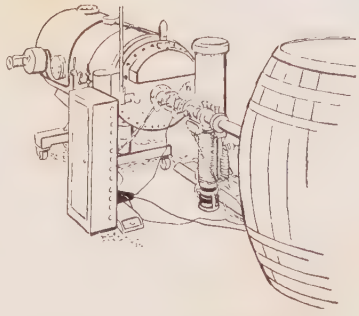

Van de Graaff pulsed-neutron source with subcritical assembly in pickle barrel.

Sjorstrand[3] of Sweden has reported measurements on a subcritical heavy-water reactor using pulsed neutrons. By this method it was possible to determine the criticality per unit volume of moderator and the effect of control-rod geometry on criticality. The overall criticality of the reactor could be measured each time some operating parameter was changed.

Pulsed Neutron Sources for Teaching

The ability to demonstrate some of the properties of the neutron can be invaluable in teaching. Experiments related to lectures can be designed to show neutron moderation with foils or other types of detectors. This can lead to a discussion of neutron diffusion and capture, and of the effects of different buckling factors and types of moderators. The addition of impurities to the water will alter the mean life, and the capture cross-sections for the impurities can be calculated and compared with other methods of measurement. The multiplicative properties of the assembly and the effect of control rods on the multiplication factor can be ascertained. *Thus the student can be shown all the steps in the design and operation of a full scale reactor — with a relatively simple piece of equipment.* The equipment investment is modest and the Division of Reactor Development of the U.S.A.E.C. has indicated willingness to support the purchase of the necessary equipment for colleges and universities.*

The sub-critical assembly can be used for group studies with adequate control for beginning students, but it is by no means limited to this type of teaching. The advanced student can use this device to carry out many important measurements of a fundamental nature which are needed by the reactor designers of today. Many of the gaps in our knowledge of reactor neutron theory can be filled through the use of this type of equipment.

Write to HVEC for a set of typical experiments which can be performed with pulsed or continuous neutron sources.

Reference

1. Campbell, P. H. Stelson Bull. APS 1, No. 4, 183, 1956
2. L. B. Borst — Nucleonics Aug. 1956. Vol. 14, No. 8, Pg. 66–68
3. N. G. Sjorstrand — Vol. 5, 52, National Conference on Peaceful Uses of Atomic Energy — Geneva, 1955 — P/789

* Contact your local U.S.A.E.C. Operations Office or write to High Voltage Enginering Corporation for information on this subject.

HIGH VOLTAGE ENGINEERING CORPORATION

BURLINGTON MASSACHUSETTS

NUCLEAR INSTRUMENTS AND METHODS 5 (1959) 1–25; NORTH-HOLLAND PUBLISHING CO.

SURVEY ARTICLE

ON BUBBLE CHAMBERS

HILDING SLÄTIS

Nobel Institute of Physics, Stockholm

Received 10 April 1959

A short survey is given on the development of the bubble chamber. Glaser's theory is briefly reproduced. Different bubble chambers are described, and photographs of tracks demonstrate the use of these chambers.

Introduction

Among the methods used for the detection of fast moving charged nuclear particles those are of a special interest which give a picture of the spatial paths or tracks passed by the particles. The well-known Wilson chamber, the nuclear photographic emulsion, the diffusion cloud chamber and the bubble chamber are such detectors. The choice of a certain detector depends mainly on the range or the energy of the particles which are of interest, the frequency of the events, whether the particles appear at random (cosmic rays) or are controlled (pulsed accelerators), the available means, and so on. The path-recording detectors have been especially significant for the discovery of new elementary particles. Thus Powell[1]), at the "Second United Nations International Conference on the Peaceful Uses of Atomic Energy" (Geneva 1958) pointed out, that in the detection of the unstable elementary particles (μ^-, π^+, π^-, π^0, K^+, K^0, n^0, Λ^0, Σ^+, Σ^-, Σ^0, Ξ^-) and their transformations nuclear emulsions were used in 10 cases, the Wilson-chamber in 8, the bubble chamber in two and counters in two cases. Bradner and Glaser[2]) at the same conference, talking about methods of particle detection for high energy physics experiments, compared track-forming detectors as well as the frequency of rare events in a 50 cm chamber (table 1). It is clear from the table how the construction of the hydrogen, the helium, the propane, the $SnCl_4$ and the xenon bubble chambers represent track detectors, the stopping power of which constitutes a beautiful series of values between about 0.01 for the cloud chamber (if the pressure is $<$ 1 atmosphere) and 200 for the photographic emulsions. Thus, the high stopping power of the photographic emulsions is also achieved by the bubble chambers, which as against the nuclear emulsions have the advantage of offering large volumes.

1. Principle and the Earliest Development of the Bubble Chamber

Making efforts to find a track-recording device, having the advantages of both the cloud chamber and the nuclear emulsions, Donald A. Glaser[3–6]) at the University of Michigan, Ann Arbor, in 1952 found that it was possible to take advantage of the instability of superheated liquids against bubble formation in the same way that a Wilson chamber utilizes the instability of super-cooled vapours against droplet formation. A macroscopic continuum theory of the stability of small bubbles in a superheated liquid shows, that bubbles carrying a single electronic charge tend to collapse more rapidly than uncharged bubbles, while bubbles carrying two or more charges are unstable against rapid growth under certain circumstances (more about this in section 2).

[1]) C. F. Powell, A/CONF. 15/P/268.
[2]) H. Bradner and D. A. Glaser, A/CONF. 15/P/730/Rev. 1.
[3]) D. A. Glaser, Phys. Rev. **87** (1952) 665.
[4]) D. A. Glaser, Phys. Rev. **91** (1953) 762.
[5]) D. A. Glaser, Nuovo Cimento **11**, Suppl. 2 (1954) 361.
[6]) D. A. Glaser, Handbuch der Physik **45** (1958) 314 (review article).

TABLE 1

Comparison of track-forming detectors. Frequency of rare events in a 50 cm chamber (D. A. Glaser, Handb. d. Physik, Berlin 1958)

	Type	Density ϱ (g/cm³)	Radiation length † λ (cm)	Scattering sagittal † δS for 2 GeV proton track 5 cm long (microns)	Magnetic field required for 10% momentum error in 5 cm relativistic track (gauss)	Stopping power of a 50 cm chamber (g/cm²)	Events/day for σ/nucleon $= 10^{-30}$ cm² = 1 microbarn	Events/pulse for σ/nucleon $= 10^{-27}$ cm² = 1 millibarn
1	1 atmosphere argon expansion cloud chamber	0.0017	11 600	0.79	2 400	0.085	0.015	0.0003
2	20 atmosphere hydrogen diffusion cloud chamber	0.0019	36 300	0.45	1 300	0.095	0.16	0.0003
3	hydrogen bubble chamber	0.05	1 380	2.3	6 900	2.5	0.43	0.008
4	helium bubble chamber	≈ 0.10	963	2.75	8 200	5.0	0.86	0.015
5	propane (C_3H_8) bubble chamber	0.44	108.3	8.2	25 000	22	3.7	0.07
6	$SnCl_4$ bubble chamber	1.5	7.35	31.5	94 000	75	13	0.23
7	xenon bubble chamber	2.3	3.1	48.5	140 000	115	20	0.34
8	nuclear emulsion (AgBr)	4.0	2.8	51.1	150 000	200	34	0.59

† Definition in section 9.

In order to test this theory and the possibility of a radiation-induced ionization, diethyl ether was heated in a thick-walled glass tube to a temperature near 130° C under a pressure of about 20 atmospheres. In the presence of a strong Co^{60} source the liquid always erupted as soon as the pressure was diminished, while when the source was removed, a time difference of 0 to 400 seconds occurred with a mean value of 68 seconds between the pressure release and the eruptive boiling. This time delay was in reasonable agreement with the time between successive traversals of the tube by a hard cosmic-ray particle, *viz.* 34 seconds.

Two similar glass tubes, forming a "coincidence telescope", showed several cases of simultaneous eruptive boiling, apparently resulting from the same cosmic-ray particle. Also the location in the two tubes of the coincident bubbles indicated that they were caused by one and the same particle.

Fig. 1 shows the first arrangement used by Glaser[5]) to demonstrate the radiation sensitivity of superheated liquids. Two 10 cm lengths of a thick-walled pyrex glass tube of 3 mm inside diameter were connected by a thick-walled capillary bent as shown in the figure. The tube was filled with liquid and gaseous ether (the vapour volume at room temperature was about a third of the left hand part of the glass tube). The larger (lower) parts of the tube were immersed in beakers of hot mineral oil and heated to about 160° and 130–150° C, respectively.

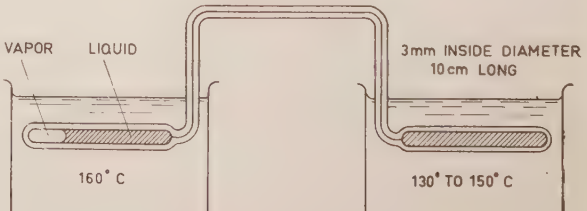

Fig. 1. Glaser's first experiment to demonstrate the radiation sensitivity of superheated diethyl ether. For details see the text. (D. A. Glaser, Nuovo Cimento 11 (1954) 361.)

The pressure in the tube was then 21 atmospheres. When the pressure was suddenly reduced by removing the left hand oil beaker and cooling the corresponding part of the tube, the other on the right became highly superheated. This state remained for about a minute on the average

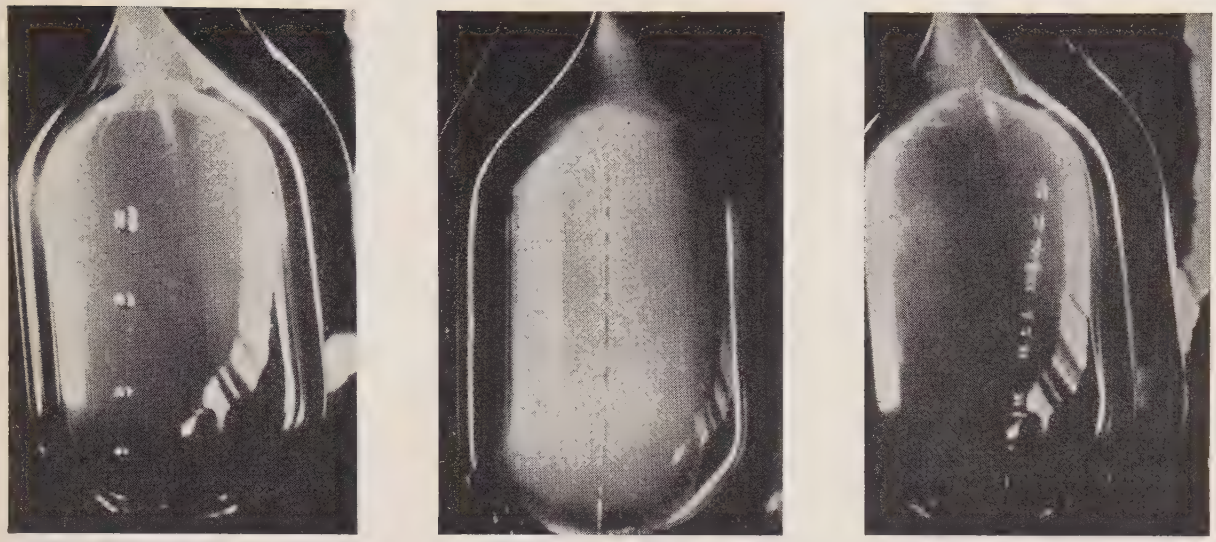

a b c

Fig. 2. Penetrating cosmic radiation tracks in Glaser's diethyl ether bubble chamber. Random expansion and counter-controlled flash-lamps. (a) 60 μsec flash delay, 20 μsec flash duration, 139° C, (b) 10 μsec flash delay, 20 μsec flash duration, 140° C, (c) 10 μsec flash delay, 5 μsec flash duration, 141° C. The track in (c) is deflected about 2° in the middle of the chamber. (D. A. Glaser, Handbuch der Physik, Bd. **45**, Berlin 1958.)

after which an eruptive boiling in the right hand part of the tube caused filling of the left hand tube with liquid ether. In the presence of a Co^{60} source of gamma rays the superheated state was destroyed immediately[7]).

In the bubble chamber the bubbles grow very rapidly. Unfortunately, it is usually not possible to see the tracks directly in the same way as in the cloud chamber. The tracks have to be photographed automatically using a flash-lamp at the proper moment. (However, it is possible to see just a glimpse of the tracks when these are automatically illuminated.) Fig. 2, which belongs to the work by Glaser[4,6]) in 1953, shows some of the first published tracks obtained in Glaser's ether bubble chamber. This consisted of a heavy-walled pyrex tube 3 cm long and with 1 cm inside diameter, connected to a pressure regulating device by means of a capillary tube 45 cm long. An oil bath thermostated to 138–143° C surrounded the bubble chamber. The pressure regulating device consisted of a brass cylinder 2 cm long and with 3 cm inside diameter. The cylinder and the liquid-containing system was closed by means of a flexible diaphragm of 3 mm Neoprene faced with Teflon to confine the ether. This arrangement permitted variation of the internal pressure by controlling the pressure of compressed gas on the outside of the diaphragm.

The bubble chamber was placed under 10 cm of lead and between two counters forming a vertical coincidence telescope, which triggered the flash-lamp used for photographing the event.

A photographic recording of an event in the bubble chamber consisted of the following phases. The ether was compressed by means of nitrogen at about 20 atmospheres, so that no bubbles remained in the liquid. After that the nitrogen gas was released, resulting in atmospheric pressure in the ether which was thereby brought into a highly supersaturated condition. On the average the liquid remained quietly in this unstable state for several seconds until an eruptive boiling started. If a coincidence of the vertical counter telescope occurred during this period of time, a picture was taken by means of a xenon flash-lamp.

Fig. 2 shows pictures of the tracks of vertical,

[7]) The author has repeated and confirmed this interesting experiment. The ether-filled pyrex glass tube was made by Mr. R. Östling at the Royal Institute of Technology, Stockholm. The author is also indepted to Mr. K. Halvarson, Esso Oil Company, for the paraffin oil used for the oil baths.

hard cosmic rays penetrating the above described Glaser bubble chamber.

The disadvantage that it is not possible to be delighted with a look at these tracks is counterbalanced by the fact that the very short time interval, some microseconds, which elapses between the passage and the photography of the track eliminates the distortions in the position of the track which depend on convective currents in the liquid. Cloud chambers are sensitive to such currents.

Already in the same year, 1953, Hildebrand and Nagle[8]) (in collaboration with Glaser) at the University of Chicago showed that also liquid hydrogen can be superheated and kept in this state for periods up to 70 seconds before boiling. The boiling was triggered immediately in the presence of a Co^{60} source. The pressures used were $3\frac{2}{3}$ and 1 atmosphere, respectively. Similar results were obtained with liquid nitrogen. The authors point out the usefulness of a bubble chamber containing liquid hydrogen for studying nuclear events involving protons. It would provide a hydrogen target of greater density and purity than can be achieved in a cloud chamber.

2. The Bubble Chamber Theory

Glaser[5]) first made some simple considerations concerning the stability of bubbles in liquids. If no charges are situated in the bubble, three forces act on the bubble surface: The vapour pressure P_T (depending on the temperature), the hydrostatic pressure P and the surface tension, for which the well-known expression $2\sigma/r$ is valid, σ being the surface tension constant (depending on the temperature) and r the bubble radius. The equilibrium condition is then

$$P_T - P = 2\sigma/r\,. \qquad (1)$$

Suppose the liquid is superheated and that $P_T - P > 0$. Equation (1) shows that the equilibrium of the bubble is unstable. If r increases, the surface tension diminishes and the pressure $P_T - P$ tends further to increase the radius r. In the same way it is seen, that if r decreases, the surface tension exceeds the pressure $P_T - P$, and the bubble collapses.

Glaser then showed that bubbles carrying a single electronic charge inside the vapour bubble always tend to collapse.

If there are several charges of the same sign, say n, on a bubble, their effect is approximated by a charge of the same size spread continuously over the sphere. The electrostatic energy E of a sphere having the radius r and the charge Q is $E = \frac{1}{2}Q^2/r$. From this expression the electrostatic force per cm^2 is easily derived and found to be $Q^2/8\pi r^4$. This is the electrostatic pressure on the bubble. Considering the dielectric constant ε, the expression for the electrostatic pressure should be divided by ε. The directions of the electrostatic pressure and the vapour pressure being the same, and considering the relation $Q = ne$ we obtain

$$P_T - P = \frac{2\sigma}{r} - \frac{n^2e^2}{8\pi\varepsilon r^4}\,. \qquad (2)$$

Fig. 3 shows $P_T - P$ as a function of r or the equilibrium conditions for bubbles of a different number of charges. The dotted curve is valid

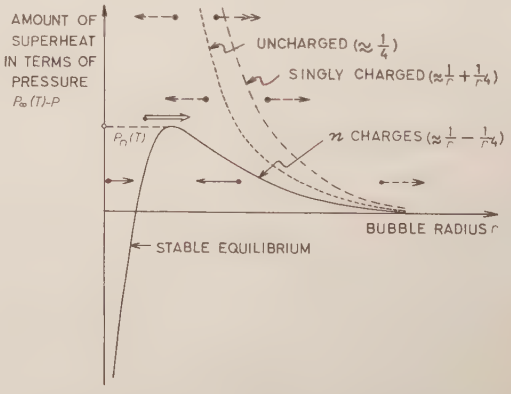
AMOUNT OF SUPERHEAT IN TERMS OF PRESSURE
UNCHARGED (≈ 1/4)
SINGLY CHARGED (≈ 1/r + 1/r4)
n CHARGES (≈ 1/r − 1/r4)
BUBBLE RADIUS r
STABLE EQUILIBRIUM

Fig. 3. Equilibrium curves for bubbles. The superheat (in terms of the pressure) as a function of the radius of the bubbles and the number n of charges on a bubble. For details see the text. (D. A. Glaser, Nuovo Cimento **11** (1954) 361.)

for neutral bubbles, the dashed curve is for singly charged bubbles. The arrows show the direction of development of the bubbles, if they collapse (arrows to the left) or grow towards infinity (arrows to the right). In the case where

[8]) R. H. Hildebrand and D. E. Nagle, Phys. Rev. **92** (1953) 517.

there are n charges the equilibrium condition is represented by the solid line. The left hand part of this curve corresponds to a stable state. The maximum point of the solid curve is easily found from the equation (2)

$$P_T - P = \left[\frac{27}{2}\frac{\pi\varepsilon\sigma^4}{n^2e^2}\right]^{\frac{1}{3}} = \text{maximum} \qquad (3)$$

$$r = \left[\frac{n^2e^2}{4\pi\varepsilon\sigma}\right]^{\frac{1}{3}}.$$

Expression (3) depends on the temperature T and may therefore be used for calculating the temperature, to which a liquid under a certain pressure should be heated to make it sensitive to ionizing radiation.

The formula has proved to be extremely useful. The theoretical values have been in good agreement with the experimental ones for $n = 6$. However, Glaser[6]) has himself made objections to the conceptions from which the equations (2) and (3) are derived. Experience shows that the radius of the bubbles under typical working conditions for organic liquids is 10^{-6} cm. It seems to be incredible that a particle having minimum ionization would be able to create 6 charges of the same sign inside such a small volume. Still more impossible is the case for α-particles. In order to get agreement with the theory, a bubble of the above mentioned size should be able to contain 900 charges of the same sign. This exceeds the amount corresponding to maximum ionization of a retarded α-particle. A mechanism other than only the occurrence of free charges has therefore to be considered. The retardation of a charged particle moving through matter originates not only from the ionization of neighbouring atoms, but also from the excitation of the atoms. In deexciting collisions between excited molecules, enough kinetic energy is released for local heating of the liquid. It is probable that this is the real cause for the creation of bubbles along the paths of ionizing particles moving through superheated liquids†.

The conception that bubbles are nucleated by moderately energetic free electrons produced by the incident particles in Coulomb encounters is analyzed by Seitz[9]).

3. Later Development of the Bubble Chamber

Early in 1953 Luis Alvarez at the Radiation Laboratory in Berkeley, University of California, drew up a plan for the development of hydrogen bubble chambers. John Wood[10]) succeeded already in 1954 to photograph proton recoil tracks appearing in a hydrogen bubble chamber irradiated with neutrons from a Po-Be-sample. The bubble chamber, the inner dimensions of which were 25 mm diameter and 12.5 mm thickness, was made of glass and immersed in a bath of hydrogen which boiled at high pressure. In this way the temperature of the bath was easily controlled by a pressure regulator. The photographs were taken using the following procedure. The hydrogen was condensed into the bubble chamber at a pressure somewhat higher than that over the bath. After temperature equilibrium had been reached the pressure in the bubble chamber was abruptly reduced to one atmosphere. An electronic circuit released after a certain time interval a light pulse in a stroboscopic lamp, thus exposing the event for the photographic camera. After this the pressure in the bubble chamber was reapplied in order to remove bubbles which might have been produced. The equipment was then reday for the next photograph.

In the article "Characteristics of Bubble Chambers" Glaser and Rahm[11]) point out the possibility of making large bubble chambers. The advantage of these have already been reported above. In addition, the possibility of using liquids containing only elements of low atomic number (in opposition to the case with nuclear emulsions) minimizes Coulomb scattering and thus permits very accurate measurements of magnetic curvature. This is important for the calculating of the momentum of the particles. Tracks of particles with minimum ionization contain about 100 bubbles per cm. The density

† *Note added in proof*. Professor Glaser has informed me that he no longer believes in the electrostatic theory for the operation of the bubble chamber. Professor Glaser and his group intend to publish some experiments giving their reasons for this view.

[9]) F. Seitz, Phys. of Fluids **1** (1958) 2.
[10]) J. Wood, Phys. Rev. **94** (1954) 731.
[11]) D. A. Glaser and D. C. Rahm, Phys. Rev. **97** (1955) 474.

of bubbles along a track increases with the ionization density, thus making bubble counting a possible method for measuring ionization. As a drawback is mentioned that the lifetime of the bubble nuclei seems to be too short to permit counter-controlled expansion after the passage of the particle to produce tracks. Therefore it is considered unlikely that the regarded types of bubble chambers will be useful for cosmic-ray experiments. On the other hand, the short sensitive time, about 10 milliseconds, and the short reset time (time between two expansions), about 5 seconds, make them ideally suited for experiments with pulsed accelerators in which the interesting events occur in short bursts and therefore in connection with intense background radiation (compare for instance figs. 18 and 22).

It is not possible here to give a detailed description of the fast development of the bubble chamber. The following persons or groups have been leading in this field: the inventor of the bubble chamber Glaser[3-6]) and the Chicago group inspired by him, Alvarez's group[12,13]) and W. Powell's team[14]) in Berkeley, the group of Steinberger[15]) at the Columbia University, New York, and the Brookhaven group with the earlier diffusion chamber experts Shutt, Thorndike and Whittemore[16]). Besides ether several other organic compounds have been used, for instance propane[14,15,17,36,37]), isopentane[18]) and fluorocarbon[19]). Apart from the already mentioned hydrogen[10,12,20]), other elements used have been helium[21]) and xenon[22]). As pointed out by Glaser[23]), a bubble chamber filled with a liquid of high density and large atomic number would be capable of detecting gamma rays with a high efficiency as well as giving information concerning the paths of charged particles. In addition, so called gas bubble chambers have been constructed. In these chambers the liquid is saturated under pressure with a gas. Thus Argan and Gigli[24]) in Genoa and independently Hahn[25,26]) in Freibourg (Switzerland) in 1956 have found that ether as well as hexan, in combination with carbon dioxide as a gas are suitable liquids for bubble chambers. These chambers have as against the common bubble chambers the advantage of being operable at room temperature.

4. "Clean" and "Dirty" Bubble Chambers

The first bubble chambers were made of one piece of pyrex glass, consisting of a cylindrical or rectangular tube connected to the expansion system by a capillary tube of the same pyrex glass. The expansion system is usually made of metal. Gradually, when the bubble chambers were larger, it was necessary for several reasons (for instance the need for a faster heat transport through the walls of the chamber) to make the chambers of metal and hence to use windows and gasketing materials. Glaser[6]) calls the former chambers as "clean" in opposition to the latter, "dirty" chambers.

In the clean chambers only the liquid in the chamber itself is superheated, while the liquid in the capillary and in the expansion part is kept at a lower temperature. This has the advantage that bubbles are formed only in connection with the passage of ionizing particles and that the eruptive boiling does not take place before such a particle has occurred. The time, during which a clean chamber is sensitive for

[12]) D. Parmentier, Jr. and A. Schwemin, Rev. Sci. Inst. **26** (1955) 954.

[13]) W. I. Linlor, Q. A. Kerns and J. W. Mark, Rev. Sci. Inst. **28** (1957) 535.

[14]) W. M. Powell, W. B. Fowler and L. O. Oswald, Rev. Sci. Inst. **29** (1958) 874.

[15]) J. Leitner, N. Samois, M. Schwartz and J. Steinberger, Nevis Cyclotron, Lab. Report, Nevis-10, May (1955).

[16]) E. M. Bolze, T. W. Morris, D. C. Rahm, R. R. Rau, R. P. Shutt, A. M. Thorndike and W. L. Whittemore, Rev. Sci. Inst. **29** (1958) 297.

[17]) L. O. Oswald, Rev. Sci. Inst. **28** (1957) 80.

[18]) I. A. Pless and R. J. Plano, Rev. Sci. Inst. **27** (1956) 935.

[19]) B. Hahn and G. Riepe, Rev. Sci. Inst. **29** (1958) 184.

[20]) D. E. Nagle, R. H. Hildebrand and R. J. Plano, Rev. Sci. Inst. **27** (1956) 203.

[21]) W. M. Fairbank, E. M. Harth, M. E. Blevins and G. G. Slaughter, Bull. Amer. Phys. Soc. **30**, No. 5 (1955) 25.

[22]) J. J. Brown, D. A. Glaser and M. L. Perl, Phys. Rev. **102** (1956) 586.

[23]) D. A. Glaser, Proceedings of the Fifth Annual Rochester Conference on High Energy Physics (Interscience Publishers, Inc., New York, 1955).

[24]) P. E. Argan and A. Gigli, Nuovo Cimento **3** (1956) 1171.

[25]) B. Hahn, Nuovo Cimento **4** (1956) 944.

[26]) B. Hahn and J. Fischer, Rev. Sci. Inst. **28** (1957) 656.

ionizing radiation after superheating of the liquid, is therefore longer than for the corresponding time in dirty chambers, where the boiling starts immediately at the rough places on the walls and the gaskets. In order not to diminish the sensitive time of the dirty chambers too much, the expansion has to be made fast and for so long, that the low pressure is maintained by providing the volume required by the newly-forming vapor. The expansion volume for a dirty chamber has therefore to be larger than for a clean bubble chamber.

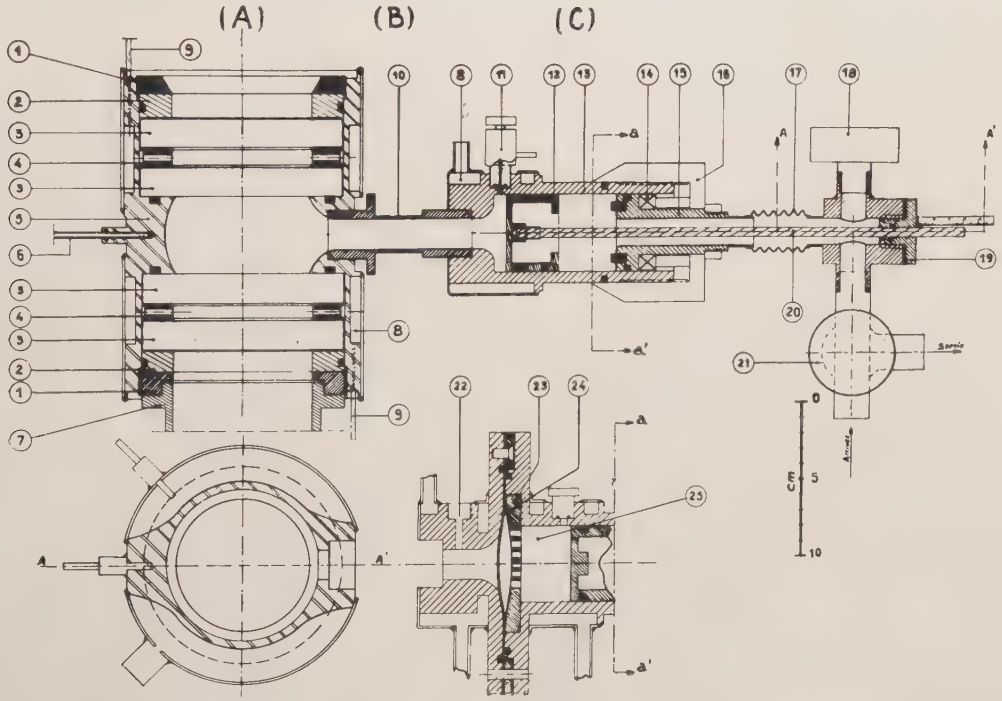

Fig. 4. Propane bubble chamber (A. Rogozinski, Rapport C.E.A. No. 607, 1957). 1. Ring nut, 2. Gasket, 3. Window, 4. Gasket, 5. Chamber wall, 6. Thermocouple, 7. Support, 8. Water circulation, 9. Water leading-in and out, 10. Tube, 11. Filler base, 12. Piston, 13. Cylinder, 14. Thrust bearing, 15. Adjusting ring, 16. Adjusting nut, 17. Tombak bellows, 18. Compressed air valve, 19. Sealing nut, 20. Control piston rod, 21. Electric valve, 22. Filling tube, 23. Stopping lattice, 24. Diaphragm, 25. Oil.

5. Propane Bubble Chambers

As a typical example of a propane bubble chamber we have chosen a chamber made by Rogozinski[27]) for "Saturne"—the 2–3 GeV proton synchrotron at Saclay. This bubble chamber was demonstrated at the "Second United Nations International Conference on the Peaceful Uses of Atomic Energy", Geneva 1958, in the French Department of the scientific exhibit. The bubble chamber was working, and glimpses of tracks released by the gamma radiation from a Co^{60} source could be seen in the light of flash-lamps†.

Fig. 4 shows a section of the bubble chamber itself and of the expansion equipment. Of the latter, two types were tried, an expansion device with a diaphragm (24) between the propane in the bubble chamber (A) and the oil in the expansion cylinder (25) (compare the lower part of the figure) and the other type an expansion equipment (C) without a diaphragm (upper part of the figure). The bubble chamber of 10 cm inside diameter and 5 cm thickness

[27]) A. Rogozinski, Centre d'Études nucléaires de Saclay, Rapport No. 607 (1957).

† In the exhibit hall of the United States an operating bubble chamber filled with liquid freon at high pressure was displayed. The temperature of the freon was 45° C. The pressure was 27 atmospheres, in the superheated state 10 atm. The tracks could be photographed or seen on a television screen.

was made of stainless steel, thoroughly polished on the inside. The chamber was equipped with double glass windows on each side. The panes were 16 mm thick, annealed, ground, polished and joined to the stainless steel cylinder in a manner shown in the figure. Fig. 4 also shows the cover of stainless steel, which together with the bubble chamber cylinder created a cavity (A, 8) for the temperature regulating water current. In a similar way the temperature of the expansion cylinder (C, 8) and the tube B (the corresponding cavity is not shown in this case) was controlled.

The propane and the nitrogen tubes, the pumps, gauges and other equipment necessary for the running of the bubble chamber are seen in fig. 5 (this equipment, however, was not used in Geneva, nor the coils for the magnetic field).

The expansion piston was of a construction already given by Steinberger[15]), and the diaphragm was made of Teflon-Mylar-Perbunan, recommended by Glaser.

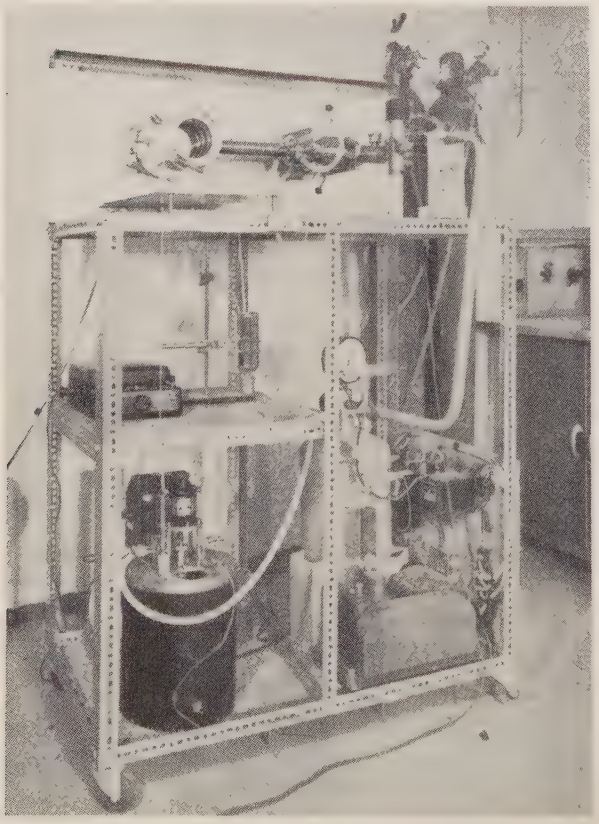

Fig. 5. The propane bubble chamber in fig. 4 with accessories. (A. Rogozinski, Rapport C.E.A. No. 607, 1957.)

Propane (C_3H_8) has a boiling point — 42.17° C, a critical temperature 95.6° C and a critical pressure 43 kp/cm². At the boiling point the density is 0.585, at 60° C and 30 kp/cm² the

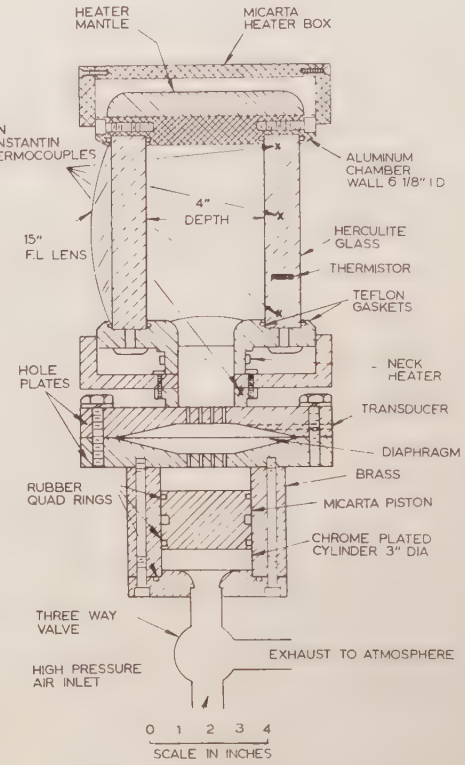

Fig. 6. The 15 cm diameter propane bubble chamber of the Steinberger group at the Columbia University. (Courtesy of Professor R. J. Plano.)

density is 0.435 g/cm³. The latter temperature and pressure were used in the bubble chamber. At room temperature and normal pressure the propane is a gas, at 10 atmospheres it is a liquid. The last mentioned pressure is used when the bubble chamber is filled. As already mentioned, the working temperature is 60° C. The liquid is superheated when the pressure is abruptly diminished from 30 to 12 atmospheres. The volume of the liquid increases by 17 per cent when the temperature is increased from 20° C to 60° C and the pressure from 10 to 30 atmospheres. Hence the bubble chamber should not be filled to more than $\frac{5}{6}$ of its volume. On the other hand, when the volume increase at a constant temperature is 3%, the pressure

changes from 30 to 10 atmospheres, making the chamber sensitive to ionizing radiation.

The minimum working period of this bubble chamber is 3 seconds. The chamber is electronically controlled. When working in connection with "Saturne" a cycle consists of the following moments (the time is called t):

$t = 0$. Start of the proton beam in "Saturne".

$t = \tau_1$. Expansion of the bubble chamber.

$t = \tau_2$. The proton beam passes the bubble chamber, 15 msec $< \tau_2 - \tau_1 <$ 20 msec.

$t = \tau_3$. Light flash $0 < \tau_3 <$ 100 msec.

$t = \tau_4$. Recompression of the chamber and forward pushing of a new film.

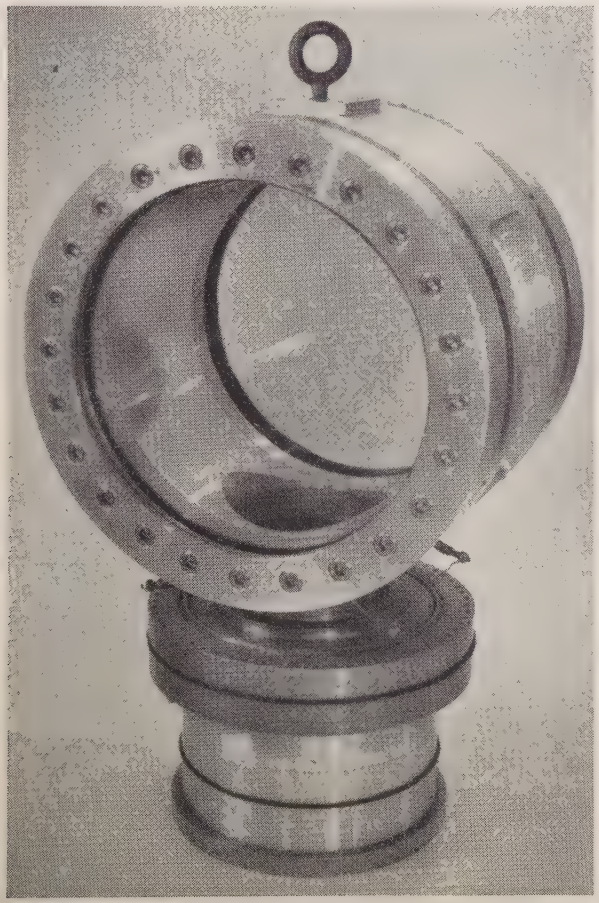

Fig. 7. Photograph of the chamber in the 30 cm diameter propane bubble chamber of the Steinberger group, Columbia University. The chamber was placed in a magnetic field of 13 400 gauss. (Courtesy of Professor R. J. Plano.)

By the courtesy of Prof. Plano in the Steinberger group, Columbia University, New York, a number of diagrammatic drawings of their propane and hydrogen bubble chambers as well as photographs of interesting events were placed at the author's disposal (figs. 6, 7, 8, 18 and 19). Fig. 6 shows diagrammatically the 15 cm diameter propane bubble chamber, fig. 7 a photograph of the chamber itself for the 30 cm apparatus and fig. 8 the optical arrangement for the stereoscopic photographing of tracks in the 30 cm diameter bubble chamber. Considering the description just given for the apparatus of Rogozinski the above figures of the Steinberger group probably need no further explanation.

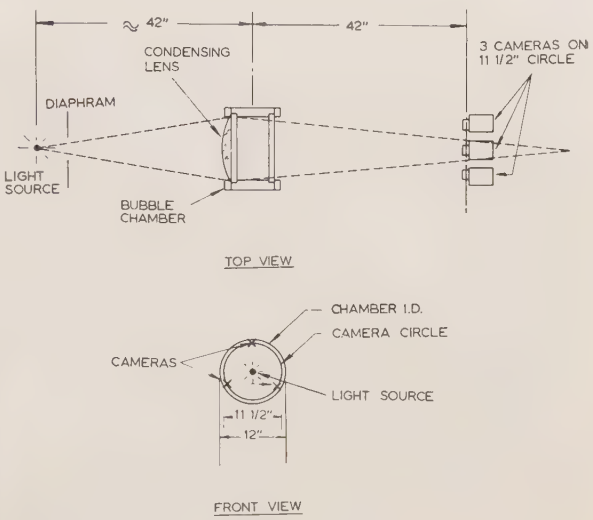

Fig. 8. Schematic diagram of the photographic system used on the 30 cm diameter bubble chamber in fig. 7. (Courtesy of Professor R. J. Plano.)

6. Hydrogen Bubble Chambers

Since Wood[10]), as mentioned earlier, succeeded in taking photographs of tracks in a small 25 mm diameter hydrogen bubble chamber, the construction of larger and larger hydrogen bubble chambers in Berkeley continued under the guidance of Alvarez. To begin with, Parmentier and Schwemin[12]) built such an apparatus with 63 mm inside diameter and immediately after that (1955) a hydrogen chamber 10 cm in diameter and 5 cm thick. We here use this latter apparatus as a typical example for the hydrogen bubble chambers.

First, it might be worth while to point out the difficulties which had to be overcome in the construction of dirty hydrogen bubble chambers. There was no experience available concerning glass-to-metal seals of this size for use at such a low running temperature, — 246 to — 253°C. Various Kovar metal-to-glass seals were tested, but the glass cracked, either on being cooled or in the warming-up process. Indium solder as well as gaskets of Teflon and gold were tried but were found to be unreliable. Finally, lead wire of about 1.2 mm thickness proved to be satisfactory. The gasket groove was made in the form of a shallow V in the end of the brass cylinder. Of course the lead must be clean and free from carbonate.

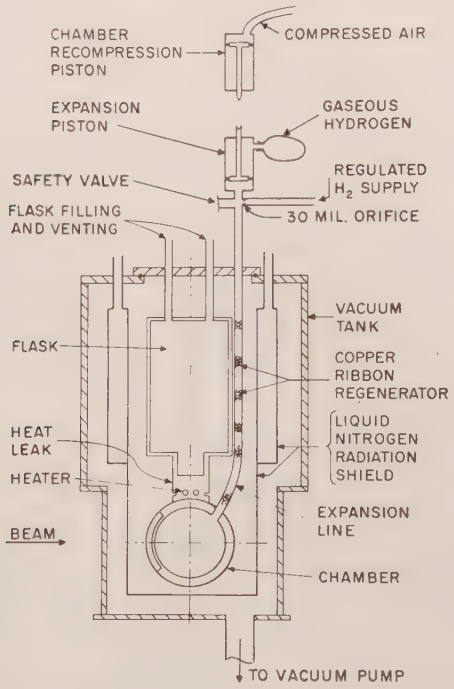

Fig. 9. Schematic diagram of the 10 cm diameter hydrogen bubble chamber of the Berkeley group. (D. Parmentier, Jr. and A. J. Schwemin, Rev. Sci. Inst. **26** (1955) 954.)

Fig. 9 shows diagrammatically the 10 cm hydrogen bubble chamber. The most important part, the cylinder for the superheated hydrogen (see the lower part of the figure) is in metallic and thermal connection with a "bottle". *viz.* a cylindrical container for liquid hydrogen, which is refilled gradually when the hydrogen in the container is diminished by evaporation. In this way the temperature of the container is kept constant at — 253°C. An electric resistance between the chamber and the container permits heating of the chamber to — 246°C. At this temperature the hydrogen is superheated if the pressure is one atmosphere. Most of the time the pressure is 5 atmospheres. The tubes for the refilling of the chamber and the expansion cylinder with the piston are seen in the upper part of the figure. The chamber and the "bottle" are enclosed in a heat-radiation shield, the upper part of which is cooled with liquid nitrogen. This radiation shield with the bubble

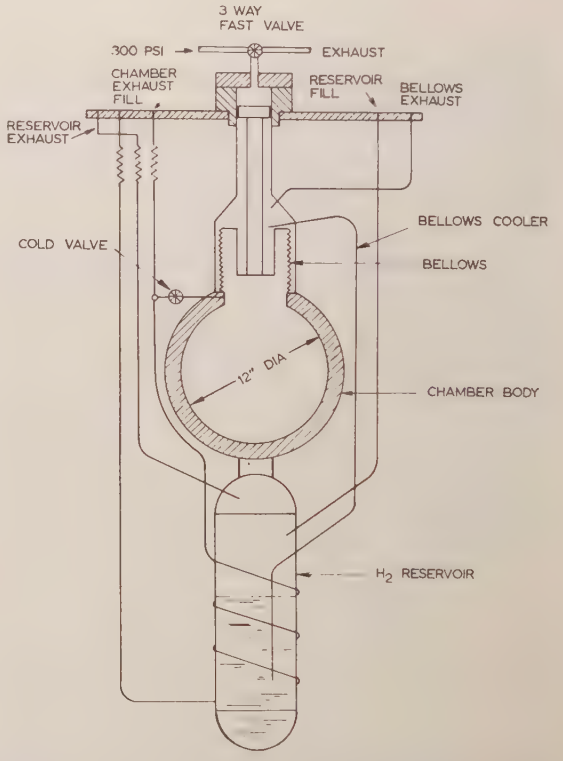

Fig. 10. Schematic diagram of the 30 cm diameter liquid hydrogen bubble chamber of the Steinberger group. (Courtesy of Professor R. J. Plano.)

chamber and "bottle" is enclosed in a vacuum tank. The vacuum tank protects the bubble chamber against heat from the surroundings and is also a protection against hydrogen leakage and hence against explosion risk. On the whole, when working with hydrogen bubble chambers, measures of precaution are an important subject, to which we will return below.

Between the expansion cylinder and the bubble chamber there is a copper ribbon heat regenerator, suggested by Garwin. The regenerator permits pulsing the chamber without prohibitive heat input and makes it possible to use shorter working periods for the bubble chamber. Instead of a cycling rate of 5 minutes without the generator, it was possible to have one picture of the tracks every four seconds with use of it. However, this short cycle is not necessary at Berkeley in connection with the Bevatron accelerator, which has a pulse rate of about five per minute.

Fig. 10 shows schematically the Steinberger group 30 cm diameter hydrogen bubble chamber. The liquid hydrogen is enclosed by the chamber connected to a bellows, which makes it possible to expand the volume. The temperature-controlling hydrogen reservoir is here placed below the chamber, as distinct from the case in fig. 9, where the "bottle" was above the chamber.

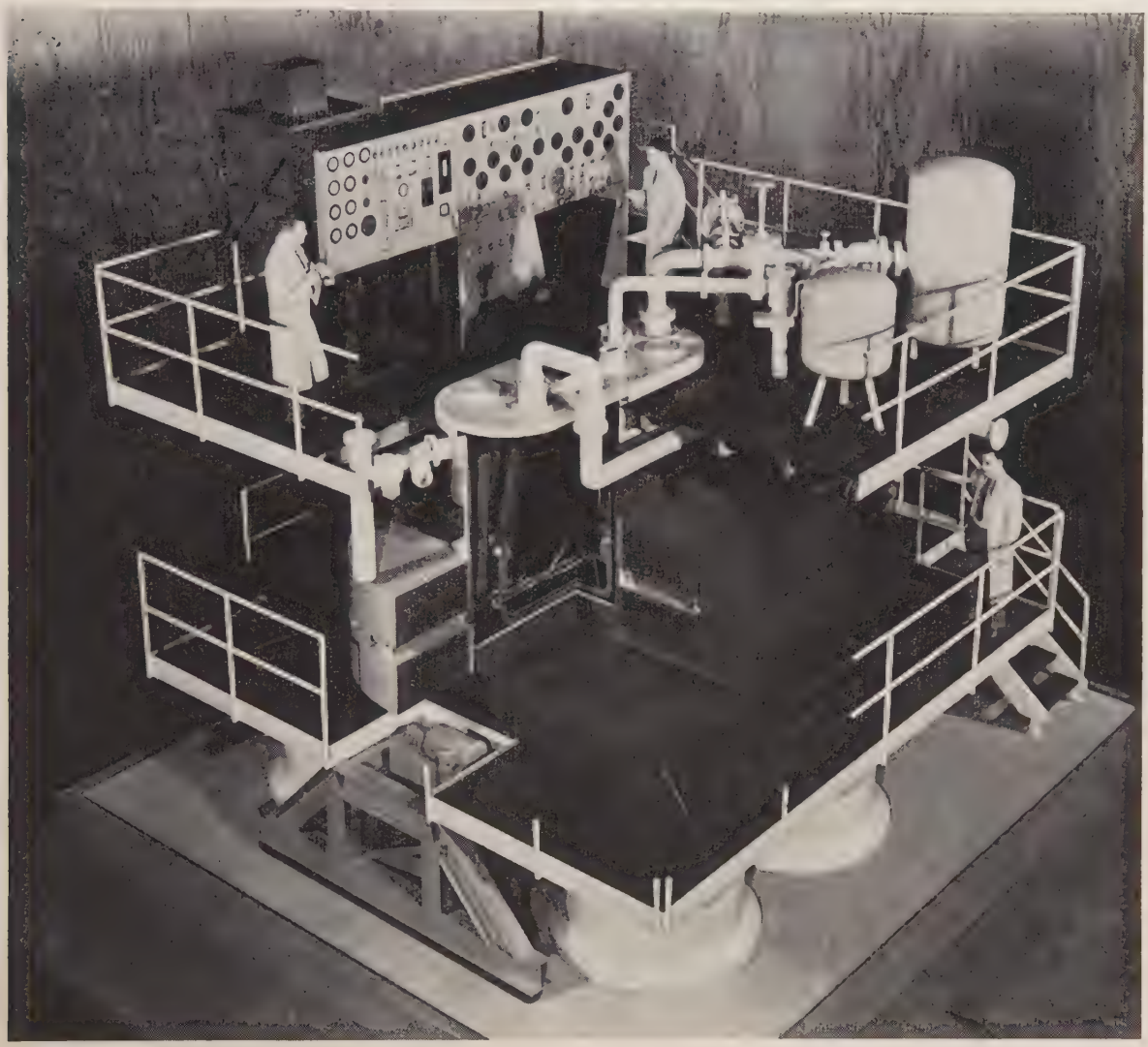

Fig. 11. Model of the 183 cm liquid hydrogen bubble chamber of the Alvarez group at Berkeley. For details see the text. (Courtesy of Professor Luis W. Alvarez.)

In Berkeley the work on bigger and bigger hydrogen bubble chambers continued. Thus the 10 cm chamber described above was followed by a 25 cm diameter chamber, 12.5 cm thick,

and finally a chamber of 183 cm length, 51 cm width and 36 cm depth, containing altogether 520 litres of liquid hydrogen. Fig. 11 shows a model of this giant. The equipment for producing liquid hydrogen, the expansion and the recompression device as well as the control panel are on the second deck. A section through the bubble chamber shows some diagrammatic tracks. The strength of the magnetic field is 17 500 gauss, and the power necessary for this is 3000 kW. The effect of the cooling machine is 2 kW. The Joule-Thomson effect gives a temperature of the hydrogen of — 253°C. The magnet "can walk on its own feet", as Professor Alvarez expresses himself. A photograph of the real hydrogen bubble chamber is shown in fig. 12. In the foreground are, from left to right, the control panel for a 38 cm bubble chamber, the chamber itself, and a 25 cm bubble chamber enclosed in a vacuum tank. In the background the large 183 cm chamber is seen. The details are easily recognized by comparison with the above demonstrated model.

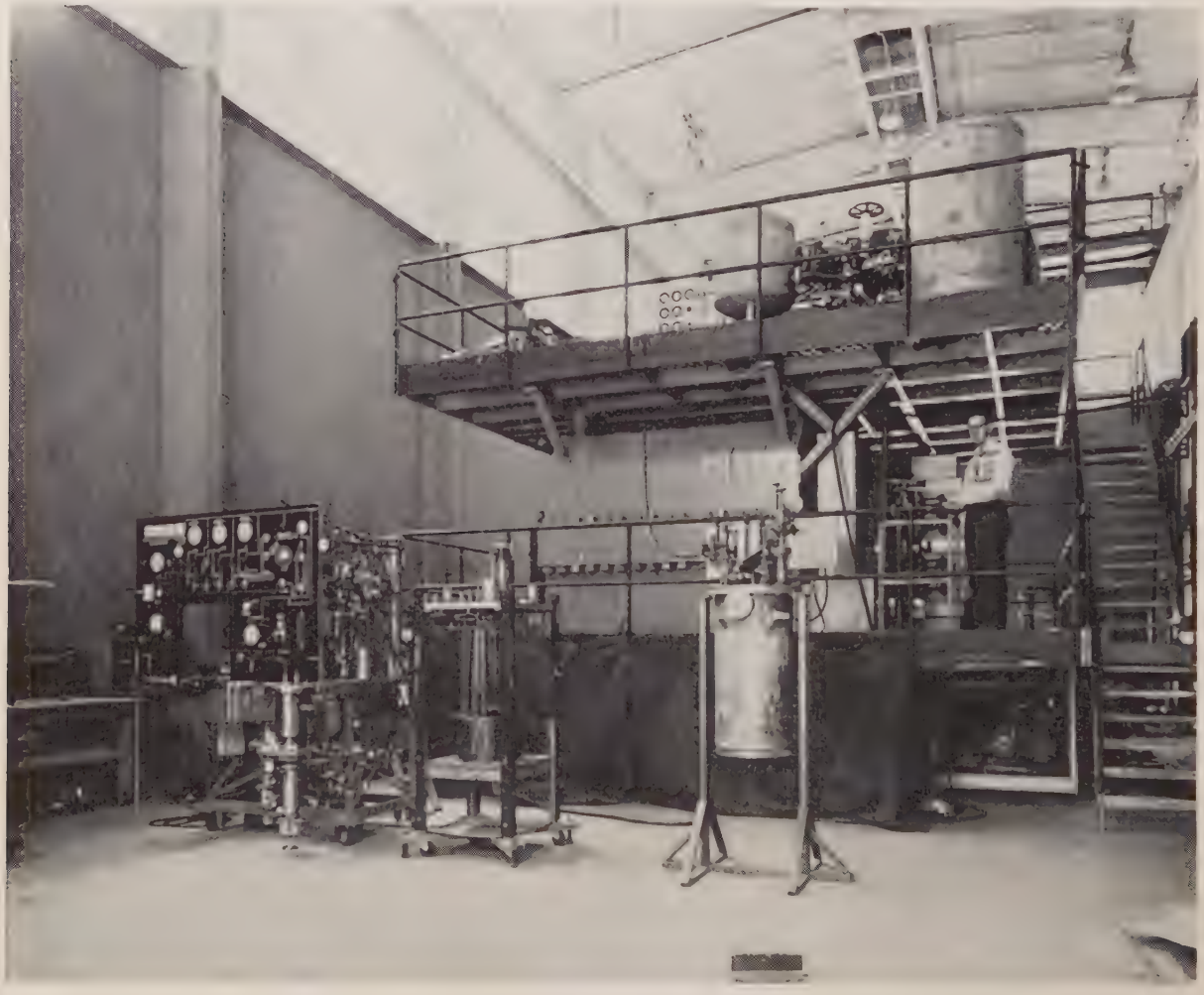

Fig. 12. Photograph of the 183 cm liquid hydrogen bubble chamber at Radiation Laboratory, University of California, Berkeley. For details see the text. (Courtesy of Professor Luis W. Alvarez.)

7. Some Existing and Planned Bubble Chambers

In addition to the already presented bubble chambers some existing or planned bubble chambers are briefly mentioned below. The list

is, however, by no means a complete one, its purpose is just to demonstrate the large interest which the bubble chamber has avoked in the high energy physics laboratories all over the world.

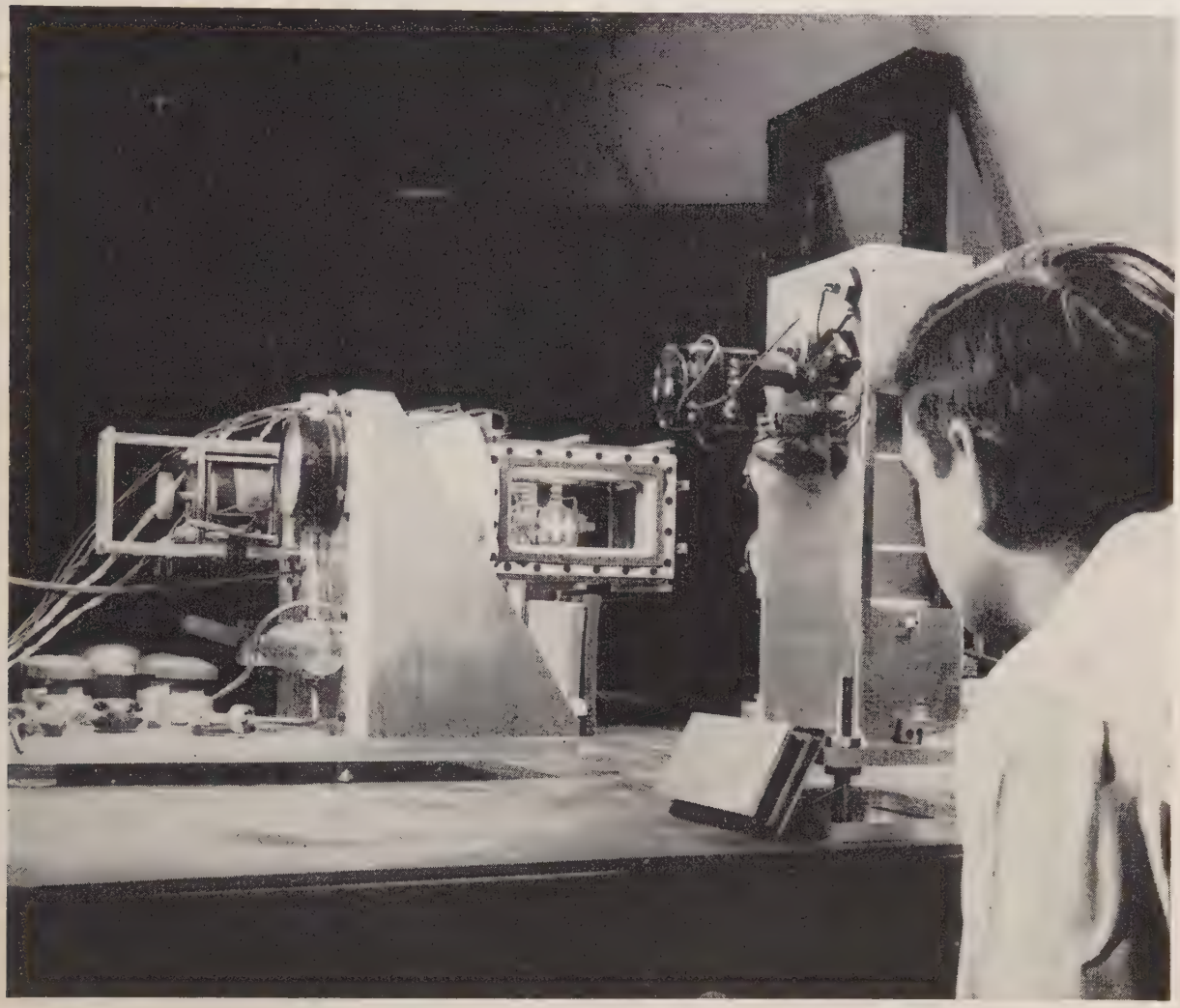

Fig. 13. First chamber ever used for high energy physics, the Glaser 15 × 7.5 cm propane bubble chamber, at that time at Brookhaven. (Courtesy of Professor Donald A. Glaser.)

In the U. K. Dee at the University of Glasgow has built a 25 cm propane bubble chamber, Wilkinson and Shaw at the University of Oxford a small propane and a small liquid hydrogen bubble chamber, respectively. Further, at the University of Birmingham Martelli is in charge of an about 23 cm long propane chamber and Riddiford has a 23 cm diameter liquid hydrogen chamber. At the Imperial College in London Barfor is in charge of a liquid hydrogen 41 cm bubble chamber. At the Liverpool Nuclear Physics Research Laboratory a 1 litre propane[28]) and a 25 cm diameter hydrogen bubble chamber are in operation, the latter in a magnetic field of 12 000 gauss. Two large bubble chambers are being constructed on a national basis. The first one is for liquid hydrogen and will be 152 × 51 × 38 cm in a field of about 10 000 gauss and is being designed by groups from

[28]) Margaret H. Alston, B. Collinge, W. H. Evans, R. W. Newport and P. R. Williams, Phil. Mag. 2 (1957) 820.

Liverpool, Imperial College and Birmingham. The chairman of the project is C. C. Butler, Imperial College. The second one is for propane and a heavy liquid, probably CF_3Br, and is being designed by University College, London (contact Dr. Stannard or Dr. Henderson), and Glasgow. The size is roughly $142 \times 38 \times 38$ cm[29]).

In France also many bubble chambers have been built. Besides the already mentioned chamber by Rogozinski[27]), A. Rousset at the Ecole Polytechnique has made a 5 litre propane bubble chamber for a study of experimental technics, as well as a 20 litre propane-methyl iodide chamber. A 300 litre chamber for a magnetic field of 20 000 gauss is under construction. Gaillard and Basu are in charge of a 20 cm diameter liquid hydrogen bubble chamber in Saclay. Also a 35 cm diameter liquid hydrogen bubble chamber will soon be available. Further, a 50 cm diameter chamber, as well as a 50×80 cm chamber, both for liquid hydrogen, are planned to be made for Saclay. All these chambers will be equipped with magnetic fields.

In addition to the already presented large U.S.A. chambers, it should be mentioned that the size of the Powell[14,30]) group propane bubble chamber is $77.5 \times 54.5 \times 16.5$ cm^3. The propane container is hydrostatically supported in oil through which the chamber is photographed. This permits the use of small glass windows with a large safety factor. (The idea of hydrostatic support for high-pressure cloud chambers is due to Johnson *et al.*)

A 10 cm diameter and a 30 cm diameter hydrogen bubble chamber have been built at CERN, of course for use in connection with the 600 MeV proton synchrotron and also for the big 25 GeV accelerator, when it is ready. The latter bubble chamber will be placed in a 15 000 gauss magnetic field[31]). A larger hydrogen bubble chamber 2 m long is planned.

A rectangular propane bubble chamber, the inner dimensions of which are $16 \times 6.5 \times 7.2$ cm is described by Kotenko, Popov and Kusnetsov[32]) at the Lebedev Physics Institute, U.S.S.R., and a $27 \times 9.5 \times 6$ cm^3 propane bubble chamber is presented by Pershin[33]) at the United Institute of Nuclear Studies, U.S.S.R.

At the time when this article was in print Professor Donald Glaser at the University of Michigan has kindly sent to the author a

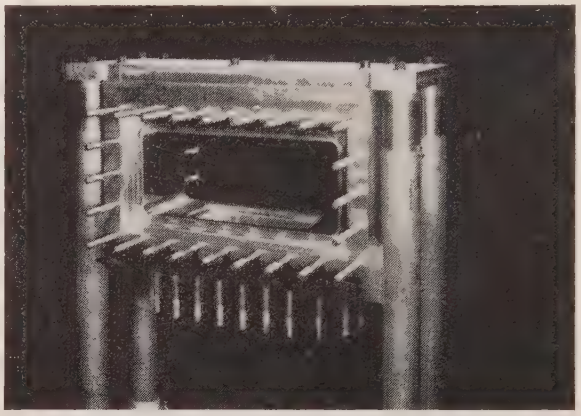

Fig. 14. The Glaser 30 cm propane chamber. (Courtesy of Professor Donald A. Glaser.)

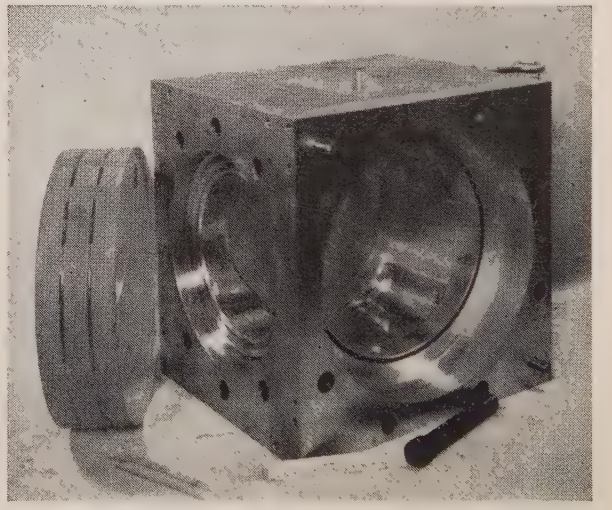

Fig. 15. Glaser's 30 cm diameter liquid xenon bubble chamber, 25 cm deep, disassembled. (Courtesy of Professor Donald A. Glaser.)

[29]) The above information concerning bubble chambers in the United Kingdom was kindly given by Dr. W. H. Evans, Univ. of Liverpool, Nuclear Physics Research Laboratory.

[30]) W. M. Powell, W. B. Fowler and L. O. Oswald, Rev. Sci. Inst. **29** (1958) 874.

[31]) European Organization for Nuclear Research, Annual Report 1957, CERN.

[32]) L. P. Kotenko, Ju. S. Popov and E. P. Kusnetsov, Pribory Tech. Exp. (Instr. and Meas. Engg.) **1** (1957) 36.

[33]) I. I. Pershin, Pribory Tech. Exp. (Instr. and Meas. Engg.) **1** (1957) 39.

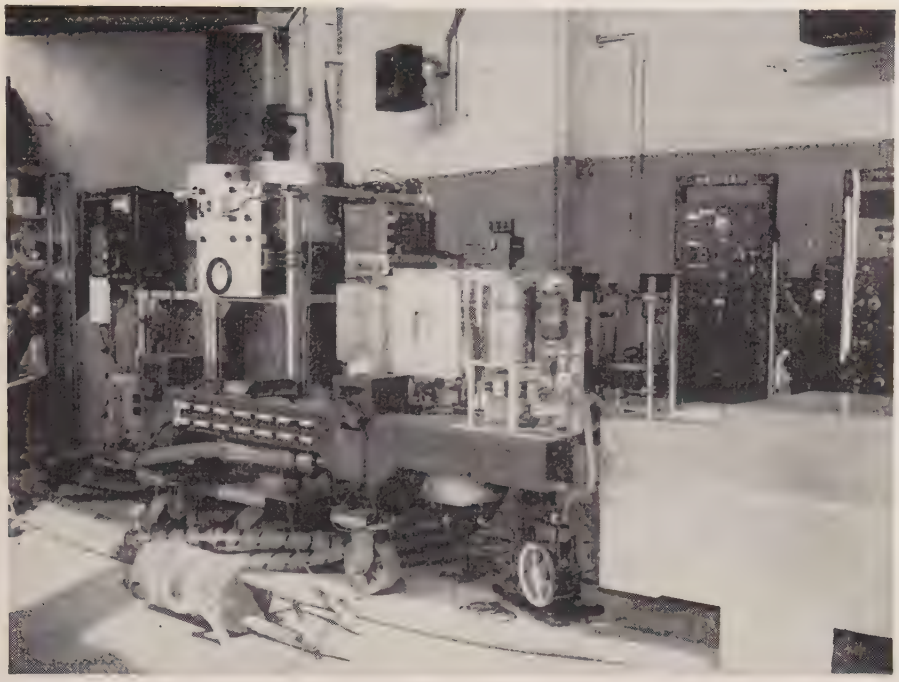

Fig. 16. Glaser's 30 cm diameter liquid xenon bubble chamber, assembled with most of its associated apparatus ready for use at the Bevatron in 1958. (Courtesy of Professor Donald A. Glaser.)

Fig. 17. Photograph taken with a carbon dioxide-propane mixture at 29.8 atm equilibrium pressure in the 1 litre bubble chamber of the Genoa group. A penetrating particle is crossing the chamber. In addition tracks of electrons are produced by the gamma-ray beam of the 31 MeV Betatron at the University of Turin (P. E. Argan, A. Gigli, E. Picasso, G. Tomasini and L. Gonella, Recent Developments in Gas Bubble Chamber Technique, Sept. 1957, Padua-Venice conference). (Courtesy of Professor Alberto Gigli.)

photograph of the first bubble chamber set-up ever used for making strange particles. The set-up includes a 15 cm propane chamber and its associated equipment without the temperature control apparatus (fig. 13). A picture of Glaser's 30 cm propane chamber (fig. 14) and the 21 litre liquid xenon bubble chamber disassembled (fig. 15) and assembled with most of its associated apparatus ready for use at the Bevatron, where the Glaser group did experiments last summer, is also shown (fig. 16). Finally, one of the photographs of the 160 000 taken, provides a rather dramatic direct proof for the neutral decay mode of the θ^0-meson (fig. 23).

A lot of information was likewise obtained from Prof. Alberto Gigli at the University of Genoa. The above-mentioned (§ 3) gas bubble chambers have been extensively developed by Gigli and his group. The characteristics of the liquid-gas solution systems, methane-propane, ethylene-propane, and ethane-propane have been investigated. The third system has proved to be the most advantageous†. A 100 litre liquid-gas solution bubble chamber is now being constructed for experiments with the Frascati 1 GeV electron-synchroton.

A rectangular propane or trifluoromonobromomethane (CF_3Br) bubble chamber, the inner dimensions of which are $50 \times 25 \times 12$ cm has been built at the Physikalisches Institut der Rheinisch-Westfälischen Technischen Hochschule Aachen (Head Prof. Dr.-Ing. W. Fucks) by M. Deutschmann and his group. A small 0.5 litre chamber for experimental studies was first constructed. Horlitz and Brandt at the Physikalisches Institut der Universität Bonn (Head Prof. Dr. W. Paul) have designed an 1 litre pentane chamber. All these German bubble chambers will be used in connection with the 500 MeV electron synchrotron by Paul and his coworkers (Schlier, Brandt, Wucherer).

H. M. Mayer and D. Lüers at the Max-Planck-Institut für Physik in Munich have constructed a 96 mm diameter propane or trifluorobromomethane bubble chamber to be used by K. Gottstein and his team in connection with the betatron at the Würzburg University (Kulenkampff and Scheer). A larger chamber is planned. Andelfinger at the Laboratorium für Technische Physik, Technische Hochschule, Munich, has studied different expansion systems ("slow system"—magnetic valve, $dp/dt = 7.5 \times 10^3$ atm/sec, and "fast system"—exploding diaphragm, $dp/dt = 2.5 \times 10^5$ atm/sec) in a small, rectangular 35 cm³ propane bubble chamber.

T. Johansson at the University of Lund, Sweden, has built a 50 mm diameter bubble chamber, which has operated with different liquids, such as propane, freon 12, freon 13 B1 or a mixture of 30% CO_2 and 70% propane. SF_6 (density 1.8 g/cm³) will be tried. A larger bubble chamber for propane and equipped with a magnetic field is planned for work with the electron synchrotron now being erected.

8. Use of the Bubble Chamber

It was already mentioned, that the bubble chamber is best suited for experiments in conjunction with high energy accelerators. These have a pulsed beam, and the well-known times for the arrivals of the particle beams in the bubble chambers can be combined with the short sensitive time of the chambers. At the same time the bubble chamber has a high stopping power for high-energy charged particles and gives therefore possibilities for a study of the interaction between the incident particles (for instance protons, mesons, neutrons, gamma-quanta) and the nuclei in the bubble chamber or for a study of the decay of elementary particles.

In the annual report 1957 of CERN[31]) a list of typical experiments in connection with bubble chambers is given:

(1) π–p-interactions
  (a) Total and differential cross section
  (b) Production of hyperon pairs
  (c) Decay modes of anti-hyperons
(2) Scattering of K^+-mesons against protons

† P. E. Argan, A. Gigli, E. Picasso, G. Tomasini, and L. Gonella, Remarks about Gas Bubble Chamber Characteristics, Sept. 1958, Geneva conference.

(3) Diffractive production of π by protons on nuclei
(4) Proton-antiproton interactions.

A team of scientists[34]) have used the 82-MeV positive pions from the University of Chicago synchrocyclotron and a 15.2 cm diameter propane bubble chamber for a study of the angular asymmetry of low-energy positrons from the decay of polarized muons coming to rest in the propane. About 60 000 stereo-photographs were obtained with an average of 7 events $\pi^+ \to \mu^+ \to e^+$ per picture.

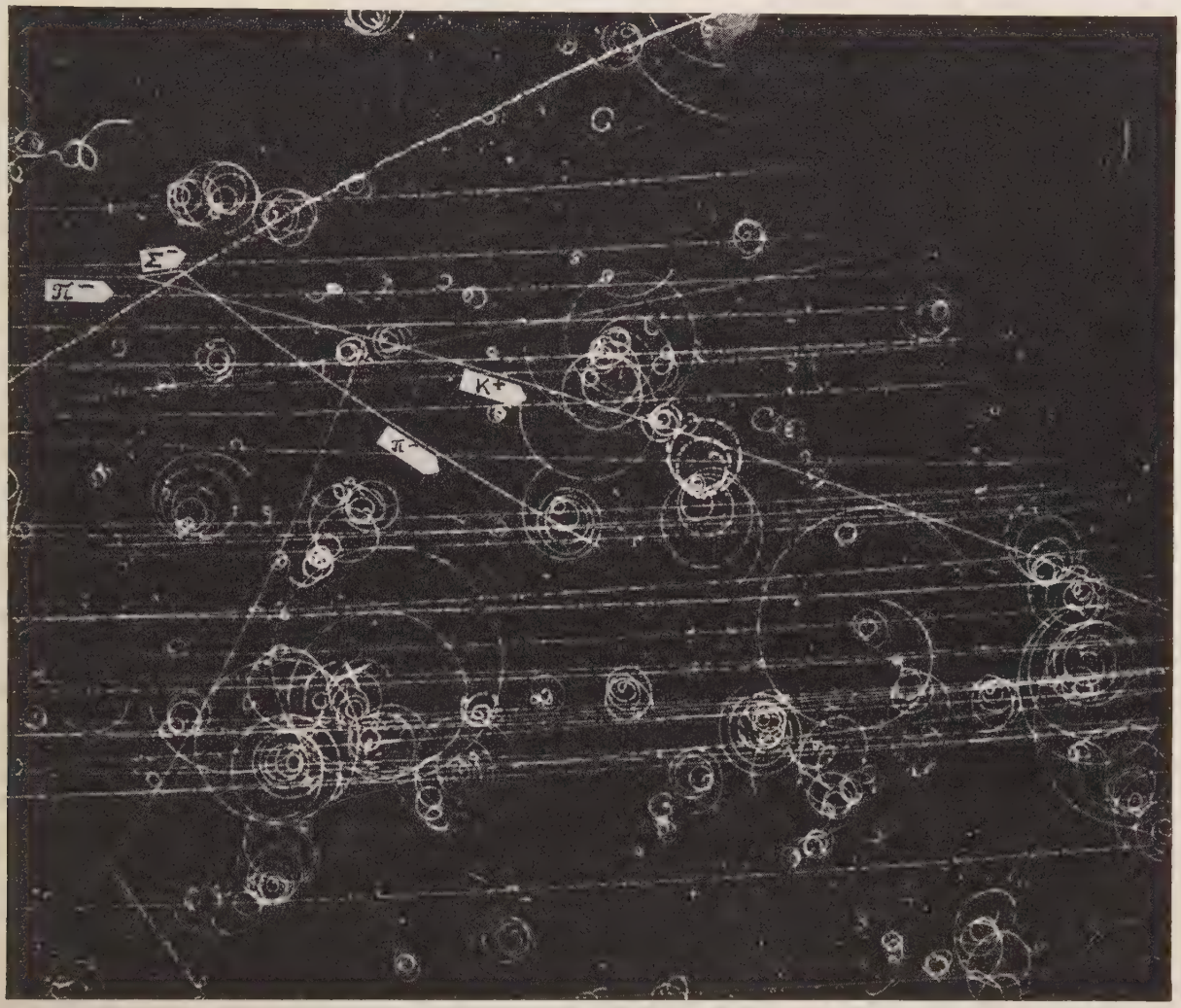

Fig. 18. A π^--meson enters from the left and interacts with a proton, creating a Σ^--hyperon and a K^+ (also called τ^+)-meson. The Σ^--hyperon decays to a π^--meson and a neutron. The neutron gives no visible track. The arrows, which indicate the nature of the particles and the direction of movement, are placed immediately to the right of the tracks, except for Σ^-, where the arrow is to the left of the track (above it in the figure). The event was photographed by the Steinberger group, Columbia University. (Courtesy of Professor R. J. Plano.)

The same $\pi^+ \to \mu^+ \to e^+$ decay was also studied by the Liverpool group[28]) and by Balandin *et al.*[35]) in their $16 \times 16 \times 4.5$ cm^3 propane bubble chamber.

Figs. 18, 19, 20 and 21 show some typical

[34]) I. A. Pless, A. E. Brenner, R. W. Williams, R. Bizzarri, R. H. Hildebrand, R. H. Milburn, A. M. Shapiro, K. Strauch, J. C. Street and L. A. Yong, Phys. Rev. **108** (1957) 159.

[35]) M. P. Balandin, U. A. Moiseyenko, A. I. Mukhin and S. Z. Otvinovsky, J. Exp. Teor. Fys. (Russian) **36** (1959) 424.

meson reactions photographed at Columbia University and Berkeley and placed at the author's disposal by the courtesy of Professors Steinberger and Plano (figs. 18 and 19) and Professor Alvarez (figs. 20 and 21).

Fig. 18 gives an example of a reaction between an incident π^--meson of 960 MeV energy and a proton in the hydrogen bubble chamber,

$$\pi^- + \mathrm{p} \rightarrow \Sigma^- + \mathrm{K}^+ ,$$

and besides the created Σ^--hyperon decays in a π^--meson and a neutron. The latter particle has no charge and accordingly gives no track.

Fig. 19 shows another reaction of an incident π^--meson (960 MeV) and a proton,

$$\pi^- + \mathrm{p} \rightarrow \Lambda^0 + \theta^0 .$$

The created hyperon Λ^0 and the K-meson θ^0 are both uncharged and do not show any visible tracks. However, the life-time for the particles is so small (about 3×10^{-10} sec), that they decay in the bubble chamber according to

$$\Lambda^0 \rightarrow \mathrm{p} + \pi^-$$
$$\theta^0 \rightarrow \pi^+ + \pi^- .$$

All these new particles give visible tracks. It is seen, that the π^--mesons give thinner tracks

Fig. 19. A π^--meson enters from the left and interacts with a proton in a point, where the corresponding track vanishes, creating two neutral particles, a Σ°-hyperon and a θ° (also called K°)-meson, which give no visible tracks. After about 3×10^{-10} sec these particles decay according to $\Lambda^\circ \rightarrow \mathrm{p} + \pi^-$, $\theta^\circ \rightarrow \pi^+ + \pi^-$, by which two $<$ -shoped figures appear in the bubble chamber. The event was photographed by the Steinberger group. (Courtesy of Professor R. J. Plano.)

than the proton, and that the negative mesons are deflected to the left, while the positive meson and the proton are deflected to the right.

Fig. 20 shows an analogous case obtained at Berkeley by Alvarez *et al.*

Fig. 21, also from Berkeley, corresponds to the first case (fig. 18), but in this case also the

In a similar way Brown, Glaser and Perl[36]) investigated the production of strange particles by 1.1 GeV kinetic energy π^--mesons penetrating a 30 cm propane bubble chamber.

The $\pi^+ \rightarrow \mu^+ \rightarrow e^+$ decays have been investigated by Barmin *et al.*[37]), using Pershin's[33]) propane bubble chamber, and Alikhanian *et al.*[38]),

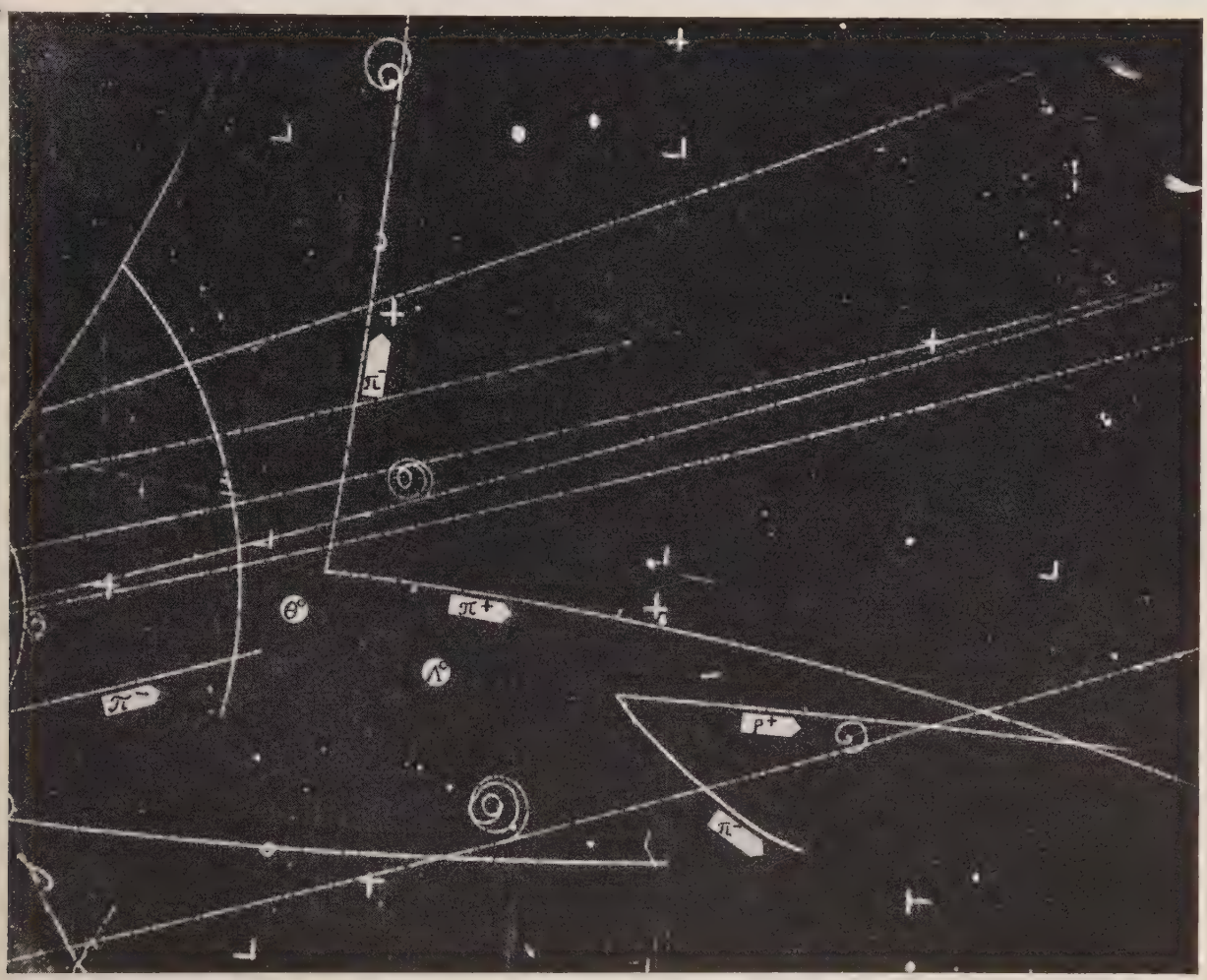

Fig. 20. This event is analogous to the event in fig. 19 and was photographed by the Berkeley group, Radiation Laboratory, University of California. (Courtesy of Professor Alvarez.)

K^+-meson decays,

$$K^+ \rightarrow \pi^+ + \pi^+ + \pi^- \ .$$

(The K^+-meson is also denoted τ^+.)

making use of the chamber described by Kotenko *et al.*[32]). Wang Kan-Chang *et al.*[39]) in-

[36]) J. L. Brown, D. A. Glaser and M. L. Perl, Phys. Rev. **108** (1957) 1036.

[37]) V. V. Barmin, V. P. Kanavets, B. V. Morozov and I. I. Pershin, Soviet Physics JETP **34** (7) (1958) 573; J. Exp. Theor. Phys. (U.S.S.R.) **34** (1958) 830.

[38]) A. I. Alikhanian, V. G. Kirillov-Urgiumov, L. P. Kotenko, E. P. Kuznetzov and Ju. S. Popov, Soviet Physics JETP **34** (7) (1958) 763; J. Exp. Theor. Phys. (U.S.S.R.) **34** (1958) 1101.

[39]) Wang Kan-Chang, Wang Tso-Tsiang, Ding Da-Tsao, L. N. Dubrovsky, E. K. Kladnitskaya and M. I. Solovyov, J. Exp. Theor. Phys. (U.S.S.R.) **35** (1958) 899.

Fig. 21. This event, observed by the Alvarez group in Berkeley, starts in a way analogous to that in fig. 18. However, here also the K^+-meson decays according to $K^+ \rightarrow \pi^+ + \pi^+ + \pi^-$. As in fig. 18, the Σ^--track is very short (here shorter than the arrow). (Courtesy of Professor Luis W. Alvarez.)

vestigated the interaction between 250–270 MeV π^+-mesons and carbon nuclei with aid of a propane bubble chamber (diam. 11 cm, depth 5.5 cm).

Whitehead *et al.*[40]) studied the charge exchange scattering of positive K-mesons in the $76 \times 46 \times 16.5$ cm^3 propane bubble chamber by Powell *et al.*[30, 41]).

Nordin *et al.*[42]) have scanned 10 000 K^--interactions observed in the Berkeley liquid hydrogen bubble chamber, identifying 45 charge-

[40]) M. N. Whitehead, R. W. Birge, W. B. Fowler, R. E. Lanou and W. M. Powell, Bull. Am. Phys. Soc., Series **2**, 3 (1958) 24.

[41]) W. M. Powell, W. B. Fowler and L. Oswald, Bull. Am. Phys. Soc., Series **2**, 3 (1958) 58.

[42]) P. Nordin, A. Rosenfeld, F. Solmitz, R. Tripp and M. Watson, Bull. Am. Phys. Soc., Series **2**, 4, No. 1 (1959) 24.

exchange scatters in which the K^0 subsequently decays via $K_1^0 \rightarrow \pi^+ + \pi^-$.

Leitner *et al.*[43]) used the Duke University liquid helium bubble chamber for the study of the absorption in helium of low-energy K^--mesons from the Berkeley Bevatron. The chamber was situated in a magnetic field of

Fig. 22. A case of antiproton-proton charge exchange, $\bar{p} + p \rightarrow \bar{n} + n$, observed by the Powell[40]) group in Berkeley. The antiproton enters from the top of the figure and disappears abruptly at a point indicated by an arrow. The antineutron and the neutron give no tracks, but the antineutron is annihilated in the lower part of the figure according to $\bar{n} + p \rightarrow 3\pi^+ + 2\pi^-$, which gives a 5-prong star with an energy release of 1500 MeV. (Courtesy of Professor W. Powell, Professor L. Agnew, and of the University of California, Radiation Laboratory.)

14 300 gauss. In about 90 000 pictures 9000 K^--mesons were observed of which about 2500 were stopped in the chamber. Preliminary evidence was found for the excistence of a ${}_{\Lambda}He^4$ hyperfragment.

Finally fig. 22 shows a case of antiproton-proton charge exchange, observed by the Powell-group[30,44]) in the large propane bubble chamber[36,37]) in Berkeley. At the end of the antiproton track the charge exchange process $\bar{p} + p \rightarrow \bar{n} + n$ takes place. In the lower part of the figure the antineutron is annihilated with a proton according to $\bar{n} + p \rightarrow 3\pi^+ + 2\pi^-$ (tentative). The bubble chamber was connected to the Bevatron, and a system of counters indicated when an antiproton entered the bubble chamber, triggering the flash-lamps for photographing only when an antiproton entered. Of course the chamber had to be expanded for every Bevatron pulse.

The Steinberger group at Brookhaven National Laboratory has in collaboration with two Italian groups from Bologna and Pisa[45]) made a study of the total and differential cross-sections for the reactions

$$\pi^- + p \rightarrow \begin{cases} \Lambda^0 + \theta^0 \\ \Sigma^0 + \theta^0 \\ \Sigma^0 + K^+ \end{cases}$$

at 910, 960, 1200 and 1300 MeV using hydrogen and propane bubble chambers in a magnetic field of 13 400 gauss.

9. Measuring of Bubble Chamber Tracks

Measuring of the position of a track relative to certain reference points at the bottom of the chamber can be made with such precision that the deviations in repeated measurements do not exceed about 5 microns in the original space[6]). Owing to the short time between the appearance and the photographing of a track, an observable convection of the liquid does not occur. However, a disturbance depending on optical inhomogeneities caused by temperature differences in the liquid does take place.

It is not customary to reproject the film tracks on adjustable screens in order to measure the size and the orientation of the tracks in

[43]) J. Leitner, E. M. Harth, M. M. Block, B. Bruckner, I. Hughes, T. Kikuchi, C. Meltzer, A. Pevsner, F. Anderson and H. Cohn, Bull. Am. Phys. Soc., Series 2, 4 (1959) 25.

[44]) L. Agnew, T. Elioff, W. B. Fowler, L. Gilly, R. Lander, L. Oswald, W. Powell, E. Segrè, H. Steiner, H. White, C. Wiegand and T. Ypsilantis, Phys. Rev. **110** (1958) 994.

[45]) F. Eisler, R. Plano, A. Prodell, N. Samios, M. Schwartz, J. Steinberger, and P. Bassi, V. Borelli, G. Puppi, H. Tanaka, P. Waloschek, V. Zoboli, and M. Conversi, P. Franzini, I. Mannelli, R. Santangelo, V. Silvestrini, Nuovo Cimento **10**, Serie X (1958) 468.

space, as in the case for cloud chambers[46]). The reason for this is of course, that it would here be necessary to adjust these screens in the liquid of the bubble chamber or at least in a liquid of the same refractive index, which in any case would be inconvenient. In addition, the method is too slow, considering the large number of photographs which have to be treated. Instead, it is preferred to make measurements on the film itself in combination with an analytical treatment in computing machines (compare the next paragraph).

It is of interest to get the velocity βc of the particles, c being the velocity of light in cm/sec and β the ratio of the velocities of the particles and that of light. The velocity βc is found from the Coulomb scattering, expressed as the average excursion "Sagitta" δS_s of the midpoint of a track segment from a chord joining its ends. If l be the length in cm of the segment, λ the radiation length (= the thickness of a material, which diminishes the particle energy to 1/e of the incident energy value) in cm and p the momentum in MeV/c, we have[6])

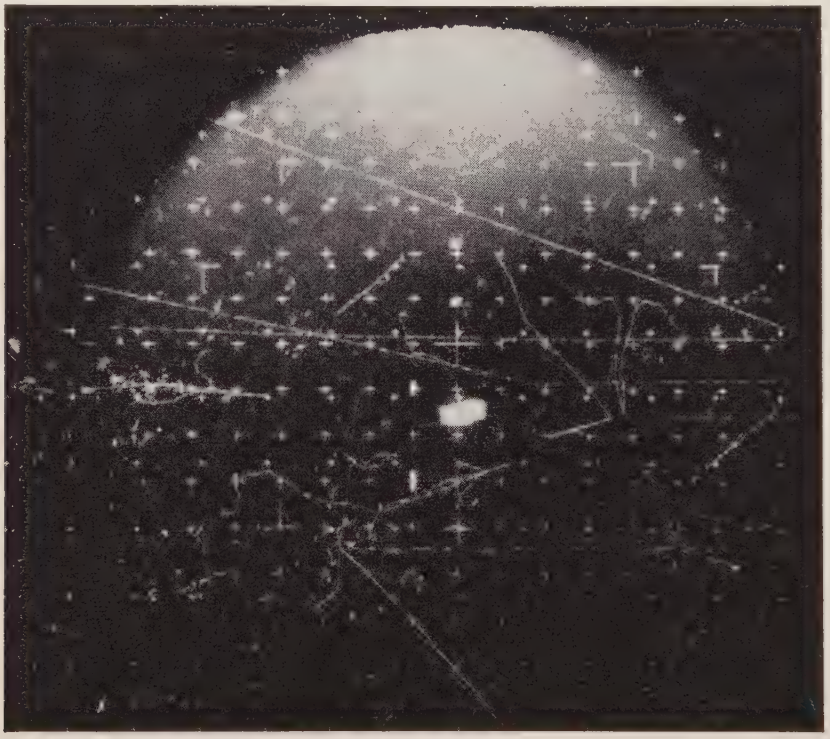

Fig. 23. Photograph No. 61 724, one of the 160 000 which were taken with the Glaser 30 cm diameter liquid xenon bubble chamber at the Bevatron in 1958. An 1.1 GeV π-meson enters from the right and interacts with a proton in the xenon chamber according to

$$\begin{array}{l} \pi^- + \mathrm{p} \rightarrow \Lambda^0 + \theta^0 \\ \qquad\quad \swarrow \qquad\quad \downarrow \\ \pi^- + \mathrm{p} \qquad 2\,\pi^0 \\ \qquad\quad\quad\quad\ \downarrow \\ \qquad\quad\quad\quad 4\,\gamma \rightarrow \ 4 \text{ electron showers,} \end{array}$$

thus giving evidence for the neutral decay mode of the θ^0-meson. (Courtesy of Professor Donald A. Glaser.)

$$\delta S_s = \frac{2.14}{p\beta c} \cdot \frac{l^{\frac{3}{2}}}{\lambda^{\frac{1}{2}}} . \qquad (4)$$

In a similar way it is possible to measure the magnetic deviation δS_H in a field-strength of H gauss,

$$\delta S_H = 3.75 \times 10^{-5} \frac{l^2 H}{pc} . \qquad (5)$$

The number of bubbles b per cm of a track

[46]) See, for instance, W. B. Fowler, R. P. Shutt, A. M. Thorndike and W. L. Whittemore, Rev. Sci. Inst. **25** (1954) 996.

depends also on the velocity. Glaser *et al.*[47]) give the following formula

$$b = \frac{A}{\beta^2} + B(T)\,, \qquad (6)$$

where $A = 9.2 \pm 0.2$ bubbles/cm for propane and B depends on the temperature.

10. Identification of Particles by Means of Machines

Regarding fig. 19, one might ask why the interpretation $\Lambda^0 \to p + \pi^-$ for the upper, $\prec$-shaped track pair is correct. Why not $\theta^0 \to \pi^+ + \pi^-$ for this event and the former interpretation for the other $\prec$-shaped track pairs?

Such an investigation is conveniently made by means of machines, as is the case, for instance, in Berkeley. This method was presented at the USA-department of the scientific exhibition in connection with the International Conference on the Peaceful Uses of Atomic Energy, Geneva 1958. The films were scanned on a projector screen in order to determine approximate 3-dimensional positions of the tracks in the chamber[48]). Interesting events were measured on a "Frankenstein" precision measuring engine. Fig. 24 shows diagrammatically such an interesting event: The track 1 is a π^--meson of 1 GeV energy. At A the meson interacts with a proton in the bubble chamber and produces two neutral particles, which give no visible tracks. At B one of these neutral tracks decays to a positive and a negative particle (3 and 4, respectively, in fig. 24). When these tracks are followed by an index on a screen, on which the tracks are projected (magnification = 30), an electronic device centers a measuring device automatically on these tracks and records the coordinates of these simultaneously on punched cards while the index is in motion. The punched cards for both of the stereoscopic pictures are then, together with "HYDRO", an instruction program, fed through an IBM 650 computing machine in order to obtain the spatial coordinates for a series of points on the paths of the particles. In addition to the position and the direction of the tracks the machine gives the momenta and certain auxiliary quantities. The nature of the neutral particle 2, which decays to 3 and 4 (fig. 18), is

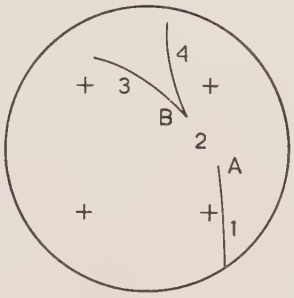

Fig. 24. "Frankensketch", an example demonstrating the identification of nuclear particle tracks by means of the machine "Frankenstein", shown at the scientific exhibit of the USA at the "Second International Conference on the Peaceful Uses of Atomic Energy", Geneva 1–13 Sept. 1958. For details see the text.

tested in another computation "COPLAN". This calculation decides if the directions and momenta computed according to "HYDRO" for 2, 3 and 4 satisfies the equations for the conservation of momentum and energy for one of the possible reactions

$$\Lambda^0 \to p + \pi^- \qquad \text{or} \qquad \theta^0 \to \pi^+ + \pi^-\,.$$

The machine gives a quantity, which is a measure of the probability of the suggested reaction, as well as the momentum for the neutral particle. In the case discussed the result was that the figuration in fig. 24 was formed rather by the decay of a Λ^0-hyperon than by the decay of a θ^0-meson.

An "International Meeting on Instruments for the Evaluation of Photographs"[49]) was held at Geneva on 15–16 Sept. 1958. The Director General, Professor Bakker, stressed the necessity for developing automatic methods of measuring track chamber photographs if physicists are to keep up with the increasing rate at which such photographs of interesting nuclear events can be produced. The bubble chamber is developing

[47]) D. A. Glaser, D. C. Rahm and C. Dodd, Phys. Rev. **102** (1956) 1653.

[48]) A Guide to the Scientific Exhibit of the United States of America (1958) 17.

[49]) CERN 58-24, Scientific and Technical Services Division, 1st October (1958) 5534/e/p.

extensively, and, under the direction of Drs. Kowarsky and Y. Goldschmidt-Clermont, a group (von Dardel and Peyroy) is working on the development of measuring devices and computing methods. Details of the above mentioned "Frankenstein" are given in the summary of the proceedings of the conference[49]). Another meeting, "Precision Instrument for the Evaluation of Photographs"[50]) was held in CERN on February 23, 1959. The aim of this meeting was to decide on specifications for a non-motorised measuring machine to be built commercially, and which would be used by various centers for the measurement of photographs from the CERN, Harwell, and Saclay accelerators†.

11. Designing for Safety in Hydrogen Bubble Chambers

It should be pointed out, that the building of and the work with especially liquid hydrogen bubble chambers is hazardous[51]). The hazards might be failure of the equipment due to overpressure or the uncontrolled escape of hydrogen gas, which may result in an explosion. The overpressure can be created by the boiling of the liquid hydrogen or by the combustion of hydrogen gas. A broken window in the bubble chamber makes the whole liquid superheated and causes a violent boiling. The construction of the bubble chamber must be such that a failure of a glass window does not destroy the limitation of the space which may be occupied by the bubble chamber liquid.

It is not possible here to give a description of all the measures necessary to ensure safety when working with bubble chambers. Detailed precautions against different kinds of hazards are given in the work by Hernandez *et al.*[51]). It might be mentioned, that the whole hydrogen bubble chamber is placed in a vacuum tank, and that the escaping hydrogen is immediately burned outside the laboratory. The building, in which hydrogen is used, should have a vent system for the equipment, good ventilation in the laboratory and no pockets near the ceiling that can trap hydrogen.

In addition to the literature already given above we refer to the review articles by Dodd[52]) and by Gottstein[53]). References are also found in the bubble chamber bibliography by Ogden[54]).

The author would like to thank the following institutions and persons for the permission to reproduce figures and information in quoted articles as well as to publish data obtained by communication:

The American Physical Society (the Physical Review),

The American Institute of Physics (The Review of Scientific Instruments),

University of California, Radiation Laboratory,

Springer-Verlag oHG. Berlin, Göttingen, Heidelberg (Handbuch der Physik, S. Flügge und E. Creutz),

Società Italiana di Fisica (Il Nuovo Cimento),

Professor Donald A. Glaser, University of Michigan, Ann Arbor,

Professor Luis W. Alvarez, University of California, Berkeley,

Professors Douglas Parmentier and Arnold Schwemin, University of California, Berkeley,

Professors J. Steinberger and Richard J. Plano, Columbia University, New York,

Professors Wilson M. Powell and Lewis Agnew, University of California, Berkeley,

Professor A. Rogozinski, Centre d'Études nucléaires de Saclay,

Professor Ralph P. Shutt, Brookhaven National Laboratory, New York,

† See also the "Meeting on the CERN PS Experimental Programme" Geneva, 16 April, 1959, Hydrogen Bubble Chamber Project CERN/PS/EP/11, Propane Bubble Chamber Project CERN/PS/EP/5, IEP Activities CERN/-PS/EP/9.

[50]) CERN (1959) 6317.

[51]) H. P. Hernandez, J. W. Mark and R. D. Watt, Rev. Sci. Inst. **28** (1957) 528.

[52]) C. Dodd, "The Bubble Chamber", Progress in Nuclear Physics, Vol. 5, Editor O. R. Frish (London 1956).

[53]) K. Gottstein, Die Naturwissenshaften **46** (1959) 97.

[54]) B. K. Ogden, "Bubble Chambers", a bibliography, CERN Service d'Information Scientifique, Genève 1959.

[55]) P. Amiot, Nuclear Instruments **3** (1958) 275.

[56]) G. Horlitz und W. Paul, Nuclear Instruments **1** (1957) 340.

Professor W.H.Evans, University of Liverpool, Dr. D. Martin, University of Liverpool,

Dipl.-Ing. C. Andelfinger, Technische Hochschule, München,

Professor Wilhelm Fucks and Dr. Martin Deutschmann, Technische Hochschule, Aachen,

Professor Alberto Gigli, Università di Genova,

Dr. K. Gottstein, Max-Planck-Institut für Physik und Astrophysik, München,

Professor W. Paul and Dr. Chr. Schlier, Universität Bonn,

Professor W. Walcher, Universität Marburg,

Dr. Luisa Zappa, Politecnico di Milano,

Dr. G. Ekspong, University of Uppsala, Sweden.

Professor S. von Friesen and Dr. T. Johansson, University of Lund, Sweden.

NUCLEAR INSTRUMENTS AND METHODS 5 (1959) 26–36; NORTH-HOLLAND PUBLISHING CO.

AN ACCURATE PHOTO-NEUTRON STANDARD

P. C. MARIN†

Laboratoire de l'Ecole Normale Supérieure, 24 rue Lhomond, Paris V, France

Received 9 May 1959

An easily reproducible, RdTh-D_2O, photo-neutron standard has been built. Its calibration is based on the associated charged particle method. We have determined its photo-neutron yield to an accuracy of 1.1%. After calibration, the ionisation current of the RdTh source was compared to the ionisation current of a standard radium source, on a Curie chamber. The yield of any substandard can be determined, apart from small geometrical corrections, by a simple comparison of the RdTh source to the radium standard on the Curie chamber. Background neutrons from (α-n) reactions in the RdTh source contribute to 3% of the total yield. The number of neutrons emitted by the source used has been determined by the recoil proton method, using an ionisation chamber and by chemical integration in a manganese nitrate solution. The total yield of the standard is known to an accuracy of 1.25%.

1. Principle of the Standard

A quasi spherical ionisation chamber, working in electron collection, is filled with very pure heavy hydrogen of known concentration and pressure. A source of RdTh (or Na^{24}), of about 0.5 mC strength, is put in the center of the chamber. If proper care is taken, one succeeds in counting about 95% of the photo-protons produced in the gas. It is obvious that for each photo-proton, a photo-neutron must have been produced. The ionisation chamber with the source in its center, represents therefore a neutron standard. Its yield will be known with an error given by the statistical error in the total number of photo-proton counts and a small error on the correction for incomplete counting mentioned above: altogether not more than 0.5%. However, the total number of neutrons produced by it will be much too small to allow any inter-comparison by existing methods (5 photo-neutrons emitted per second, per mC of RdTh, for a chamber of 2 cm radius filled under 5 atmosphere pressure). Therefore, two steps are taken to arrive at a standard of more suitable intensity:

1. The RdTh (or Na^{24}) source is replaced by a source of higher activity: 50 mC for the final measurements.

2. The heavy hydrogen in the ionisation chamber is replaced by heavy water.

In this way a standard of roughly 10 000 times bigger intensity is obtained. But two problems of inter-comparison are added which will necessarily contribute to the final error with which the yield of the final standard will be known.

a. The change in the number of deuterium atoms per cm^3 when the gas is replaced by heavy water.

b. The intercomparison of the two γ-ray sources. Furthermore, the γ-ray absorption and diffusion in heavy water has to be accounted for.

It was found possible, without undue increase of the total error, to use as a standard, instead of the ionisation chamber, a capsule which was identical to the one used for making the chamber, in all but the fact that it had no electrodes. We show in later section that we can supply other laboratories with standard capsules which can be corrected for geometrical differences to an inaccuracy of only 0.04% in the final neutron yield. The procedure for obtaining this consists in having precision machine produced capsules, filled with heavy water of known purity. As regards the RdTh sources, they can be compared

† Most of the experimental work described below, has been done in the Clarendon Laboratory, Oxford.

on our Curie chamber, to an accuracy better than 0.1%. It would of course be more convenient to distribute simply the containers filled with heavy water and let other laboratories get their RdTh source intercompared with radium standards by the various competent national institutions. However, this procedure would notably increase the uncertainty on the yield of the substandards since international radium standards are not known to better than 1%. This error could be decreased to less than 0.1% by an intercomparison of radium standards. However, a few tenths of a percent must be added to take into account the variation of the ratio I_{RdTh}/I_{Ra} from one Curie chamber to another.

The background neutrons emitted by the RdTh source are the most disturbing feature of this standard. We believe that this neutron emission is not a primary phenomenon but is due to the interaction of the α-rays with impurities. It has not, so far, been possible to prepare the source in a way to make this neutron background reproducible. It varies from source to source and has to be determined in a way that we shall discuss later.

The uncertainty on the background neutrons can be reduced to less than 0.15%. If Na^{24} is used the problem of the background neutrons disappears. On the other hand, the work has to be done with a source of 15 hours period. This involves frequent new standardisations on the Curie chamber.

2. The D_2O Capsule

The standard (fig. 1) is made of two half spheres of 2 cm radius separated by a partition of about 6 mm thickness. The RdTh source can be introduced in the center of the chamber in a little hole, 3 mm diameter. The spheres have been tool-pressed to make separate assembled standards as identical as possible. The metal used for both the spheres and the partition was "Heat Treatable High Strength Alloy" for its good mechanical properties. The assembly of the two half spheres and of the partition was done with Araldite type 1. About 33.5 g of heavy water are needed to fill up the chamber. Filling up the capsule has to be done in a dry atmosphere to avoid exchange between D_2O and the ordinary water vapor. The two half spheres once filled up are plugged with small rubber corks. After introducing the RdTh source in the center of the capsule, the remaining

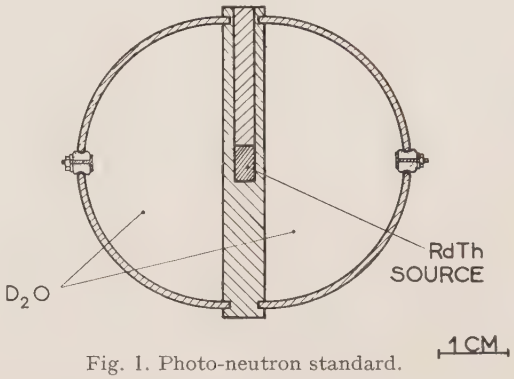

Fig. 1. Photo-neutron standard.

hole in the partition is plugged with an aluminium rod. In this way absorption and dispersion of the γ-rays are regularized.

The reproducibility of the standard can be affected by small geometrical differences:

1. In the dimensions of the capsule. The correction to apply for small changes in the sensitive volume is straighforward and can be done to an accuracy of 0.01%. The correction to apply for a small change Δd, in the partition thickness, is $-2.16\,\Delta d/r$ (r radius of the hemisphere), the residual uncertainty resulting from it being less than 0.03%.

2. In the distribution of the radioactive powder inside the source container. We have estimated to 0.1% the maximum variation of the yield from one standard to another due to these changes. This we have done by looking at the source with a G.M. counter through a lead collimator of 0.5 mm diameter.

3. In the thickness of the walls of the source container (irridiated platinum). These do not alter in the same way the ratio of the ionisation currents on the Curie chamber and the photo-neutron yields of the standards. Measurements of the dimensions of the containers of the two sources used and of their weight point out to a correction of $0.025 \pm 0.01\%$.

Table 1 summarizes the various uncertainties arising from these corrections:

TABLE 1

Corrections	$\Delta Y/Y$
Thickness of the partition	0.03%
Sensitive volume of the capsule	0.01%
Distribution of the radioactive powder in the source container	0.10%
Thickness of the sourse container	0.01%
Total	0.15%

3. γ-Ray Absorption and Diffusion in D_2O

Absorption and diffusion of the 2.62 MeV γ-rays in D_2O has two effects:

1. Due to pair production and Compton effect, a decrease of $4.56\% \pm 0.02\%$, occurs in the number of photo-neutrons of average energy 196 keV produced.

2. Due to the degraded γ-rays, a small number of photo-neutrons ($0.35 \pm 0.013\%$) of energy ranging from 0 to 196 keV are emitted.

Altogether the decrease of the photo-neutron yield due to absorption and diffusion of the 2.62 MeV γ-rays in D_2O is $4.21 \pm 0.03\%$.

4. The Photo-Proton Chamber

4.1. DESCRIPTION AND USE

Counting of the photo-proton pulses is the most difficult part in the calibration of our standard. Due to positive ion effect and to wall effect, the shape of the pulse height distribution from the photo-protons, depends strongly upon the geometry of the ionisation chamber. The geometry of the chamber should be chosen so as to reduce to a minimum the loss of counts due to these two effects. After several trials with chamber geometries of various kinds, we have fixed our choice upon the type shown on fig. 2.

The ionisation chamber uses a capsule identical to the one employed in the final neutron standard. However, two small cylindrical electrodes, 1 mm diameter, have been introduced in the capsule in order to collect the ionisation produced by the photo-protons (the correction for the small decrease of sensitive volume is only 0.1%). These electrodes are held by two kovar-glass seals with guard rings soldered on brass cylinders, which are araldited on the capsule. Pumping and filling is done through two copper tubes soldered on to the brass cylinders.

A negative high tension (3500 volt) is applied on the capsule. The collection electrode is connected to the grid of the first preamplifier valve and the guard ring grounded to avoid breakdown pulses in the collection electrode.

After degassing and pumping at 120° for several days, the photo-proton chamber is filled under 5 atm with deuterium prepared by a method described by R. Wilson *et al.*[1]). In order to achieve an electron capture less than 1%, with a filling of 10 atm and a collecting voltage of 3500 volt, the oxygen concentration should be less than 10^{-6} according to Wilkinson[2]). In fact, this concentration seems to be even more dangerous as is shown by Wilson *et al.*[1]).

After amplification the pulses are sent in a

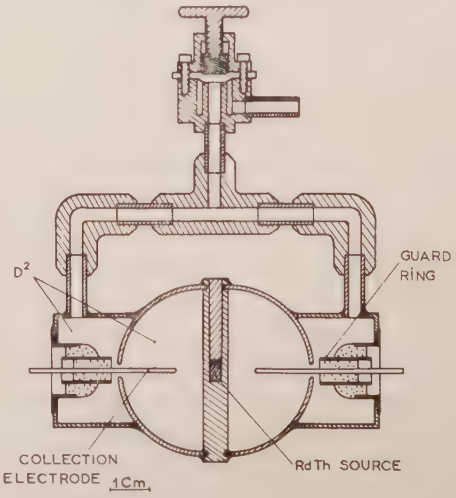

Fig. 2. Photo-proton chamber.

25 channel kicksorter and a scaler with an adjustable bias. In order to increase the signal to noise ratio, we have reduced as much as

[1]) R. Wilson, L. Beghian, C. H. Collie, H. Halban and G. R. Bishop, Rev. Scient. Instr. **21** (1951) 699.

[2]) D. H. Wilkinson, Ionisation Chambers and Counters, p. 42.

possible the input capacitance (9 pF). The input valve (6AK5) was selected amongst a set of valves of the same type for its small grid noise and the grid leak resistor was about 500 MΩ. The values of the time constants (0.8 μsec) were chosen so as to achieve the best signal-to-noise and electron pulses ratio.

The pulse height distribution (fig. 6) shows a clearly resolved photo-proton line due to the 2.615 MeV γ-rays. The photo-proton spectrum due to the momentum of the incident γ-ray is also indicated in broken line. The pulse height distribution shows a tail on the low energy side of the photo-proton line. The tail on the high energy side up to 250 keV is due to piling-up of pulses from secondary electrons. Careful evaluation of the loss of counts below 112.5 keV is done in § 4.2 and 4.3. The validity of the correction applied has been checked by comparing, in the energy interval between 111 and 140 keV, the theoretical and the experimental distributions of pulses.

4.2. CORRECTIONS FOR POSITIVE ION EFFECT

For the 196 keV photo-protons the pulse loss resulting from positive ion effect is relatively small with the actual geometry of the chamber, since the RdTh source is rather remote from the region of fast variation of the potential. However, a precise calculation of the influence of this effect on the pulse height distribution has been done. Shockley's theorem[3]) gives for the pulse induced on the collecting electrode by the movement of a charge q, the following expression

$$u(t) = \frac{q}{c} \frac{V(t) - V(0)}{V_c - V_e} \qquad (1)$$

where $V(t)$ and $V(0)$ are the potentials of the equipotential surfaces on which one finds the charge q at time t and at time 0. V_c and V_e are the potential of the collection and external electrodes.

In order to calculate the pulse height distribution resulting from the positive ion effect, we have drawn the equipotential surfaces in the chamber by the electrolytic bath method. This was done by using a model homothetic of our chamber in a ration 10/1. Fig. 3 shows the distribution of the equipotential surfaces. The pulse height distribution at the output of the amplifier was then calculated with the approximation of monokinetic photo-protons of zero range in the following way. From expression (1) for a certain number of trajectories and initial

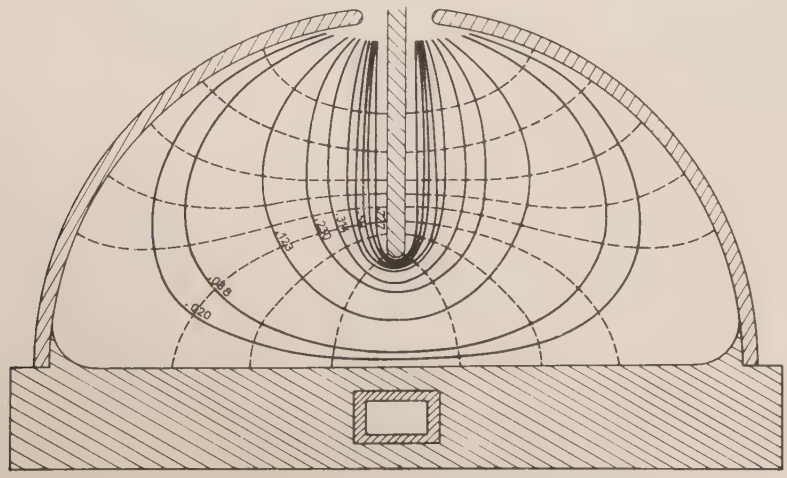

Fig. 3. Equipotential surfaces in the photo-proton chamber.

and the values of the drift velocity for electrons and positive ions in deuterium, the shape of the output pulse from the chamber was calculated positions of the ion pairs (altogether 72 cases). The positive ion mobility was taken as 10.6

[3]) W. Shockley, J. Appl. Phys. 9 (1951) 635.

cm^2/sec volt[4]). Electron drift velocity in deuterium was deduced from the drift velocity in ordinary hydrogen by correcting for the difference of mass. A measurement of the electron drift velocity in deuterium for values of $E/p \leqslant 0.6$ confirms this approximation[5]). For each trajectory the output signal after passing through an integrating and a differentiating time constants (0.8 μsec) was calculated by means of the following formula:

$$u(t) = \exp(-t/\tau)\left[\left(1 - \frac{t}{\tau}\right) I + J\right]$$

with

$$I = \int_0^t \exp(t'/\tau)\, v(t')\, \frac{dt'}{\tau}$$
$$J = \int_0^t \exp(t'/\tau) \times \frac{t'}{\tau} \times v(t')\, \frac{dt'}{\tau} \qquad (2)$$

where $v(t')$ represents the signal induced by the motion of the electron and the positive ion on the collecting electrode.

The surface corresponding to the same maximum output signal were then calculated (fig. 4), and the number of photo-protons created between two successive surfaces evaluated. The pulse height distribution resulting from positive ion effect in the chamber is finally shown on fig. 5. An arrow indicates the value of the counting bias used (112.5 keV). Due to this effect, the fraction of the photo-proton pulses which is not recorded is 1.24%.

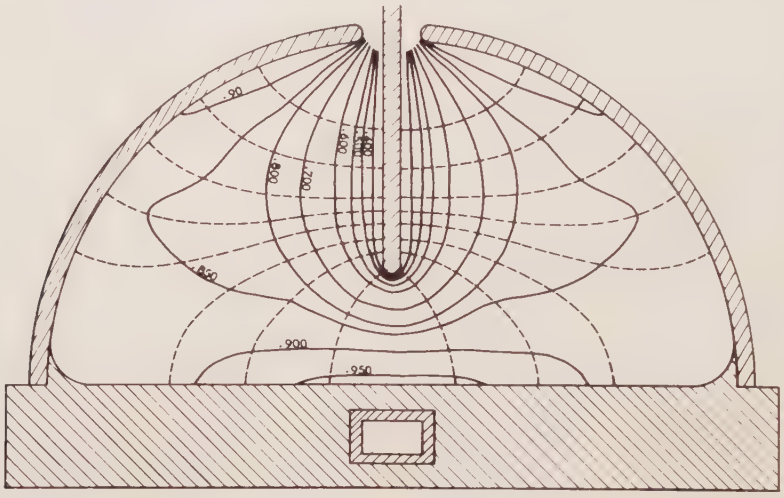

Fig. 4. Surfaces corresponding to the same output signal from the amplifier.

4.3. WALL EFFECT IN THE PHOTO-PROTON CHAMBER

Some of the photo-protons produced near the inner surface of the chamber will lose part of their energy in the walls. A correction has therefore to be applied for those which will not be recorded. This correction is important (4.9%) and has to be estimated precisely. In order to cal-

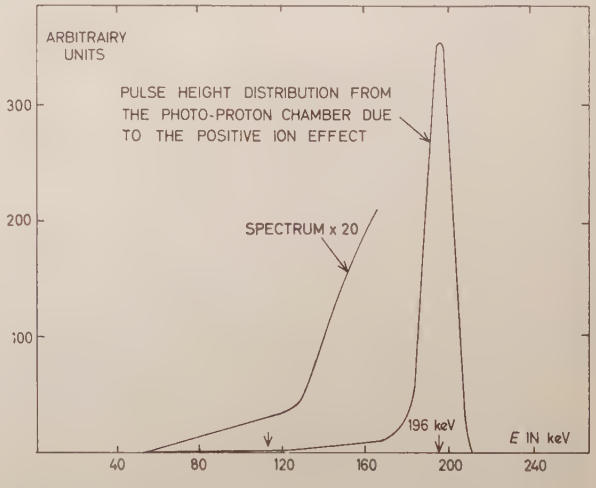

Fig. 5. Pulse height distribution from the photo-proton chamber due to the positive ion effect.

[4]) W. H. Bennett and C. D. Thomas, Phys. Rev. 62 (1951) 41.

[5]) P. C. Marin, Etalonnage absolu de source de rayons γ et de neutrons (Thesis, Paris University, 1958) p. 90.

culate this correction, one needs the range-energy relation for protons in deuterium. This relation was deduced from the experiment of Crenshaw[6]) who measured the stopping power of deuterium, for protons of energy between 70 and 335 keV.

The calculation of the wall effect is particularly simple with the approximation of isotropic angular distribution and fixed range for the photo-protons and uniform irradiation of the chamber. One shows easily that the percentage of particles suffering wall effect is $\frac{1}{4}\,\Sigma\,S/V$ where Σ is the range of the particles, S the inner surface limiting the volume V. In fact, none of these conditions is realised in our case. The angular distribution of the photo-protons is very anisotropic:

$$I(\varphi) = a + b \sin^2 \varphi \,.$$

For the energy 2.615 MeV of the γ-rays, the value of b/a measured by Bishop *et al.*[7]) is 1/0.24. Furthermore, the energy of the photo-protons emitted at an angle φ compared to the direction of the incident γ-ray is:

$$E(\varphi) = (196 + 26.6 \cos \varphi) \text{ keV} \,.$$

Finally the irradiation of the chamber is far from being uniform. The evaluation of the wall effect was done, without these approximations, in the range between 0 and 168 keV (energy of the photo-proton emitted opposite to the incident γ-ray). This was done partly by graphical integration, partly by calculation. One finds that the fraction of the photo-protons which suffer wall effect and give a pulse height between 0 and 168 keV is altogether 7.44% (5.80% for the partition and 1.64% for the spherical part of the chamber). By using the formula $\frac{1}{4}\,\Sigma\,S/V$ one would get 8.28%. The percentage of photo-protons giving pulses below 112.5 keV (counting bias) is 4.9%. If one adds to it the loss of pulses due to positive ion effect 1.24%, one then gets a total loss of 6.14%.

In order to check the validity of the corrections applied, we have plotted on the left of fig. 6, for the energy region between 111 and 140 keV, the contributions to the spectrum due to these two effects, as well as the counting rate obtained experimentally in this region. The ordinates have been increased by 10. The agreement is good, within the statistics which is of the order of 5%. We therefore think that the uncertainty on the total correction is less than 0.3%.

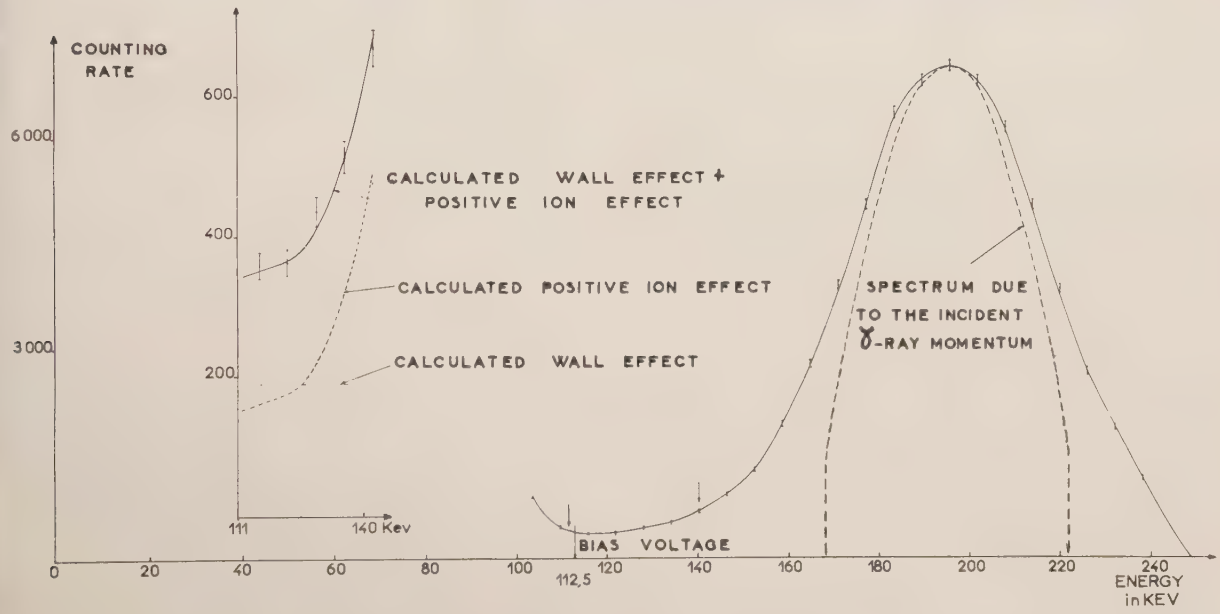

Fig. 6. Photo-proton pulse-height distribution.

[6]) C. M. Crenshaw, Phys. Rev. **62** 1951) 54.

[7]) G. R. Bishop, L. E. Beghian and H. Halban, Phys. Rev. **83** (1951) 1052.

4.4. PHOTO-PROTON COUNT

A large part of the background was eliminated by simultaneously counting the signals with two scalers biased respectively at 112.5 and 250 keV. The correction was then only 0.3%. The counting rate was measured over periods of one hour, alternatively for each half of the chamber and for three different fillings. Altogether, 115 000 pulses have been recorded, thus giving a statistical error of 0.3%. Individual counting rates were found within the statistics as well as total counts for each filling.

4.5. EVALUATION OF THE RATIO OF THE DEUTERON NUCLEI CONCENTRATIONS: C_2/C_1

The deuteron nuclei concentration C_2 in D_2O can easily be determined to an accuracy of 0.01%. The concentration C_1 in the gas filling of the chamber has been determined in the following way. The gas contained in the chamber was allowed to expand in a volume such that the final pressure was closed to the atmospheric pressure. This final pressure was measured with a manometer tube. The volume of the chamber and the total volume of expansion were measured by filling with distilled water and weighing to an accuracy of 0.02%. The number of molecules of gas was then finally known to an accuracy of 0.10%. However, a correction had to be applied for the ordinary hydrogen content in the deuterium used. The ratio H/D was measured with mass spectrograph by two different groups in Oxford. The results were 2.73% and 3.10% each of which with an accuracy of 0.15%. The difference between the two measurements is a bit larger than the sum of the two errors, so we took for the ratio H/D the value $2.91 \pm 0.20\%$, which has a safe margin of error. The uncertainty of the ratio C_2/C_1 is then 0.30%.

5. Comparison of the Intensities of the two RdTh Sources on the Curie Chamber

The comparison has been done on the Clarendon Laboratory Curie Chamber. For an argon filling, the linearity of this instrument measured with radon sources between 300 and 1.7 mC was found to be better than 0.01%[8]). The comparison was made via an intermediate RdTh source of intensity 8.7 mC. Variation in the ionisation current reaching 0.15% have been observed with the 50 mC and 0.66 mC sources, when rotated around their axes. These variations are likely due to a non-uniform distribution of the radioactive powder in the capsule. For each source, an average was taken on the ionisation current measured every 45 degrees.

The ratio of the source intensities was finally found to be:

$$R = 74.86 \pm 0.03_1$$

the relative error being 0.04%.

6. The Background Neutrons from the RdTh Source

Neutron emission from RdTh and radium sources is well known[9, 10]). This emission can be spontaneous or due to the interaction of the α-particles emitted by RdTh, radium and their daughter substances, with the carrier of the source or with the capsule (photo-fissions of Th^{232} by the 2.62 MeV γ-rays emitted by ThC'' is negligible). Spontaneous emission of neutrons by RdTh and the daughter substances is very small or nul. In particular, measurements done with an active deposit source have shown that the number of neutrons emitted is less than one per second, per mC of activity[11]).

Background neutrons are a very disturbing feature for our standard. We tried, before all, to reduce it by a convenient preparation of the sources. We then measured their number in two ways: by the proton recoil method using a hydrogen filled chamber and by chemical integration in a manganese nitrate solution.

6.1. PREPARATION OF THE SOURCES

Three sources have been prepared, using spec. pure Thoria (0.02%) as carrier, with the following characteristics:

[8]) P. C. Marin, Brit. J. of Appl. Phys. **7** (1951) 188.
[9]) O. R. Frisch, H. Halban and Jorgen Koch, Mat. Fys. Medd. Dan. Vid. Selsk. **15** (1951) 10.
[10]) G. R. Gamertsfelder and M. Goldhaber, Phys. Rev. **69** (1951) 368.
[11]) A. V. Kogan and L. I. Rusinov, JETP (1957) 365.

Source No. 2991: carrier 1 mg, activity 0.03 mC
Source No. 2992: carrier 1 mg, activity 0.50 mC
Source No. 3382: carrier 10 mg, activity 50 mC

Spectroscopic analysis of the content of the first two sources gave an evaluation of the percentage of impurities brought in the precipitation and those due to the incomplete purification of the RdTh. From this, we deduced the percentage of impurities, one should expect from the 50 mC source. Table 2 shows impurities existing in an appreciable amount in this source, which can emit neutrons, when bombarded by the α-particles, from the RdTh and its daughter substances. In order to estimate the number of neutrons emitted, we have assumed that the cross-section for the α-n reaction is equal to the cross-section σ_c for the formation of the compound nucleus. The last row of table 2 gives the expected number of neutrons for each type of impurity.

However, apart from the impurities in the carrier, one has to account for the presence of nitrogen in the capsule. The inner volume of the capsule is 10 mm^3 and the weight of Thoria, 10 mg. The density of Thoria being about 4, 75% of the capsule is filled with air. One should then expect neutrons from the reaction N^{14} (α-n) F^{17} to be emitted (threshold of — 4.74 MeV). The expected number of neutrons calculated as above should be about 5000 if the α-particles were not slowed down by Thoria. In practice, one should expect the number of neutrons emitted by the 50 mC RdTh source to range between a few hundreds and a few thousands per second.

Another interesting remark can be deduced from the preceding discussion, concerning the energy spectrum of the background neutrons. At most, 30 neutrons emitted per second will have an energy greater than 4 MeV. Most of the others will have much less energy. In particular, the neutrons from the reaction N^{14} (α-n) F^{17} will have a maximum energy of 2.95 MeV. This result is important for the measurement of the background neutrons by the proton recoil method, the wall effect being considerable for neutrons of an energy of greater than 4 MeV. We can confidently expect to detect the background neutrons in good condition.

Table 2

Element	B^{10}	Cr^{52}	Mn^{55}	Fe^{65}	Cu^{65}
Natural abundance (%)	81.3	83.8	100	91.7	30.9
Concentration in the source carrier (%)	0.10	0.05	1.60	5.35	0 16
Q for the α-n reaction (MeV)	+ 1.07	— 3.4	— 3.4	— 5.2	— 5.85
$\sigma_c \times 10^{24}$ ($E_\alpha = 8.77$ MeV) (cm^2)		0.07	0.07	0.17	0.13
Expected number of neutrons emitted per second	120	1	40	30	1

6.2. MEASUREMENT OF THE BACKGROUND NEUTRONS BY THE RECOIL PROTON METHOD

For this purpose, we have used an ionisation chamber identical to the one described by L. E. Beghian and H. Halban[12]). Its shape is cylindrical (diameter 42 mm, length 160 mm) with hemispherical ends. The walls are of aluminium alloy and have a thickness of 1 mm. The central electrode has a diameter of 1 mm. A kovar-glass seal with guard ring transmits the pulses to the preamplifier. The chamber was filled with very pure hydrogen (from a hydrogen liquefier) under a pressure of 10 or 15 atm. A voltage of 3000 volt was applied on the external electrode and the guard ring was grounded to earth. The RdTh source was located on the axis of the chamber at an adjustable distance. It was maintained in this position by two thin aluminium tubes sliding along the chamber. The

[12]) L. E. Beghian and H. Halban, Proc. Phys. Soc. A 42 (1951) 395.

energy calibration was made by irradiating the same chamber filled with deuterium, by the 2.62 MeV γ-rays from ThC''.

The recoil proton spectrum was measured down to 270 keV. It was corrected for positive

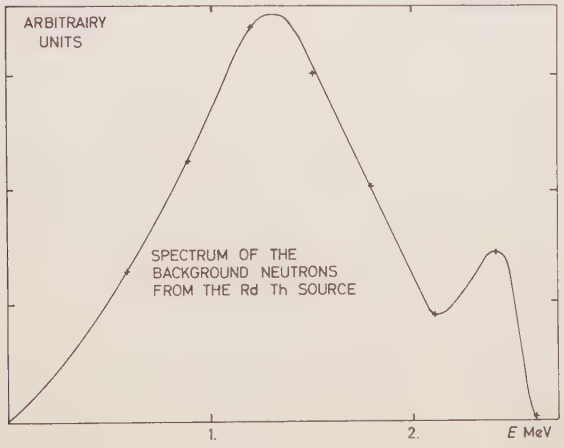

Fig. 7. Spectrum of the background neutrons from the RdTh source.

ion effect (the correction for wall effect amounts to only 2 to 3% and was neglected). The energy spectrum of the background neutrons was then calculated, taking into account the variation of the neutron-proton cross-section with energy. It is shown on fig. 7. Finally, the number of background neutrons was evaluated. The total error arising from statistics and various uncertainties in the solid angle, on the efficiency of the counter and on the wall effect is 7%. Using the final value of the photo-neutron yield given in section 7, we obtain for the ratio R of background neutrons/photo-neutrons the value:

$$R = 2.88 \pm 0.20\% \,.$$

6.3. MEASUREMENT OF THE RATIO OF BACKGROUND NEUTRON/PHOTO-NEUTRONS BY THE METHOD OF CHEMICAL INTEGRATION

For this measurement we have used the apparatus shown on fig. 8. The standard is fixed on the apex of a cone, made in aluminium 1 mm thick, and covered on both sides with a thin layer of araldite. The cone dips into a cylinder. Both the cone and the cylinder are filled with a 50% manganese nitrate solution. Fig. 8 shows the dimension of the set up. If the emission of the neutrons is isotropic and if the dimensions of the reflector are large enough, the ratio of background to the photo-neutron activity will be the same as if the irradiations were done in a sphere of a radius equal to the cone height. In practice, this can be achieved, with the present system, by using 4 times less solution than with a sphere. The isolation of the cone, for thermal neutrons is good, the average distance from the cone surface to the cylinder surface being 7 times the diffusion length (2.22 cm).

The experiment was conducted in the following way. Irradiations were successively made with the standard and then with the RdTh source alone. After thorough mixing the 3 liters of solution contained in the cone were put around a NaI crystal scintillator 4.5 × 5 cm. The whole was housed in a lead castle 6 cm thick. A DuMont photo-multiplier detected the γ-rays due to the 156 minutes activity of Mn^{55}. With a bias set at 400 keV, the counting rates were respectively 700 c/m and 20 c/m for the irradiation with the photo-neutrons and with the background neutrons. The background of the scintillator itself was 120 c/m. However, the stability of this background and the possibility of counting for a long time made the experiment

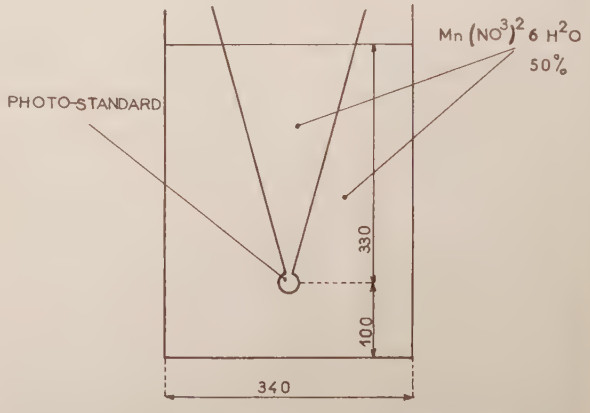

Fig. 8. The chemical integration in the manganese nitrate solution.

feasible. Table 3 shows that the reproducibility of the counting rates is good within the statistics.

Subsidiary irradiations made in a sphere of 24 cm radius and in the cone set up, show

TABLE 3

	Total activity due to the standard	Activity due to the background neutrons	$R = \frac{\text{background neutrons}}{\text{photo-neutrons}}$
Sphere: radius 24 cm	4236 ± 14	109.9 ± 3.1	
	4187 ± 11	110.8 ± 2.9	
	4206 ± 10	105.4 ± 2.7	2.62 ± 0.03%
	4250 ± 10	104.0 ± 3.0	
	4192 ± 10	107.9 ± 2.9	
	4224 ± 10		
Average:	4216 + 10	107.6 ± 1.3	
Same sphere surrounded by water	4228 ± 10	111.8 ± 3.0	
	4227 ± 10	110.8 ± 2.9	
	4197 ± 25	115.0 ± 3.0	2.73 ± 0.04%
		109.9 ± 3.5	
Average:	4223 ± 7	112.0 ± 1.5	
Cone height: 33 cm	2029 ± 6.0	57.0 ± 3.1	
	2004 ± 6.0	60.5 ± 3.1	
	2013 ± 6.5	58.2 ± 3.1	3.08 ± 0.07%
		64.7 ± 3.1	
		60.3 ± 3.1	
Average	2015 ± 7.5	60.1 ± 1.4	

(table 3) that some of the neutrons still escape from the cone due to its finite height. A correction for this loss was attempted by using the curves of density distribution of thermal neutrons in water obtained with a RdTh-D_2O source and with a source of D-D neutrons (of a maximum energy of 3.8 MeV[13, 9]). The observed increase in activity between the irradiations made with the 24 cm radius sphere and with the 33 cm height cone (15%) is in good agreement with the value calculated from the curve mentioned above (14.7%). From these, we expect the correction introduced to account for the loss of neutrons due to the finite height of the cone, to be 8 ± 2%.

Finally, another correction of 0.16% ± 0.02% was applied to account for the photo-neutrons produced in the natural deuterium content of the manganese nitrate solution. This correction was obtained from the activity found in the solution after irradiation with a Na^{24} source (taking into account the variation of the cross-section for the photodisintegration of the deuteron between 2.62 and 2.76 MeV). The final result gives for the ratio background neutrons/photo-neutrons, the value:

$$R = 3.17 \pm 0.16\% .$$

The weighted average value of the two methods gives for the ratio R the value:

$$R = 3.06 \pm 0.13\% .$$

7. The Final Yield of the Photo-Standard

We give below the main data needed to make corrections for small differences between our standard and any substandard of this type:

Capsule

Weight of bi-distilled water at 15° C for the filling of the capsule: 33.008 ± 0.03 g.

Thickness of the partition: 6.050 ± 0.005 mm.

Diameter of the central hole: 3.130 ± 0.005.

Depth: 44.990 ± 0.005.

[13]) Amaldi, Hafstad and Tuve, Phys. Rev. **31** (1951) 896.

50 mC RdTh *Source*

Source No.: 3382 supplied by Amersham, double capsule made with iridiated platinum, height 5.000 mm, diameter 3.053 mm, thickness 1 mm, total weight 540.7 mg, carrier Thoria 10 mg weight.

The intensity of the source on our Curie chamber was 43.87 millicurie radium equivalent on the 1/1/1955. The radium source used had an activity of 0.960 mC (National Physical Laboratory).

The number of photo-neutrons emitted, at this date, was $58\,414 \pm 654$ neutrons per second. The total intensity (photo-neutrons + background neutrons) was $60\,094 \pm 751$.

Table 4 recalls the various sources of errors which affect the final value of the yield of our neutron standard, and their values.

Table 4

Statistical error on the photo-proton count:	0.30%
Uncertainty of the correction applied for wall effect and positive ion effect:	0.30%
Uncertainty of the corrections for geometrical differences between the D_2O capsule and the photo-proton chamber:	0.15%
Error on the ratio of the intensities of the two RdTh sources:	0.04%
Error on the ratio of the deuteron concentrations C_2/C_1:	0.30%
Uncertainty of the correction for the γ-ray absorption in D_2O:	0.03%
Error of the correction for the background neutrons emitted by the RdTh source:	0.13%
Total	1.25%

By adding all these errors, one obtains a total uncertainty of 1.12% on the photo-neutron yield of the standard and 1.25% on the total yield (photo-neutrons + background neutrons).

8. Conclusion

We have built a RdTh-D_2O photo-neutron standard which has been calibrated by the associated charged particle. Its yield for a RdTh source of intensity 43.87 millicurie radium equivalent on a Curie type ionisation chamber, is $58\,414 \pm 654$ photo-neutrons (that is $1.332 \pm 0.015 \times 10^6$ per curie radium equivalent). The accuracy on the yield, 1.12%, is the best obtained to-day to our knowledge. Subsidiary standards can easily be made by using one of our D_2O capsules and correcting for small geometrical differences. Furthermore, RdTh sources should be made with the same geometry as our source and compared on the Clarendon Laboratory Curie chamber to the radium standard which we used. Any substandard made in this way should have a yield known to an accuracy comparable to the one we obtained.

For our particular RdTh source, the number of background neutrons was found to be $3.06 \pm 0.13\%$, thus giving an accuracy of 1.25% on the total yield.

Acknowledgment

I would like to express my gratitude to Professor H. Halban for inspiring this work and for the many advices and suggestions he gave me.

I also wish to thank Dr. G. R. Bishop for his help at various stages of this work and for his most valuable advices.

I am also very grateful to A.E.R.E. Harwell and especially to Dr. Bretscher for the kind loan of the 50 mC RdTh source.

The construction of the various ionisation chambers which we used would not have been possible without the technical advices and the constant help of Mr. V. Round.

NUCLEAR INSTRUMENTS AND METHODS 5 (1959) 37–43; NORTH-HOLLAND PUBLISHING CO.

MEASUREMENT OF PHOTONUCLEAR ABSORPTION CROSS SECTIONS

J. KOCKUM

Radiation Physics Department, University of Lund, Lund

and

N. STARFELT†

Institute of Physics, University of Lund, Lund

Received 25 April 1959

The total photonuclear cross sections for carbon, aluminium, sulphur, and iron have been measured in the energy region of the giant resonance. A total absorption scintillation spectrometer was used to study the transmission of the bremsstrahlung spectrum from a 30 MeV synchrotron through long absorbers. The integrated total photonuclear cross section between 10 and 27 MeV as well as the width of the giant resonance was obtained. The measured widths are definitely larger for the deformed nuclei aluminium and iron than for the spherical carbon nucleus, whereas the width for sulphur has an intermediate value.

1. Introduction

The giant resonance in photonuclear reactions has been the subject of numerous theoretical and experimental investigations. The dipole sum rule theory[1]) predicts a lower limit of the total integrated cross section $\int_0^\infty \sigma(E)\,\mathrm{d}E$ of 0.060 NZ/A MeV-barns, where N, Z and A are the neutron, proton, and mass numbers, respectively. Another well established feature is the slow decrease of the resonance energy with increasing atomic number. However, considerable difficulties are encountered in the calculation of the width of the giant resonance. Recently several authors[2–5]) have shown that the width depends on the deformation of the nucleus. Large nuclear deformation results in a wide resonance, whereas spherical nuclei exhibit the narrowest peaks. In the most deformed nuclei a splitting of the giant resonance into two different peaks should occur.

Absorption cross sections have been determined from experiments mainly through addition of the measured partial (γ,n) and (γ,p) cross sections. A method using the dispersion relation to derive absorption cross sections from measured elastic scattering cross sections has also been employed[6]). Johansson[7]) made a systematic study of the experimental width of the giant resonance for different elements. He pointed out the difficulties in obtaining total cross sections through addition of partial ones. It was therefore considered of value to obtain direct measurements of absorption cross sections.

This type of measurements has been reported by Haslam *et al.*[8]) and recently by Ziegler[9]). Haslam *et al.* used photo-induced radioactivities to detect gamma rays before and after transmission through a carbon absorber. Ziegler[9]) employed a magnetic pair spectrometer to measure the shape of a 32 MeV bremsstrahlung spectrum from a betatron with and without long absorbers inserted into the beam.

† Now at Research Institute of National Defence, Stockholm 80.

[1]) J. S. Levinger and H. A. Bethe, Phys. Rev. **78** (1950) 115.
[2]) M. Danos, Bull. Am. Phys. Soc., Ser. II, **1** (1956) 135.
[3]) M. Soga and J. Fujita, Nouvo Cimento **6** (1957) 1494.
[4]) K. Okamoto, Phys. Rev. **110** (1958) 143.
[5]) J. S. Levinger, Nuclear Physics **8** (1958) 428.
[6]) E. G. Fuller and Evans Hayward, Phys. Rev. **101** (1956) 692.
[7]) S. A. E. Johansson, Arkiv för fysik **13** (1958) 331.
[8]) R. N. H. Haslam, R. S. Horsley, H. E. Johns and L. B. Robinson, Canad. J. Phys. **31** (1953) 636.
[9]) B. Ziegler, Z. Physik **152** (1958) 566.

Koch[10]) suggested the possibility of measuring photonuclear cross sections by analysis of a continuous bremsstrahlung spectrum transmitted through a long absorber. The absorber should be long enough for the photonuclear effect to give appreciable attenuation. This implies the use of a high intensity bremsstrahlung source and a high efficiency spectrometer. A total absorption scintillation spectrometer is ideal for this purpose. Another feature of this spectrometer is that it can be used in conjunction with a multichannel pulse-height analyzer, thus making it possible to record the number of counts in a large number of energy intervals simultaneously. This is of great importance in this kind of experiment, in which the variation in the counting rate with photon energy is fairly small. Magnetic spectrometers have better resolving power than the scintillation spectrometer, but their lower detection efficiencies require the use of shorter absorbers. Thus, when employing a magnetic spectrometer smaller variations in counting rate have to be detected with an instrument which can record the counting rate in only one energy interval at a time. This imposes extremely high requirements on the stability of the whole apparatus.

In the present investigation a large NaI(Tl) scintillation spectrometer was used in the study of the transmission of the bremsstrahlung from a 30 MeV synchrotron through long absorbers of carbon, aluminium, sulphur and iron. Considerable difficulties were encountered in the analysis of the experimental data to obtain information about the photonuclear cross sections. Higher maximum bremsstrahlung energy, and more accurate knowledge of the atomic gamma-ray attenuation coefficients would improve the results considerably.

2. Experiment

The experimental arrangement is shown in fig. 1. The bremsstrahlung from the 30 MeV synchrotron passed through a narrow hole in a shielding wall consisting of 70 cm of lead and 64 cm of borated paraffin. The beam was further collimated by a 28 cm long lead collimator with an opening diameter of 1.0 cm. The well-collimated beam was then allowed to penetrate through the absorber and enter the scintillation spectrometer through a 4 cm diameter hole in the shield of borated paraffin and lead. The diameter of the beam at this collimator was slightly smaller than the collimator aperture. The spectrometer consisted of two NaI(Tl)

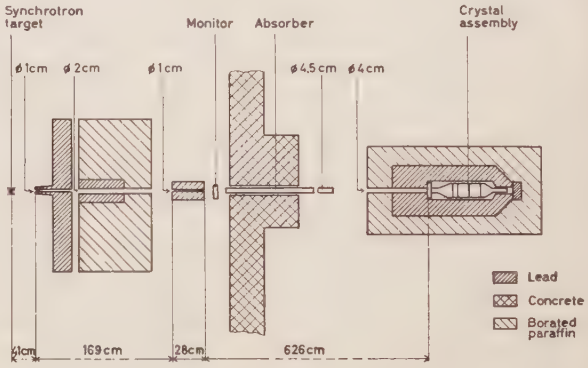

Fig. 1. Experimental arrangement.

crystals, 12.7 cm in diameter and 10.2 cm long, mounted to form a 20.4 cm long cylinder. Each crystal was connected to a DuMont 6364 photomultiplier; the one closer to the synchrotron, by means of a 4 cm lucite light guide; and the other one, without any extra light guide. The use of a light guide was necessary because of the non-uniformity of the photomultiplier cathode surface. The pulses from the photomultipliers were added, amplified, and sorted in a gated 100-channel pulse-height analyzer. The gate was opened by a pulse from the synchrotron and was left open for a few milliseconds at the time of the occurrence of the yield pulses from the accelerator. In this way the background counting rate was decreased, e.g. by a factor of 5 at 20 MeV.

The repetition rate of the synchrotron was 50 pulses per second and the maximum yield was 3 roentgen per minute as measured at a distance of 1 meter from the platinum target. The beam intensity was monitored by means of a transmission ion chamber mounted in the

[10]) R. S. Foote and H. W. Koch, Rev. Sci. Instr. **25** (1954) 746.

beam between the collimator and the absorber.

Data about absorbers, recording time, number of counts, and background are given in table 1. The background counting rate was measured with a 10 cm long cylindric lead absorber inserted between the absorber under investigation and the spectrometer.

Table 1
Experimental data

Absorber	(g/cm²)	Attenuation at 20 MeV	Number of counts above 10 MeV	Relative background, 20 MeV	Running time (hours)
Carbon	629	5.3×10^{-5}	163 900	1%	5
Aluminium	490	2.4×10^{-5}	96 000	10% †	7
Sulphur	408	4.1×10^{-5}	163 400	2%	5.5
Iron	345	1.5×10^{-5}	126 000	10% †	9
Aluminium	67.5	0.21	51 400	2%	2

† These experiments also include runs where no gating was used.

The short aluminium absorber was used in a run to give the unattenuated synchrotron spectrum. It was necessary to use an absorber in this case too, because the synchrotron injector could not be operated at very low currents. Without an absorber the counting rate in the spectrometer would be too high and pile-up of pulses would occur.

Energy calibration of the spectrometer was performed before the experiment with the use of gamma-ray lines produced in proton induced reactions in a van de Graaff generator[11]). The pulse height versus energy curve was found to be linear up to 20.3 MeV, the highest gamma-ray line obtainable. During each run with the synchrotron energy calibration was made with the 4.45 MeV gamma-ray line from a Po-Be source. The zero-energy point on the pulse-height analyzer scale was determined by means of a precision pulser.

3. Results and Discussion

The experimental pulse distributions were first corrected for background and subsequently converted to photon spectra by multiplication with the response function matrix given in ref. [11]). The resulting spectra are shown in figs. 2 and 3 together with the uncorrected pulse distributions. The points represent 2 MeV energy intervals and were obtained through addition of the number of counts accumulated in several pulse-height analyzer channels. Fig. 2 shows the spectrum obtained with the short aluminium absorber. This spectrum is known from other experiments[12]) and theory[13]) and the degree of agreement between the spectrum from the present experiment and the calculated spectrum provides a check on the method of analysis. The agreement is good except at both

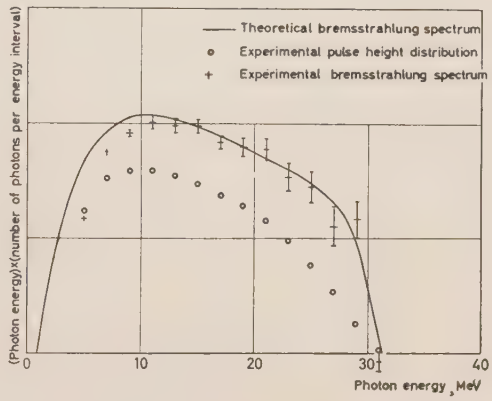

Fig. 2. 30.5 MeV bremsstrahlung spectrum, attenuated in 26 cm of aluminium. The circles represent the pulse-height distribution obtained with the NaI(Tl) spectrometer, the crosses the photon spectrum obtained by multiplying the pulse-height distribution with the inverse response-function matrix[11]). The solid curve is the theoretical bremsstrahlung spectrum[13]).

[11]) J. Kockum and N. Starfelt, Nuclear Instruments 4 (1959) 171.

[12]) E. G. Fuller, E. Hayward and H. W. Koch, N.B.S. Report 5439 (1957).

[13]) A. S. Penfold and J. E. Leiss, University of Illinois (1958).

ends of the spectrum, the high-energy end giving the greatest reasons for concern. Here the irregularities are due to small errors in the response-function matrix which are inevitable because of the lack of accurate experimental information. These irregularities were investigated further by making a new matrix corresponding to slightly better energy resolution of the spectrometer than was experimentally obtained. Multiplication of the pulse-height distribution with this new matrix did not change the result in the middle of the spectrum but made the errors at the high-energy end larger. This opens up a possibility of improving the matrix by trial and error. However, in the energy region of the giant resonance the response function is better known through experiment, besides which small errors in the matrix are amplified only in that part of the spectrum near the high-energy end. The

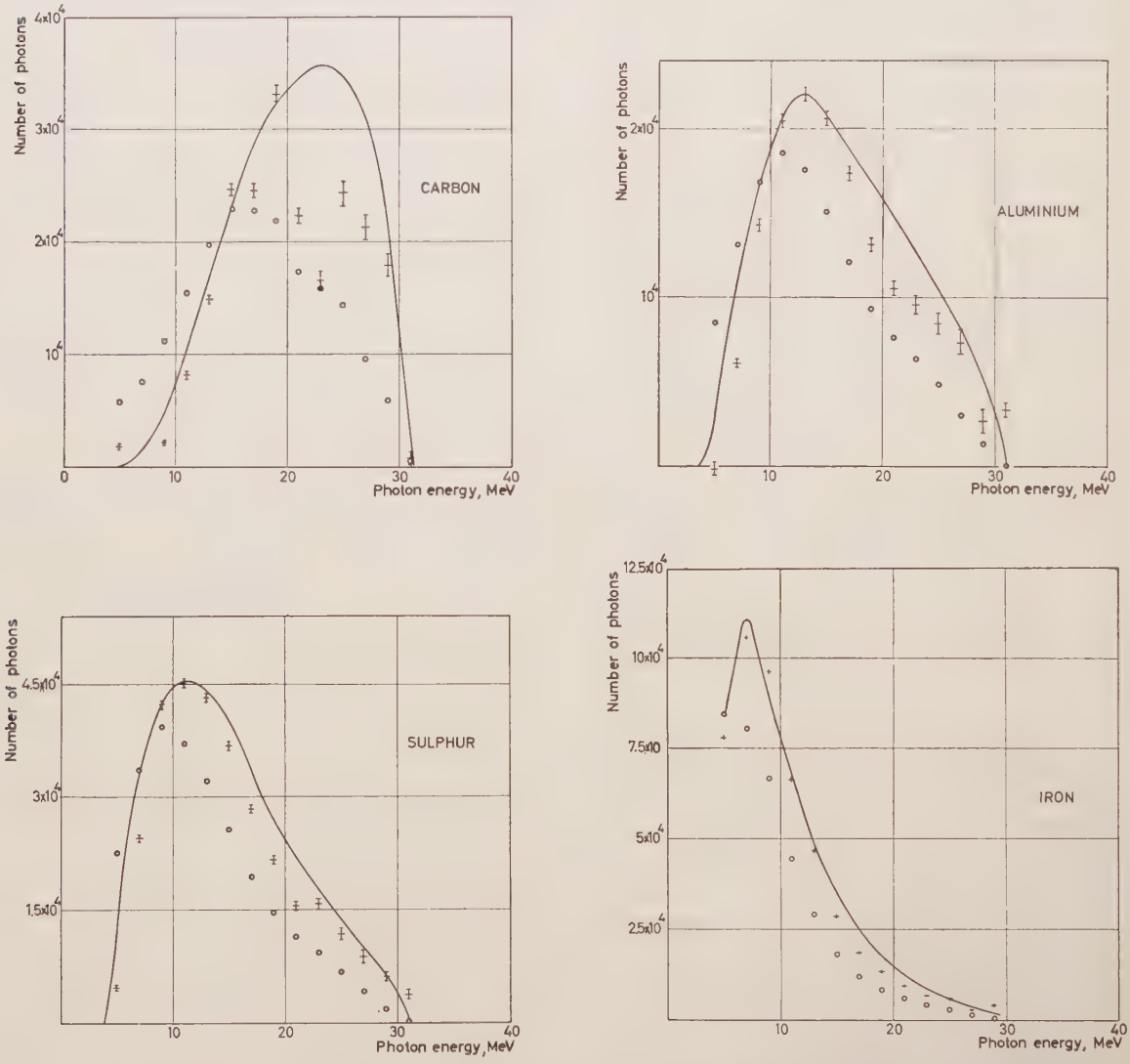

Fig. 3. 30.5 MeV bremsstrahlung spectra attenuated in long absorbers. The circles represent the pulse-height distributions obtained with the NaI(Tl) spectrometer, the crosses the photon spectrum obtained by multiplying the pulse-height distributions with the inverse response-function matrix[11]). The solid curves show the spectra that would be obtained if the photonuclear cross section were zero. They were obtained from the spectrum in fig. 2 using White's atomic absorption coefficients[14]).

deviation between the expected and the observed photon distribution at low energies is not due to errors in the matrix, but is most likely a result of small errors in the atomic absorption coefficients used in the reduction of the experimental data. The errors shown on the curves in figs. 2 and 3 are due only to statistical errors in the experiment.

The spectra expected for the different absorbers if only atomic attenuation processes were effective were calculated from the theoretical spectrum in fig. 2 at energies above 9 MeV and from the experimental points in the same figure below this energy. The atomic absorption coefficients, μ_a, for this calculation were taken from White's first tables[14]), which Wyckoff and Koch[16]) found to agree better with experiment than the new ones[15]). This choice of absorption coefficients influences the final photonuclear cross-section results to some extent; e.g. if the new absorption coefficients of carbon were used

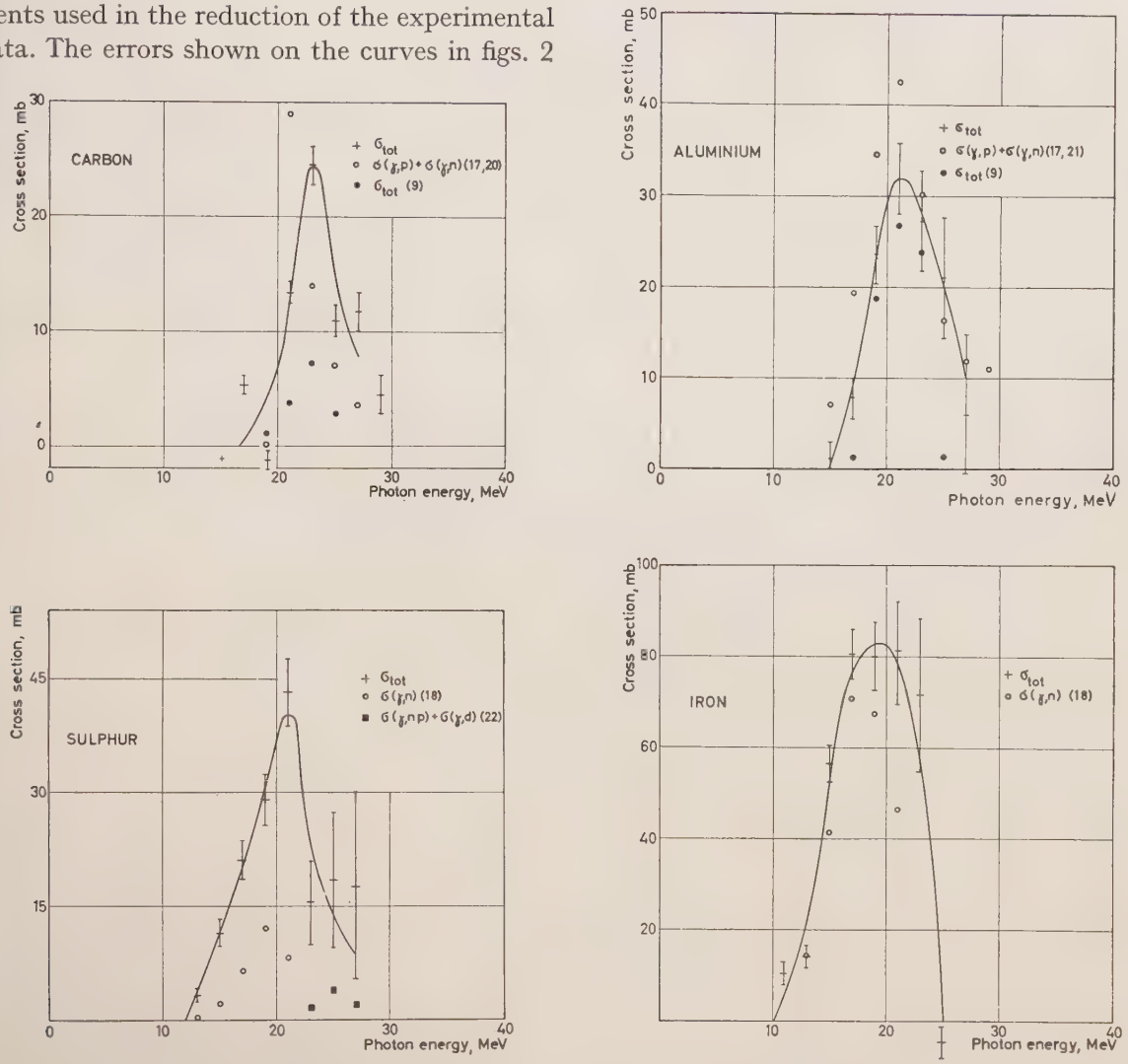

Fig. 4. Experimentally determined photonuclear absorption cross sections (crosses). The open circles show the sum of the (γ,n), and (γ,p) cross sections and the filled squares the (γ,np) + (γ,d) cross section where available[17,18,20–22]). The filled circles give the total photonuclear absorption cross section as measured by Ziegler[9]).

[14]) Gladys R. White, N.B.S. Report 1003 (1952).
[15]) Gladys White Grodstein, N.B.S. Circular 583 (1957).
[16]) J. M. Wyckoff and H. W. Koch, Conf. on Photonuclear Reactions, N.B.S. (1958).

a peak cross section 10% lower than that in fig. 4 would be obtained. $N_0(k)$ denoting the bremsstrahlung spectrum from the synchrotron the spectra calculated as stated above represent $N_0(k)\exp(-\mu_a l)$. Here k is photon energy and l absorber length. These spectra were normalized to the measured spectra at energies well below the giant resonance as shown in fig. 3. This normalization influences the accuracy of the final results, especially in the low energy part of the giant resonance. In aluminium, for instance, an error of 3 percent appears as an energy independent error in the photonuclear cross section of about 4 millibarns.

Photonuclear absorption cross sections μ_n were obtained by division of $N_0(k)\exp(-\mu_a l)$ by the experimentally obtained spectra $N_0(k)\exp(-(\mu_a+\mu_n)l)$. The resulting cross sections, σ, are shown in fig. 4. The errors shown are due only to the statistical inaccuracies in the experimental spectra, $N_0(k)\exp[-(\mu_a+\mu_n)l]$. The curves $N_0(k)\exp(-\mu_a l)$ are here assumed to be without errors. The cross section curves in fig. 4 are seen to be determined with reasonable accuracy up to energies well above the peak of the curves. However, in some cases the combined errors in the values at 27 and 29 MeV are very large. This is due to the above mentioned errors in the response-function matrix. The magnitude of the errors in these points depends to some extent on the shape of the spectrum, but even where they are shown in fig. 4 these points are of very small significance. Such difficulties can be partly overcome or at least removed from the energy region around the giant resonance by increasing the maximum energy of the bremsstrahlung spectrum. The synchrotron used in this experiment is now being rebuilt to yield energies up to 40 MeV. This is expected to improve the results of the present kind of experiments.

Published values of the sum of the (γ,n) and (γ,p) cross sections as well as the $(\gamma,np)+(\gamma,d)$ cross section are shown in fig. 4 for comparison where available, refs.[17-22]). For sulphur a differential cross-section curve has been reported only for the (γ,n) and $(\gamma,np)+(\gamma,d)$ processes, but Johansson[23]) determined the integrated (γ,p) cross section to be about 4 times as large as the (γ,n) cross section. The cross-section curves are adjusted to give the same resolution as our experiment (each point is an average over a two-MeV interval). This influences the most narrow cross-section curve (carbon) more than the others. Our cross-section curves agree fairly well with previously reported values. The discrepancies at higher energies may be due to the fact that our curves represent total absorption but are compared to partial cross-section curves. Moreover, the difference method used in the yield measurements introduces large uncertainties above the peak of the giant resonance. Ziegler's[9]) results for carbon and aluminium are also given in fig. 4. A comparison between Ziegler's and our measurements shows a resonable agreement for aluminium but a definite discrepancy for carbon, where Ziegler's cross section is surprisingly low.

TABLE 2

Experimentally determined giant resonance data; peak energy, E_{max}, width at half height, ΔE, and integrated cross section, $\int_{10\,MeV}^{27\,MeV}\sigma dE$, and values of $\int_0^\infty \sigma dE$ predicted by the dipole sum rule.

Absorber	E_{max} (MeV)	ΔE (MeV)	$\int_{10\,MeV}^{27\,MeV}\sigma dE$	$\int_0^\infty \sigma dE$
Carbon	23	4.6	0.12	0.18
Aluminium	21.5	7.8	0.24	0.40
Sulphur	21	6.6	0.30	0.48
Iron	19.5	9.4	0.76	0.84

Integrated cross section, 10–27 MeV, energy of maximum cross section, and width at half

[17]) J. Halpern and A. K. Mann, Phys. Rev. **83** (1951) 370.
[18]) R. Montalbetti, L. Katz and J. Goldemberg, Phys. Rev. **91** (1953) 659.
[19]) L. W. Jones and K. M. Terwilliger, Phys. Rev. **91** (1953) 699.
[20]) W. C. Barber, W. D. George and D. D. Reagan, Phys. Rev. **98** (1955) 73.
[21]) F. Ferrero, R. Malvano, S. Menardi and O. Terracini, Nuclear Physics **9** (1958) 32.
[22]) L. Katz and A. S. Penfold, Phys. Rev. **81** (1951) 815.
[23]) S. A. E. Johansson, Phys. Rev. **97** (1955) 1186.

height of the experimental cross-section curves are given in table 2. The values of the peak energy of the giant resonance are consistent with a $A^{-\frac{1}{6}}$, but not with a $A^{-\frac{1}{3}}$ law. The width for the non-deformed nucleus, carbon, is definitely smaller than those for the other three nuclei, of which aluminium and iron are known to be deformed in the ground state. Sulphur, which is probably not deformed in the ground state, exhibits a somewhat narrower giant resonance than aluminium and iron.

The method of measuring photonuclear absorption cross sections described in this paper should be useful in a systematic study of width and position of the giant resonance for different nuclei. Better statistics and higher maximum bremsstrahlung energy and also better knowledge of the atomic gamma-ray absorption cross sections should considerably improve the accuracy of the results especially at energies above the maximum in the cross-section curve.

Acknowledgement

The authors wish to express their sincere gratitude to Dr. S. A. E. Johansson and to Dr. K. Lidén for constant support and for many fruitful discussions and to Mr. L. Hansson for skilful technical assistance.

NUCLEAR INSTRUMENTS AND METHODS 5 (1959) 44–49; NORTH-HOLLAND PUBLISHING CO.

MESURE DE TEMPS DE MONTEE D'IMPULSIONS ELECTRIQUES INFERIEURS A LA MILLIMICROSECONDE

A. SARAZIN, J. SAMUELI et G. DUCROS

Institut d'Etudes Nucléaires, Alger

Reçu 5 Mai 1959

A system based on time-pulse height conversion is described, which enables electrical pulse rise times of less than one millimicrosecond and their statistical fluctuations to be measured, in the range from 0 to 5×10^{-9} sec.

The method has been used to study pulses from a mercury switch and from scintillations in a plastic scintillator or gas induced by ionizing radiations.

De très nombreuses études de physique nucléaire conduisent à des mesures de temps courts et sont effectuées à l'aide de dispositifs constitués de détecteurs de particules suivis d'une électronique rapide. La connaissance du temps de montée des impulsions fournies par les détecteurs, présente un grand intérêt car ce sont généralement ceux-ci qui limitent la résolution en temps de l'appareillage. D'autre part, la détermination de la forme d'impulsions électriques liées à certains phénomènes physiques, donne des indications sur les processus d'émission (scintillateurs, semi-conducteurs, etc.).

La détermination des temps de montée par la méthode oscillographique présente de grandes difficultés dès que l'on atteint la millimicroseconde, car il est impossible d'amplifier le signal sans le déformer. L'attaque d'un oscilloscope à ondes progressives ne peut se faire qu'avec des signaux de grande amplitude. L'adaptation d'impédance et l'obtention de deux signaux en opposition de phase posent également des problèmes très complexes.

De plus, pour des impulsions non récurrentes, il est très difficile d'effectuer rapidement par la méthode oscillographique un nombre suffisant de mesures pour obtenir une précision statistique convenable. Il est évident que les fluctuations des temps de montée échappent à cette méthode de mesure, alors que leur connaissance présente un grand intérêt dans la détermination de la résolution des appareillages destinés aux mesures de temps courts et dans l'étude des phénomènes donnant naissance aux impulsions.

1. Principe de la Méthode

La méthode proposée est basée sur la mesure du temps mis par l'impulsion pour franchir deux seuils d'amplitudes connues. Pour cela l'impulsion étudiée est coupée sur deux voies différentes par des discriminateurs dont on peut faire varier les seuils. Les deux signaux ainsi obtenus sont appliqués à des circuits de mise en forme destinée à les standardiser.

Ces impulsions sont alors envoyées à un circuit de conversion temps-amplitude opérant la mesure du temps les séparant.

Les mesures d'intervalles de temps de l'ordre de la millimicroseconde s'effectuent généralement à l'aide de circuits à coïncidences rapides[1]). L'extrapolation de ces circuits a conduit à la conversion temps-amplitude qui transforme la mesure du temps séparant deux impulsions, en une mesure d'amplitude[2,3]).

L'utilisation d'un sélecteur multicanaux classique devient alors possible pour des mesures directes de temps: chaque canal du sélecteur

[1]) Z. Bay, I.R.E. Transactions NS **3** (1956) 4, 12; Nucleonics **14** (1956) 4, 56.

[2]) G. C. Neilson et D. B. James, Rev. Sci. Inst. **26** (1955) 1018.

[3]) J. Samueli et A. Sarazin, J. Phys. et Rad. **19** (1958) 109A.

correspond à une valeur d'intervalle de temps entre les deux impulsions d'entrée; l'histogramme est donc le relevé du nombre de couples d'impulsions séparées par un temps t en fonction de t.

Les mesures effectuées à l'aide de tels circuits permettent d'obtenir non seulement la valeur moyenne de la variable aléatoire étudiée t, mais encore ses divers moments. Appelons $f(t)$ la densité de probabilité de t. Pour une valeur de t l'indication de l'appareillage sera $T = t + X$ où X est une variable aléatoire indépendante de t, liée à la limite de résolution des circuits de conversion: c'est l'indication aléatoire de ces derniers pour deux signaux simultanés. Si on désigne par $P(X)$ la densité de probabilité de X qui définit la courbe de résolution des circuits de conversion et par $N(T)$ la densité de probabilité qui définit la réponse des circuits à l'ensemble des paires d'impulsions séparées par toutes les réalisations de la variable aléatoire t, on a d'après une relation classique dans l'addition des variables aléatoires indépendantes

$$N(T) = \int_{-\infty}^{+\infty} P(T - t)\, f(t)\, \mathrm{d}t\,. \qquad (1)$$

Une méthode de détermination de $f(t)$ consiste à utiliser des relations entre les moments des diverses variables aléatoires introduites[1]). Posons

$$M_K(N) = \overline{(X + t)^K} = \int_{-\infty}^{+\infty} T^K N(T)\, \mathrm{d}t\,.$$

On a

$$M_K(N) = \sum_{j=0}^{K} C_K^j\, X^{K-j}\, t^K\,.$$

A cause de l'indépendance de X et t

$$M_K(N) = \sum_{j=0}^{K} C_K^j\, X^{K-j}\, t^K = \sum_{j=0}^{K} C_K^j M_{K-j}(P) \cdot M_j(f)\,.$$

Pour $K = 1$, on a, évidemment $\bar{t} = \overline{(X + t)} - \bar{X}$ soit:

$$\int_{-\infty}^{+\infty} t \cdot f(t)\, \mathrm{d}t = \int_{-\infty}^{+\infty} t \cdot N(t)\, \mathrm{d}t - \int_{-\infty}^{+\infty} t \cdot P(t)\, \mathrm{d}t\,.$$

La valeur moyenne de la variable aléatoire t (temps séparant les deux impulsions) est égale à la distance des abscisses des centres de gravité des surfaces $N(T)$ et $P(T)$, (les surfaces étant normées). L'obtention de la densité $f(t)$ peut se faire par l'intermédiaire des fonctions caractéristiques de X et T c'est-à-dire des transformées de Fourier des densités. On a

$$p(\nu) = \overline{\exp\,(+\,2\pi i \nu X)} = \int_{-\infty}^{+\infty} P(X) \exp\,(+\,2\pi i \nu X)\, \mathrm{d}X$$

$$n(\nu) = \overline{\exp\,(+\,2\pi i \nu T)} = \int_{-\infty}^{+\infty} N(T) \exp\,(+\,2\pi i \nu T)\, \mathrm{d}T$$

$$f(t) = \int_{-\infty}^{+\infty} \varphi(\nu) \exp\,(-\,2\pi i \nu t)\, \mathrm{d}\nu\,.$$

Dans l'espace des fréquences ν, la relation (1) devient:

$$n(\nu) = p(\nu) \cdot \varphi(\nu) \qquad (2)$$

relation d'ailleurs évidente puisque T est la somme des variables aléatoires X et t. Donc,

$$f(t) = \int_{-\infty}^{+\infty} \frac{n(\nu)}{p(\nu)} \exp\,(-\,2\pi i \nu t)\, \mathrm{d}\nu\,.$$

2. Montage Electronique

La figure 1 donne le schéma du dispositif de conversion qui comprend tout d'abord deux voies identiques de mise en forme.

Chacune de ces voies est constituée par un tube limiteur chargé par une ligne à retard qui, pour tout signal négatif d'amplitude et de largeur suffisantes, fournit une impulsion standardisée. Ce tube est suivi d'un étage amplificateur.

A la sortie des tubes amplificateurs V_2 et V_4 on est donc en présence de deux signaux identiques séparés par le temps à mesurer. Ces deux impulsions attaquent alors un circuit d'addition constitué par V_5 et V_6 dont la charge commune est de nouveau une ligne à retard. Les signaux subissent ainsi une seconde mise en forme avant d'être additionnés. Appelons τ le temps de propagation dans la ligne. Si nous choisissons 2τ inférieur au temps de montée des impulsions standardisées qui arrivent sur les grilles des tubes d'addition, ces impulsions sont coupées avant d'avoir atteint leur maximum et ont une forme triangulaire.

Les figures 2 et 3 indiquent respectivement la forme du signal sur une voie et le processus d'addition.

Soient S la pente des impulsions rendues triangulaires, $2A$ leur largeur à la base et t le

temps les séparant. L'amplitude du signal de sortie du circuit additif est:

$$St + 2S\,(A - t) = S\,(2A - t)\,.$$

Ce signal est coupé par une diode polarisée au seuil SA. Le signal de sortie proportionnel à $S(A - t)$ est alors amplifié en augmentant son temps de montée de façon à pouvoir être envoyé sur un sélecteur RIDL à 100 canaux. sélecteur latéral, un signal de coïncidence est envoyé sur l'analyseur 100 canaux qui enregistre alors l'information fournie par le convertisseur temps-amplitude.

3. Mesures

L'ensemble décrit nous a servi à l'étude d'impulsions récurrentes et non récurrentes. Les premières étaient fournies par un relais

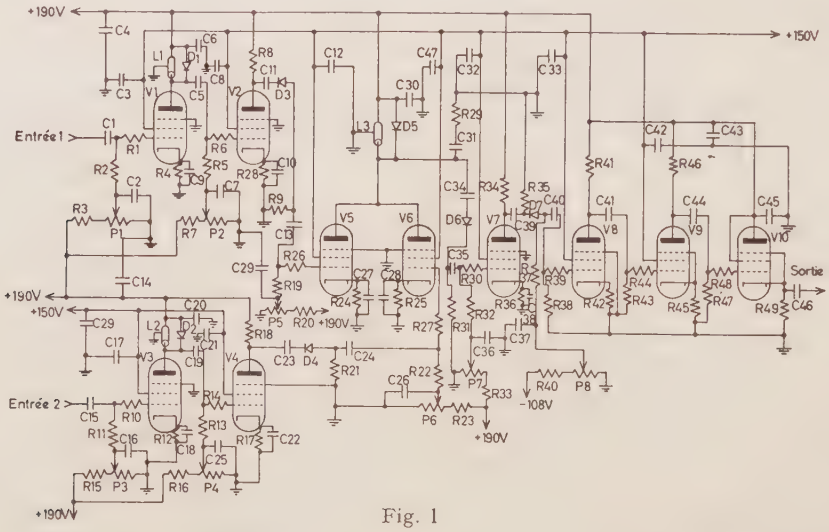

Fig. 1

V_1 à V_7	E180F	D_3-D_4	GEX66
V_8	EF80	D_5	.0A9
V_9-V_{10}	EL83	D_6	IN82A
D_1-D_2	OA5	D_7	15P2

L_1, L_2	1.5 mètre	Z =	170 ohms
L_3	0.7 mètre	Z =	170 ohms
P_1 à P_8	5000 ohms		

Résistances (ohms)

1, 6, 10, 14, 26, 27, 30	68	31, 39, 41, 44, 48	1 000
45	120	2, 5, 11, 13, 19, 22, 32	4 700
49	150	37	6 800
42	180	35	27 000
8, 9, 18, 21, 29, 34	200	38	47 000
4, 12, 17, 24, 25, 28, 36	390	3, 7, 15, 16, 20,	
46	470	23, 33, 40, 43, 47	100 000

Capacités

43	470 picofarads
1, 5, 6, 9, 10, 11, 13, 15, 18, 19, 20, 22, 23, 24, 27, 28, 30, 31, 34, 35, 38, 39, 40, 41	10 000 picofarads
3, 8, 12, 17, 21, 32, 44, 46, 47	22 000 picofarads
2, 7, 16, 25, 26, 29, 33, 36, 37, 52, 45	0.1 microf.
4, 29	16 microf.

Nota

Les filaments des tubes sont découplés par 100 picofarads. La tension chauffage est stabilisée à 0.5% et les hautes tensions à 1/1000.

Le circuit complet de mesure est donné figure 4. L'impulsion étudiée est appliquée directement à des discriminateurs à diodes polarisées suivis de deux étages cathodynes. Un troisième cathodyne transmet l'impulsion à un circuit de sélection latéral qui permet de fixer l'amplitude des impulsions étudiées. Lorsqu'un signal correspond à l'amplitude acceptée par le à mercure; les secondes par un scintillateur plastique.

Ce sont les impulsions étudiées qui, dans chaque cas, servent à l'étalonnage et à la détermination de la résolution du circuit.

Les deux seuils des discriminateurs étant égaux, on introduit artificiellement des retards variables dans l'une des deux voies avec des

câbles de longueurs différentes. Le sélecteur multicanaux enregistre alors pour chaque valeur du retard la courbe de résolution $P(T)$ définie

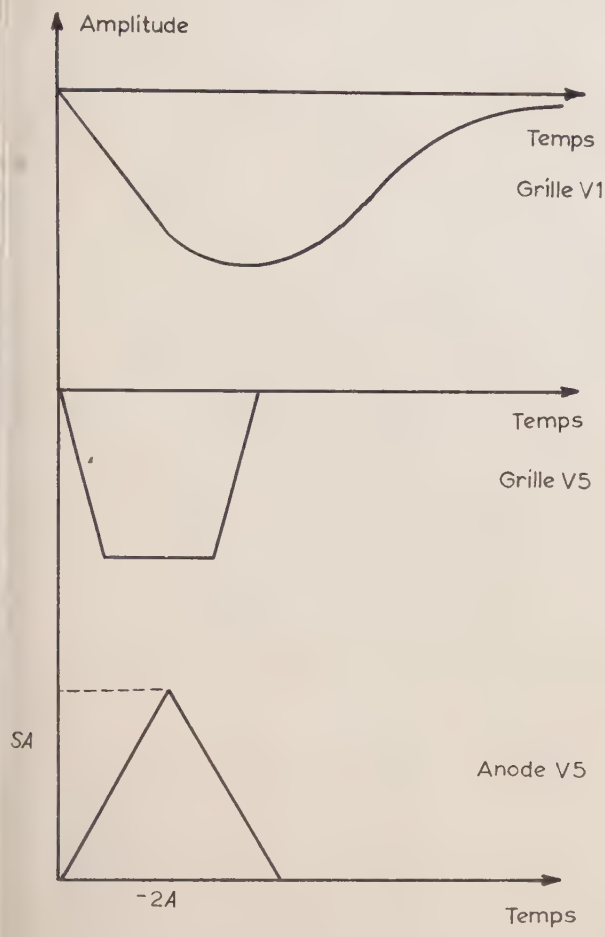

Fig. 2

précédemment. L'abscisse du centre de gravité de la surface limitée par $P(T)$ et l'axe des T définit l'amplitude correspondant à un retard donné.

Pratiquement pour des mesures de temps de montée $P(T)$ est gaussien et l'abscisse du centre de gravité coïncide avec l'abscisse du maximum. La demi-largeur à mi-hauteur de $P(T)$ définit la résolution du circuit, l'ensemble des valeurs obtenues pour des retards différents constitue la courbe d'étalonnage.

Lorsqu'on effectue la mesure du temps de montée, les seuils sont ajustés à des valeurs différentes et le sélecteur enregistre la courbe $N(T)$.

Dans le cas où $N(T)$ est également gaussien la valeur de l'abscisse de son maximum donne immédiatement la valeur moyenne du temps mis par l'impulsion pour passer du premier au second seuil.

La figure 5 donne le montage qui précède le convertisseur dans le cas des impulsions récurrentes du générateur à relais à mercure.

L'impédance de sortie du générateur était de 75 ohms. Pour réduire au maximum l'influence des capacités parasites un diviseur à résistances ramenait l'impédance à l'entrée du circuit à 7 ohms.

L'amplitude des impulsions aux bornes de cette impédance était de 7 volts. Nous avons étudié point par point l'impulsion de 0 à 5 volt et trouvé un temps de montée linéaire de pente 9.6×10^{-11} seconde par volt. La valeur du temps de montée de 0 à 5 volts a été trouvée égale à $(4.8 \pm 0.5) \times 10^{-10}$ seconde.

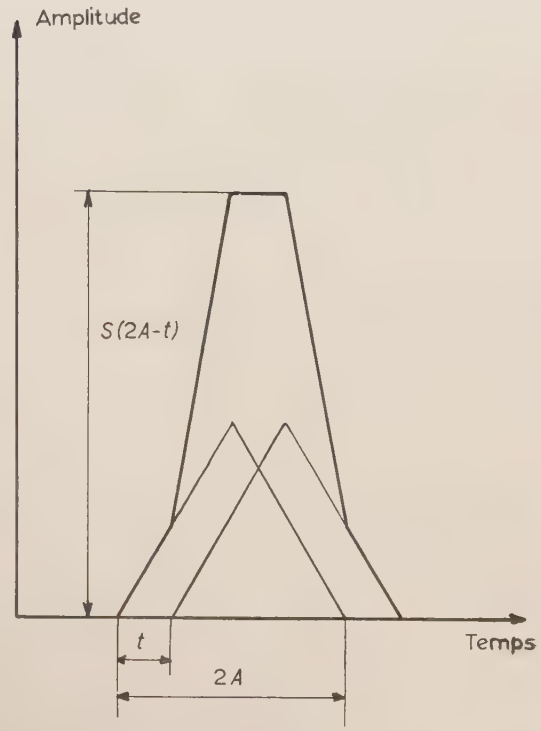

Fig. 3

Dans la seconde application, le but était la détermination de la constante de décroissance d'un scintillateur plastique. Le photomultipli-

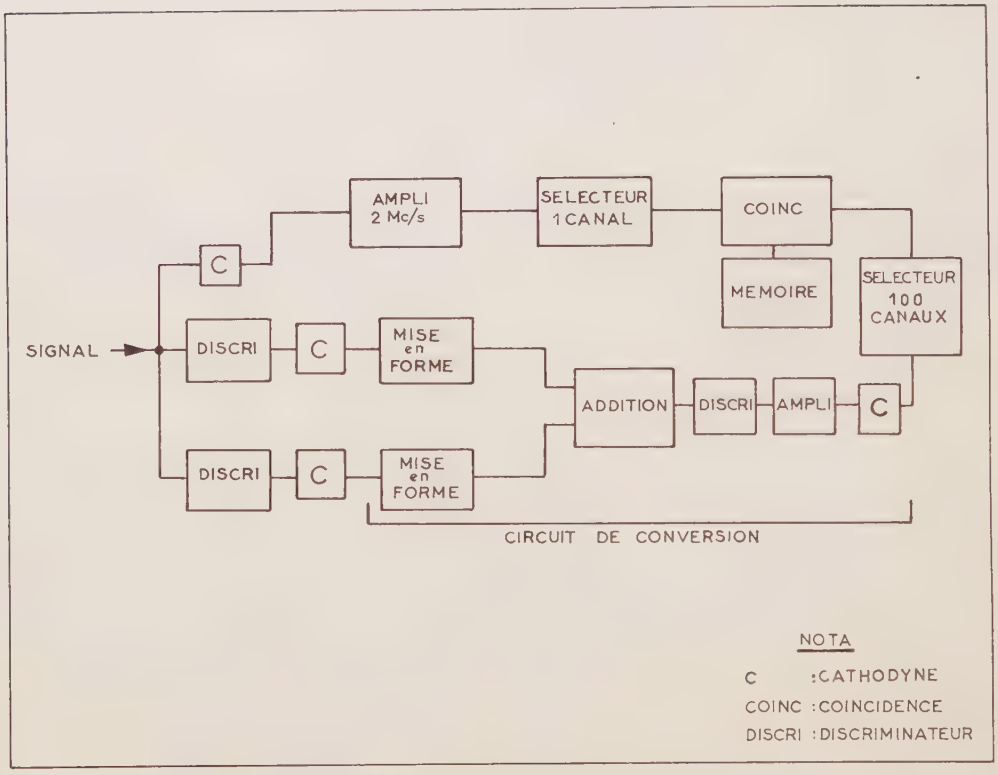

Fig. 4

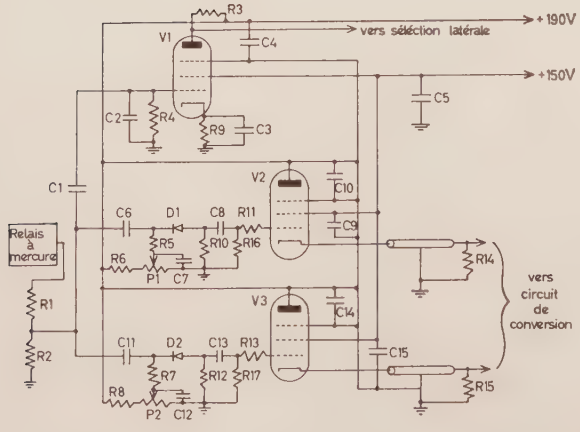

Fig. 5

V_1 EF80 — V_2, V_3 E180F — D_1, D_2 IN56A

Résistances (ohms)

P_1, P_2	10 000	14, 15	75	16, 17	47 000
2	7	9	150	3, 4, 6, 8	100 000
1, 11, 13	68	5, 7	10 000	10, 12	560 000

Capacités (picofarads)

1	5	—	2	68	—	3 à 15	10 000

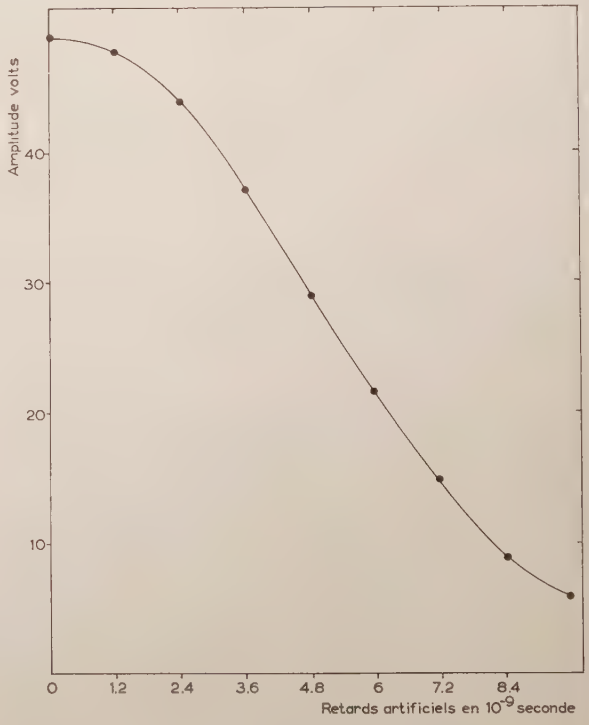

Fig. 6

cateur utilisé était un 51AVP Radiotechnique et le scintillateur "Nuclear Enterprise" était excité par les particules béta d'une source de phosphore 32.

En première approximation la réponse d'un ensemble scintillateur solide-photomultiplicateur à des particules est de la forme:

$$V(t) = \frac{Q}{C_A} \frac{\tau_1}{\tau_0 - \tau_1} [\exp(-t/\tau_0) - \exp(-t/\tau_1)]$$

où

τ_0 est la constante de décroissance du scintillateur

$\tau_1 = RC_A$, la constante de temps de l'électronique

R la résistance de charge anodique du P.M.

C_A la capacité parasite d'anode

Q la quantité d'électricité totale arrivant sur l'anode pour une impulsion.

Si on intègre l'impulsion, c'est-à-dire si τ_1 est très supérieur à τ_0 on a sensiblement:

$$V(t) \approx \frac{Q}{C_A} (1 - \exp(-t/\tau_0))$$

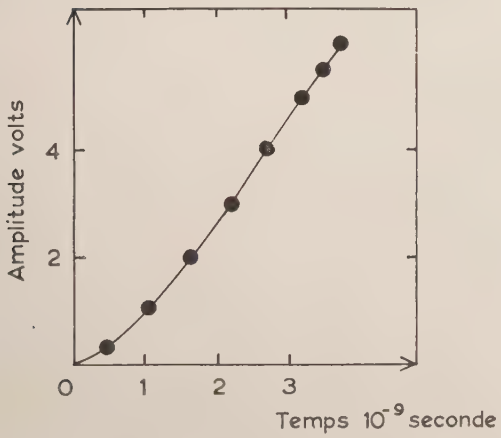

Fig. 7

c'est-à-dire que pour $t = \tau_0$ l'amplitude de l'impulsion est la fraction 1 — 1/e de l'amplitude maximum. Le sélecteur latéral fixait cette amplitude à 8 volts.

On obtient donc τ_0 en mesurant le temps de montée de l'impulsion de 0 à 63% de son amplitude.

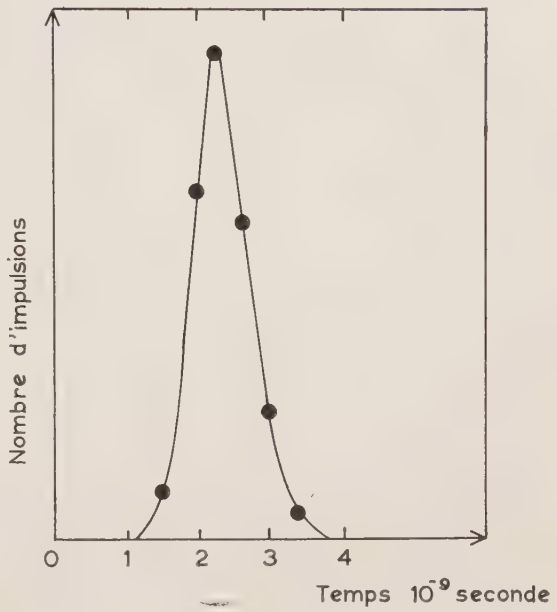

Fig. 8

Les figures 6, 7 et 8 indiquent la courbe d'étalonnage, le tracé de l'impulsion et les fluctuations.

La constante τ_0 a été trouvée égale à $(3.8 \pm 0.7) \times 10^{-9}$ sec.

Des mesures portant sur la scintillation du xénon excité par des particules alpha ont été effectuées par M. Bougnot avec cet appareillage†.

Remerciements

Les auteurs souhaitent exprimer tous leurs remerciements à M. le Professeur A. Blanc-Lapierre, Directeur de l'Institut d'Etudes Nucléaires d'Alger pour les conseils et l'aide qu'il leur a apportés.

† Publication à paraître.

NUCLEAR INSTRUMENTS AND METHODS 5 (1959) 50–55; NORTH-HOLLAND PUBLISHING CO.

THE ENERGY DEPENDENCE OF THE CORNELL THICK-WALLED IONIZATION CHAMBER†

F. J. LOEFFLER, T. R. PALFREY and G. W. TAUTFEST

Department of Physics, Purdue University, Lafayette, Indiana

Received 20 April 1959

The absolute response of a thick-walled ionization chamber of the Cornell design has been determined in the energy region of 60–322 MeV. The determination is the result of (1) intercomparisons with chambers calibrated absolutely at other laboratories, (2) absolute calibration at two energies at this laboratory, and (3) measurements of the relative energy dependence by pair-spectrometer and $Cu^{63}(\gamma,n)Cu^{62}$ activation methods. A plot of the results obtained is given and a comparison with the prediction of shower theory is made.

1. Introduction

The determination of photon cross sections from activation measurements made as a function of the peak energy of the incident bremsstrahlung is a well-known technique in nuclear physics. In order to avoid gross distortions in the derived photon cross section, the behavior of the monitor used in the activation measurements as a function of the bremsstrahlung energy must be accurately known. To date, the most widely used monitor for photon beams up to a peak energy of 500 MeV has been the ionization chamber developed at Cornell. A description of this chamber has been given in a Cornell University progress report[1]). The chamber is constructed with 1-inch Cu walls which are of a thickness such that the charge collected is largely due to ionization by electrons of a shower near the shower maximum for a large range of energies. Since the number of electrons at the shower maximum per incident photon is roughly proportional to the photon energy[2]), the charge collected is roughly proportional to the total energy in the beam. To the extent to which these assumptions are valid, the sensitivity of the chamber when expressed in units of MeV/coulomb is independent of photon energy.

A number of articles[1,3,4,5]) have reported calibrations of chambers of this design at energies in the neighborhood of 300 and 500 MeV, but the agreement between laboratories is only $\approx 10\%$. The present work was undertaken because of these discrepancies in the absolute response of the chamber and to determine the dependence on photon energy.

2. Procedure

2.1. INTERCOMPARISONS

The chamber used in these experiments was constructed at Cornell University and was brought to Purdue in 1952. It was one of a number that were intercalibrated[1]) there by the use of (1) a pair spectrometer and (2) the Blocker-Kenney-Panofsky shower method[2]). The absolute response of the chamber was obtained at three energies with an accuracy of 5%: the results (at 0° C and 760 mm Hg) are 3.74×10^{18} MeV/coulomb at 315 MeV, 3.59×10^{18} MeV/coulomb at 250 MeV, and 3.47×10^{18} MeV/coulomb at 197 MeV[6]).

† Supported in part by the U.S. Atomic Energy Commission.

[1]) Corson, DeWire, McDaniel and Wilson, The Cornell 300-MeV Synchrotron, Office of Naval Research (1953).

[2]) Blocker, Kenney and Panofsky, Phys. Rev. **79** (1950) 419.

[3]) Walker, Oakley and Tollestrup, Phys. Rev. **97** (1955) 1279.

[4]) D. C. Oakley and R. L. Walker, Phys. Rev. **97** (1955) 1283.

[5]) D. R. Dixon and K. C. Bandtel, Phys. Rev. **104** (1956) 1730.

[6]) Private communication from J. DeWire.

In April 1958 this chamber was taken to the National Bureau of Standards and compared with the response of the P-2 monitor chamber which has been developed there[7]). This chamber is constructed with a dural wall 3.7 inches thick and has been calibrated by calorimetric methods[7]) and by counting the number of photons in the beam with a NaI(Tl) spectrometer[8]). The absolute response of the chamber in the energy region 10–180 MeV is believed to be known to 3%[9]). The Cornell chamber response was compared with that of the P-2 chamber in the X-ray beam from the NBS 180-MeV synchrotron at peak bremsstrahlung energies of 60, 90 and 130 MeV. A number of runs were taken at each energy with a reproducibility of 1%. The ratio of the Cornell chamber response to that of the P-2 chamber per unit P-2 response was 0.645 at 60 MeV, 0.646 at 90 MeV, and 0.676 at 130 MeV. These ratios yield the following absolute response of the Cornell chamber at STP; 3.40×10^{18} MeV/coulomb at 60 MeV, 3.28×10^{18} MeV/coulomb at 90 MeV, and 3.16×10^{18} MeV/coulomb at 130 MeV.

2.2. SHOWER METHOD

The "balanced converter" method of Blocker, Kenney and Panofsky[2]) was used to determine the absolute response of the chamber at peak bremsstrahlung energies of 318 and 250 MeV. The collimated X-ray beam from the synchrotron was brought through a clearing magnet and thin-walled monitor chamber by an evacuated pipe to a second thin-walled monitor chamber. The number of electrons produced by the bremsstrahlung beam in a foil placed immediately in front of the second chamber was measured as a function of the thickness and atomic number of the foil. Foils of C, Al, Cu, Sn and Pb were used ranging in thickness from 10^{-3} to 10^{-1} radiation lengths. As described by the authors[2]), these measurements allow the ionization due to Compton electrons to be subtracted from the total ionization observed. The remainder is compared with the theoretical number of pair electrons created in the foils to determine the number of photons in the beam. The response of the thick-walled chamber was then compared with that of the first monitor chamber.

A number of runs were taken for each thickness of foil of a given atomic number. The grand average of the runs when corrected to STP yields $3.94 \pm 0.15 \times 10^{18}$ MeV/coulomb at 318 MeV and $3.49 \pm 0.15 \times 10^{18}$ MeV/coulomb at 250 MeV. The errors are based on the internal consistency of determinations from various combinations of foils of different atomic number at a given energy.

2.3. RELATIVE ENERGY DEPENDENCE

a. Pair Spectrometer

An ideal electron-positron pair spectrometer samples one region, Δk, of the bremsstrahlung spectrum and gives a total number of counts proportional to the number of photons between k and $k + \Delta k$. The number of pairs counted, N_p, when the radiator is bombarded with Q effective quanta, will be given by:

$$N_p = QNt \int\int \Phi_+(k,E_+)\, \Phi(k,k_0)\, \varepsilon(k)\, \mathrm{d}k\mathrm{d}E_+ \qquad (1)$$

where Nt is the target thickness in atoms-cm^{-2}, $\Phi_+(k,E)_+$ is the differential positron cross section, $\Phi(k,k_0)$ is the bremsstrahlung spectrum, and $\varepsilon(k)$ is the efficiency of the pair spectrometer. Simultaneously the ionization chamber will measure a number of coulombs q:

$$q = Q \int k\, \Phi(k,k_0)\, \mathrm{d}k / R(k_0) \qquad (2)$$

where $R(k_0)$ is the ionization chamber response in MeV/coulomb.

Normalizing to the same number of coulombs one can combine equations (1) and (2) at two different peak energies of the bremsstrahlung to find the ratio of monitor responses at these two energies, k_0 and k'_0:

$$R(k_0) = R(k'_0)\, \frac{N_p}{N'_p} \frac{\int k\, \Phi(k,k_0)\, \mathrm{d}k}{\int k\, \Phi(k,k'_0)\, \mathrm{d}k} \times \frac{\int\int \Phi_+k,E_+)\, \Phi(k,k'_0)\, \varepsilon(k)\, \mathrm{d}k\mathrm{d}E_+}{\int\int \Phi_+(k,E_+)\, \Phi(k,k_0)\, \varepsilon(k)\, \mathrm{d}k\mathrm{d}E_+}. \qquad (3)$$

[7]) J. S. Pruitt and S. R. Domen, N.B.S. Report No. 6218.
[8]) Leiss, Pruitt and Schrack, N.B.S. Report No. 6149.
[9]) Private communication from E. V. Fuller.

If, for all k_0 measured, k is below the knee of the bremsstrahlung spectrum and k is high enough so that the pair cross section is slowly varying, then moderately high resolution of the pair spectrometer will make $\varepsilon(k)$ a very sharp function, and the relative monitor response function is very nearly given by:

$$R(k_0) = R(k'_0) \frac{N_p}{N'_p} \frac{k_0}{k'_0} \frac{\Phi(k,k'_0)}{\Phi(k,k_0)} \tag{4}$$

in which the primes refer to measurements at a second value of k_0, and where k now signifies the photon energy for which the spectrometer is set.

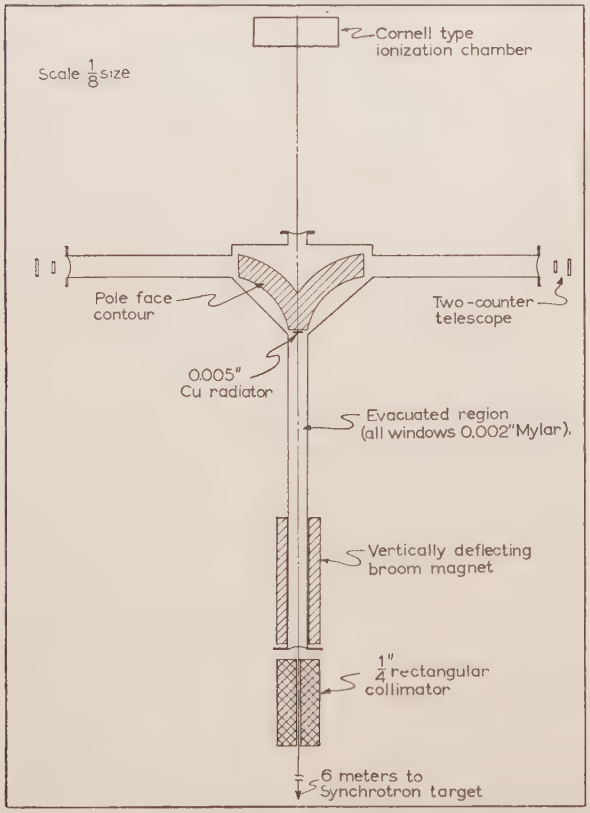

Fig. 1. Pair spectrometer arrangement. (Shielding and return iron not shown.)

In the instrument used in this experiment, shown in fig. 1, the resolution was 6% in photon energy, full width at half maximum. The principal effect of this width is to shift slightly the value of k at which $\Phi(k,k_0)$ in eq. (4) should be evaluated.

Both positrons and negatrons were deflected through 90° and detected in counter telescopes consisting of two 1″ × 1″ plastic scintillators 0.125″ thick. A four-fold coincidence of 4×10^{-8} sec resolution indicated a pair. The background counting rate with the 0.005″ Cu radiator removed from the evacuated system was measured to be less than 1% of the foil-in rate.

The major problem in operating a one-channel pair spectrometer at fairly high resolution is that the ratio of singles to pairs is approximately proportional to the resolution. As a consequence chance coincidence rates are not usually negligible. In this experiment the chance rate was continually monitored by taking delayed coincidences between one positron counter and one electron counter, and, from time to time, the counting rate for delayed quadruple coincidences (true positron coincidence delayed with respect to true electron coincidence) was measured. Since by far the largest source of chance rate was between true electrons and true positrons, these measurements allowed satisfactorily precise knowledge of the effect of chance coincidences. The chance rate did not exceed 7% of the total rate in any run.

In deciding to what extent one can reliably go from eq. (3) to eq. (4), one must take into account the effects which reduce the resolution or otherwise influence the numbers to be used in eq. (4). The 6% finite-target finite-detector resolution, measured by floating wire methods, has to be modified for the effects of:

1. The angles between the photon and the e^+ and e^- in pair production.

2. Multiple scattering of the emergent particles in the converter.

3. Radiation by the electron and positron in the converter.

4. Scattering into the detector system of particles which would not otherwise have been counted, e.g. from the exit snout of the vacuum tank.

5. Effect of the spreading out in time of the gamma-ray beam on the average peak energy k_0.

The first four of these effects have been estimated and have the principal result of changing

slightly the effective value of k to use in eq. (4). Since k appears in the ratio of $\Phi(k,k_0)$ to $\Phi(k,k'_0)$, the net effect in these relative determinations is negligible at the resolution used. The fifth effect requires that the value of k_0 used be calculated

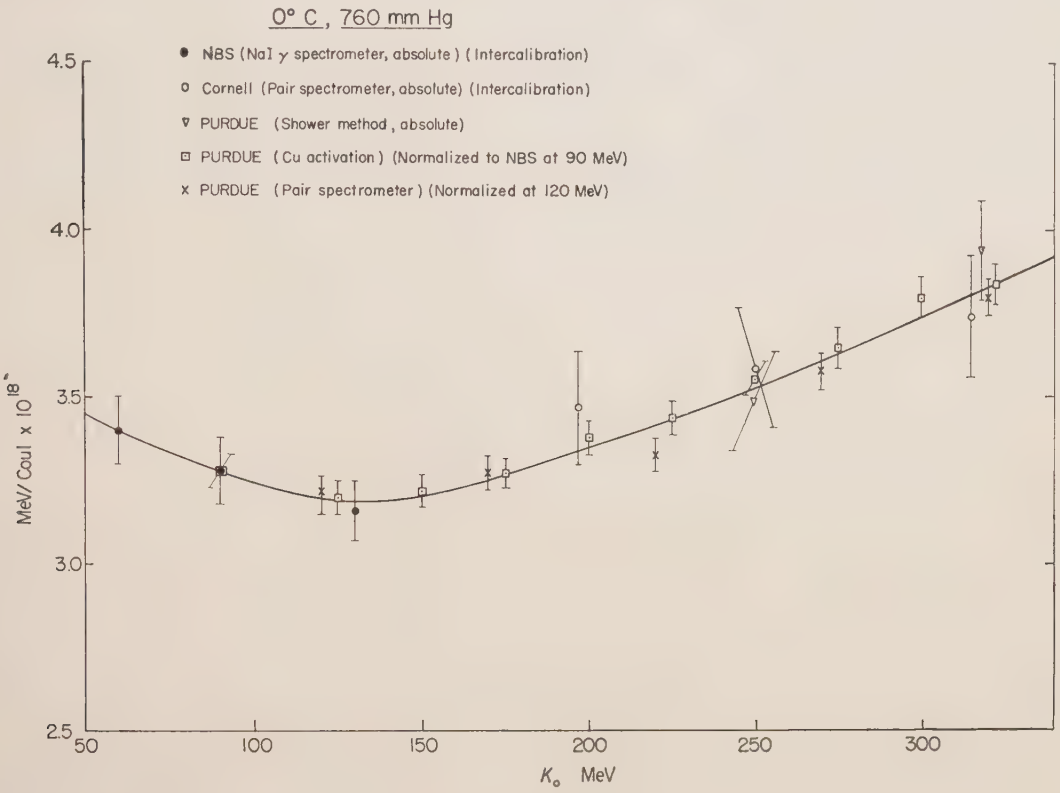

Fig. 2. Measured response of the Cornell chamber as a function of peak bremsstrahlung energy.

from the known electron energy in the synchrotron as a function of time, and that the values of k_0 and k'_0 used be the appropriate average energies.

Data was taken at central values of k of 56, 73 and 75 MeV for k_0 of 121, 173, 220, 269 and 320 MeV. The normalization point k'_0 was chosen to be 121 MeV; R (121 MeV) was set equal to 3.21 ± 0.05. The results are shown in fig. 2.

b. $Cu^{63}(\gamma,n)Cu^{62}$ *Activation*

The cross section for the reaction $Cu^{63}(\gamma,n)Cu^{62}$ has been measured up to 38 MeV by Berman and Brown[10]). They find that the cross section has the familiar resonance shape, rising to a peak value at a photon energy of 18 MeV and dropping rapidly to an insignificant value at 38 MeV. Their reported value for the integrated cross section is 0.55 MeV-barn. Leiss has compared the excitation of the reaction with the response of the Kerst-Edwards chamber[11]) in the energy range 100–270 MeV and finds that the yield curve is consistent with zero cross section above 38 MeV. We have measured the yield of the reaction by counting the 9.9 min positron activity in copper foils of natural isotopic abundance following exposure in the bremsstrahlung beam from the synchrotron. The activity was counted in 4π geometry with constant discriminator setting. Drift in the counter electronics was corrected for by normalizing to the activity of a standard In^{114}

[10]) A. I. Berman and K. L. Brown, Phys. Rev. **96** (1954) 83.

[11]) J. Leiss, Doctoral Thesis University of Illinois (1955) (unpublished).

source. Assuming that the $Cu^{63}(\gamma,n)Cu^{62}$ reaction has the value determined by Berman and Brown[10]) and that the cross section is zero for photon energies above 40 MeV, we have calculated a yield curve in the energy range 80–322 MeV and, by fitting our yield points, obtained the energy dependence of the thick-walled ionization chamber in this energy range.

3. Monitor Response Calculations

In order to obtain a semiquantitative understanding of the shape of the monitor response was constructed which estimated the ionization on the basis of (1) the attenuation of the photons before they reach a point in the copper from which their pair or Compton electrons could reach the air of the chamber, and (2) a weighting of the ionization by the thickness of copper from which the electrons from a given photon could be coming and still contribute to the ionization. The two parts of $I(k)$ were fitted smoothly to each other in the neighborhood of 20 MeV and the indicated integrations were carried out.

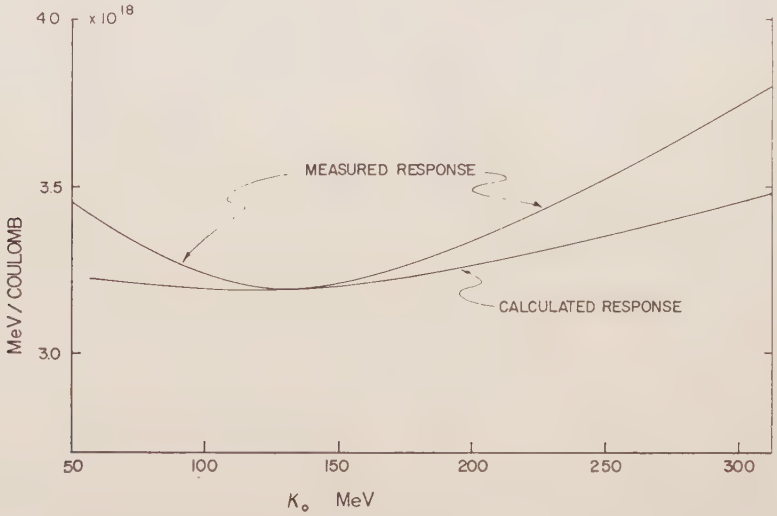

Fig. 3. Comparison of measured response of the Cornell chamber to a calculated response as a function of peak bremsstrahlung energy.

curve (fig. 2), an attempt was made to calculate the expected response. If $I(k)$ is the expected ionization in a Cornell type ionization chamber per photon of energy k incident normal to the chamber wall, and $\Phi(k,k_0)$ is the bremsstrahlung spectrum of peak energy k_0, then the expected ionization per unit energy in the incident beam is given by the expression:

$$R^{-1}(k_0) = \int_0^{k_0} k\Phi(k,k_0)\,\mathrm{d}k \Big/ \int_0^{k_0} I(k)\Phi(k,k_0)\,\mathrm{d}k\,.$$

In the calculations performed we used the spectra given by Leiss and Penfold[12]). For the ionization above 20 MeV we used the Monte Carlo results of R. R. Wilson[13]), with arbitrary normalization. Below 20 MeV a simple theory

The results of the calculation are compared to the experimental curve in fig. 3 with arbitrary normalization at 120 MeV.

The qualitative features of the curve are reasonably well reproduced. In order to obtain better agreement it would be necessary to decrease for energies below 10 MeV the values of $I(k)$ calculated on the model used—hardly surprising in view of the crudity of the estimate of the ionization below 20 MeV. In order, however, to imitate the observed rise of the chamber response above 150 MeV peak brems-

[12]) Analysis of Photo Cross Sections, Penfold and Leiss, Physics Research Laboratory, University of Illinois (May 1958).

[13]) R. R. Wilson, Phys. Rev. **86** (1952) 261.

strahlung, it would also be necessary to increase the ionization at high photon energies above that given by the Monte Carlo curves, possibly by inclusion of the effects of back-scatter.

4. Results

The measurements described above are presented in figure 2 as a function of peak bremsstrahlung energy. The solid line is a smooth fit to the experimental points. In fig. 3, the predicted response is shown with the smoothed experimental data.

Acknowledgements

We wish to thank Mr. R. Fessel for his assistance in taking and reducing the shower data, and Mr. L. Mortara and Mr. F. Liu for their assistance in all phases of the pair spectrometer work. Mr. Edward Metcalf was always helpful in operating the synchrotron. We are grateful for the cooperation and hospitality of Drs. J. Leiss and S. Penner at the National Bureau of Standards during the intercalibration, and for the interest and helpful discussion with Professor J. DeWire of Cornell University.

NUCLEAR INSTRUMENTS AND METHODS 5 (1959) 56–60; NORTH-HOLLAND PUBLISHING CO.

PRECISION SCHMITT TRIGGER†

ARIEH FISCHMANN-ARBEL

Scientific Department, Ministry of Defence, Israel

Received 17 April 1959

A modified Schmitt Trigger is described which combines the principle of the original circuit with the stability of a cathode coupled difference amplifier. Its hysteresis may be closely controled by choosing suitable circuit values. Compared with the conventional Schmitt Trigger, this circuit represents an improvement in drift and hysteresis by at least one order of magnitude.

1. Introduction

The performance of a discriminator is determined by its hysteresis, and by its drift as compared with the maximum signal it is capable to accept without being overloaded. The hysteresis limits the maximum sensitivity of the discriminator; the drift determines the accuracy of discrimination, and is usually constant over the total range.

In pulse height analysis it is desirable to obtain ratios between maximum applicable pulse input and drift of 1000:1. The drift of a conventional Schmitt Trigger being of the order of 0.1 volt, maximum pulse amplitudes of 100 volts are required to obtain this accuracy. The hysteresis is usually of the order of 1 volt.

It has been the purpose of this investigation to build a discriminator having a drift of not more than 10 mV, and a hysteresis of less than 100 mV. This enables one to use pulse amplifiers giving a maximum output of 10 volts only, with the obvious advantages of saving power, increasing speed and linearity and also making possible their transistorization.

2. The Schmitt Trigger Prototype

Among the various discriminators, the Schmitt Trigger occupies a unique position. Firstly, because it acts as a true discriminator comparing the instantaneous value of two potentials independent of rise time and repetition frequency; secondly because at very large signals it acts as a cathode follower which is difficult to overload; finally, it is capable of accepting positive or negative pulses, because of its symmetrical action.

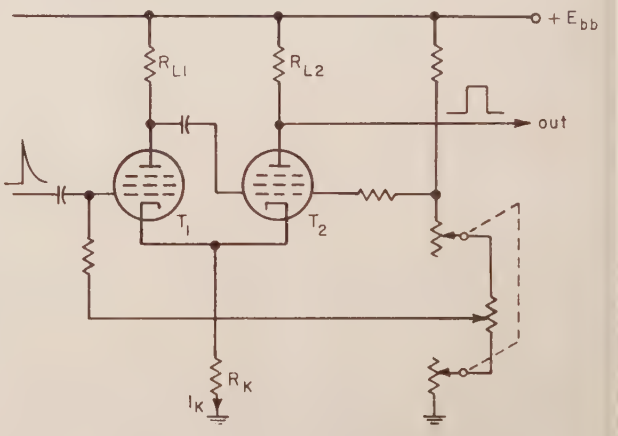

Fig. 1. AC coupled Schmitt Trigger.

Fig. 1 shows the AC coupled version of a Schmitt Trigger which has the advantage of greater loopgain over the DC coupled circuit. If properly designed it will still be insensitive to changes in rise time and repetition frequency of the incoming pulses, in spite of the AC coupling. In the appendix it is shown that

$$R_{L1} = \frac{1}{gm_1} + \frac{1}{gm_2} \qquad (1)$$

is the condition for the loop gain to be greater than one, assuming that R_k and the internal

† Patent pending.

resistances of T_1 and T_2 are considerably greater than R_{L1} and R_{L2}. It is further approximately true that the hysteresis equals $\Delta i \cdot R_{L1}$†, where Δi denotes the change of platecurrent in each tube, during the regenerative action. In a conventional Schmitt Trigger, Δi is only slightly smaller than the total cathode current I_k, and the hysteresis is accordingly considerable.

Although condition (1) disregards the existence of stray capacities, it is clear that their presence will affect the loopgain adversely at high frequencies. In other words, unless R_L is considerably greater than $(1/gm_1) + (1/gm_2)$, the rise time of the regenerative output pulse will be poor. On the other hand, a large R_L adversly affects the hysteresis.

The exact level of comparison is determined by the potential difference between the grids of T_1 and T_2, at which condition (1) is obtained. At this point, one tube is nearly fully conducting, whereas the other one is still very close to cut off. Changes in the heater voltage of T_1 and T_2 will therefore have an unequal influence on their gm, and will considerably affect the stability of the discrimination level.

3. The New Circuit

Fig. 2 shows the new circuit in principle. It should again be assumed that R_k and the internal resistances of T_1 and T_2 are considerably greater than R_{L1} and R_{L2}. R_k may therefore be replaced by a constant current source. D_1 and D_2 will be considered to be ideal diodes.

If T_1 is initially cut off, and a positive pulse is delivered to its grid, the following three phases of operation may be distinguished:

1. If $i_{p1}R_{L1} < i_{p2}R_{L2}$, D_1 is conducting. R_{L1} and R_{L2} are therefore connected in parallel, and as $i_{p1} + i_{p2} =$ constant, no output is obtained. The currents through R_{L1} and R_{L2} are

$$i_1 = I_k \frac{R_{L2}}{R_{L1} + R_{L2}}, \quad \text{and} \quad i_2 = I_k \frac{R_{L1}}{R_{L1} + R_{L2}}. \tag{2}$$

2. If $i_{p2}(R_{L2} + R_3) \geq i_{p1}R_{L1} \geq i_{p2}R_{L2}$, D_1 and D_2 are cut off and a positive output is obtained.

† More accurately, the hysteresis equals $\Delta i \cdot R_{L1}$ minus twice the voltage difference between the grids of T_1 and T_2, at the beginning of the regenerative action.

3. If $i_{p1}R_{L1} > i_{p2}(R_{L2} + R_3)$, D_2 is conducting and again no output is obtained as now R_{L1} is

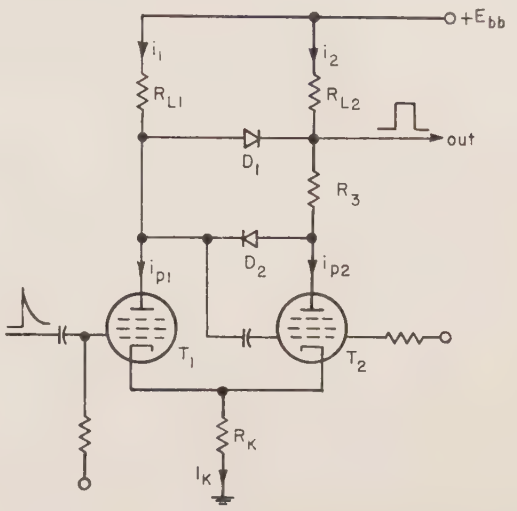

Fig. 2. Modified Schmitt Trigger.

connected in parallel with $(R_{L2} + R_3)$. Now the currents through R_{L2} and R_{L1} are

$$i_1 + \Delta i = I_k \frac{R_{L2} + R_3}{R_{L1} + R_{L2} + R_3}, \quad \text{and}$$
$$i_2 - \Delta i = I_k \frac{R_{L1}}{R_{L1} + R_{L2} + R_3}. \tag{3}$$

During phase 1 and 3 the input signal merely affects the current distribution between the tubes T_1 and T_2, but no output is obtained. During phase 2 however, the circuit is fully regenerative as both diodes are open. The break away point of D_1 may be accurately controlled by choosing suitable values for R_{L1} and R_{L2}. If, as an example,

$$R_{L1} = R_{L2} \tag{4}$$

the break away will occur when $i_{p1} = i_{p2}$. This makes the stability of the threshold comparable with that of a cathode coupled difference amplifier which is only little affected by common mode signals, including variations in the heater supply. At the same time, the expression $(1/gm_1) + (1/gm_2)$ attains its maximum possible value, providing maximum regenerativity for a given R_{L1}.

The change of plate current in each tube, during the regenerative action, may be found from (2) and (3):

$$\Delta i = I_k \left(\frac{R_{L2} + R_3}{R_{L1} + R_{L2} + R_3} - \frac{R_{L2}}{R_{L1} + R_{L2}} \right) = \\ = I_k \frac{R_{L1} R_3}{(R_{L1} + R_{L2})(R_{L1} + R_{L2} + R_3)}.$$

The hysteresis is equal to

$$\Delta i R_{L1} = \frac{I_k R_{L1}^2 R_3}{(R_{L1} + R_{L2})(R_{L1} + R_{L2} + R_3)} \qquad (5)$$

and the amplitude of the positive output pulse equals

$$\Delta i R_{L2} = \frac{I_k R_{L1} R_{L2} R_3}{(R_{L1} + R_{L2})(R_{L1} + R_{L2} + R_3)} \qquad (6)$$

In order to obtain maximum sensitivity, we want the hysteresis to be as small as possible. (5) shows that in order to achieve this end we must make $R_{L2} \gg R_{L1}$, and $R_3 \ll R_{L1}$, $R_3 \ll R_{L2}$. But (6) shows that the amplitude of the outpulse equals the hysteresis times R_{L2}/R_{L1}; considering condition (4) to be the most desirable relation between R_{L1} and R_{L2}, the conditions for (6) to be large seem to contradict the conditions for (5) to be small.

This difficulty may be overcome if advantage is taken of the fact that (4) is based on static conditions, whereas (5) and (6) describe the dynamic behaviour of the circuit.

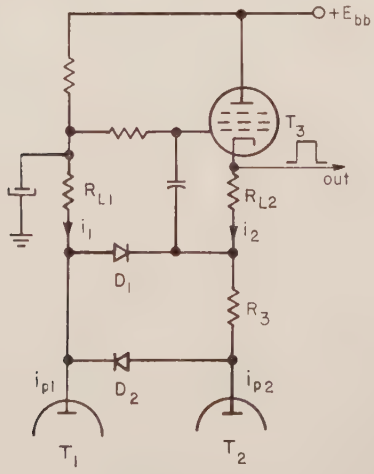

Fig. 3. Improved Modification of Schmitt Trigger.

Fig. 3 shows a configuration in which the dynamic resistance of R_{L2} is considerably greater than its static value. Using (10) from the appendix, the hysteresis is now

$$\Delta i \cdot R_{L1} = \\ = I_k \frac{R_{L1}^2 R_3}{(R_{L1} + R_{L2})\,[R_{L1} + R_{L2}\,(\mu_3 + 1) + R_3 + r_{p3}]} \qquad (7)$$

and the output pulse

$$I_k \frac{R_{L1} R_3\,(\mu_3 R_{L3} + r_{p3})}{(R_{L1} + R_{L2})\,[R_{L1} + R_{L2}\,(\mu_3 + 1) + R_3 + r_{p3}]} \approx \\ \approx I_k \frac{R_{L1} R_3}{(R_{L1} + R_{L2})}. \qquad (8)$$

Insertion of practical values into (7) and (8) shows that an output voltage of a few volts at a hysteresis of less than 50 mV may be obtained. The circuit will operate equally well with either positive or negative input pulses.

A practical example of the new circuit is shown in fig. 4. It is used in connection with a scaler having a resolution of 0.5 μs with an input sensitivity adjustable between 0.1–10 volts, for positive and negative pulses. An input attenuator is provided to extend the sensitivity from 1–100 volts.

D_3 should be a silicon diode. It serves to suppress positive pulses at the output, if large negative pulses are analyzed at minimum sensitivity of the discriminator.

For positive input pulses, D_3 is biased into cut off. By choosing judiciously this cut off voltage and a suitable diode, the change of sensitivity owing to a change at different temperatures in the characteristics of D_1 may be compensated, for all practical purposes. Additional drift may be caused by heater voltage fluctuations, owing to the combined influence of assymetry between T_1 and T_2 and the change in the transconductance of T_3. It is minimized by adjusting P_1. Compensation may only be achieved if the weaker tube is inserted into the base of T_2. P_1 is essential with an unregulated heater supply, if the maximum drift should be below 10 mV.

The diodes D_1 and D_2 should be of the quick recovery, high conductance type. Their capacity should be as low as possible. Gold bonded computer types are excellent.

Using a stabilized heater supply, a maximum drift of 1.5 mV per day was measured after a warm up period of 30 minutes, for positive input pulses. If the heater supply voltage varies by ± 10%, the drift will still be below 5 mV, if

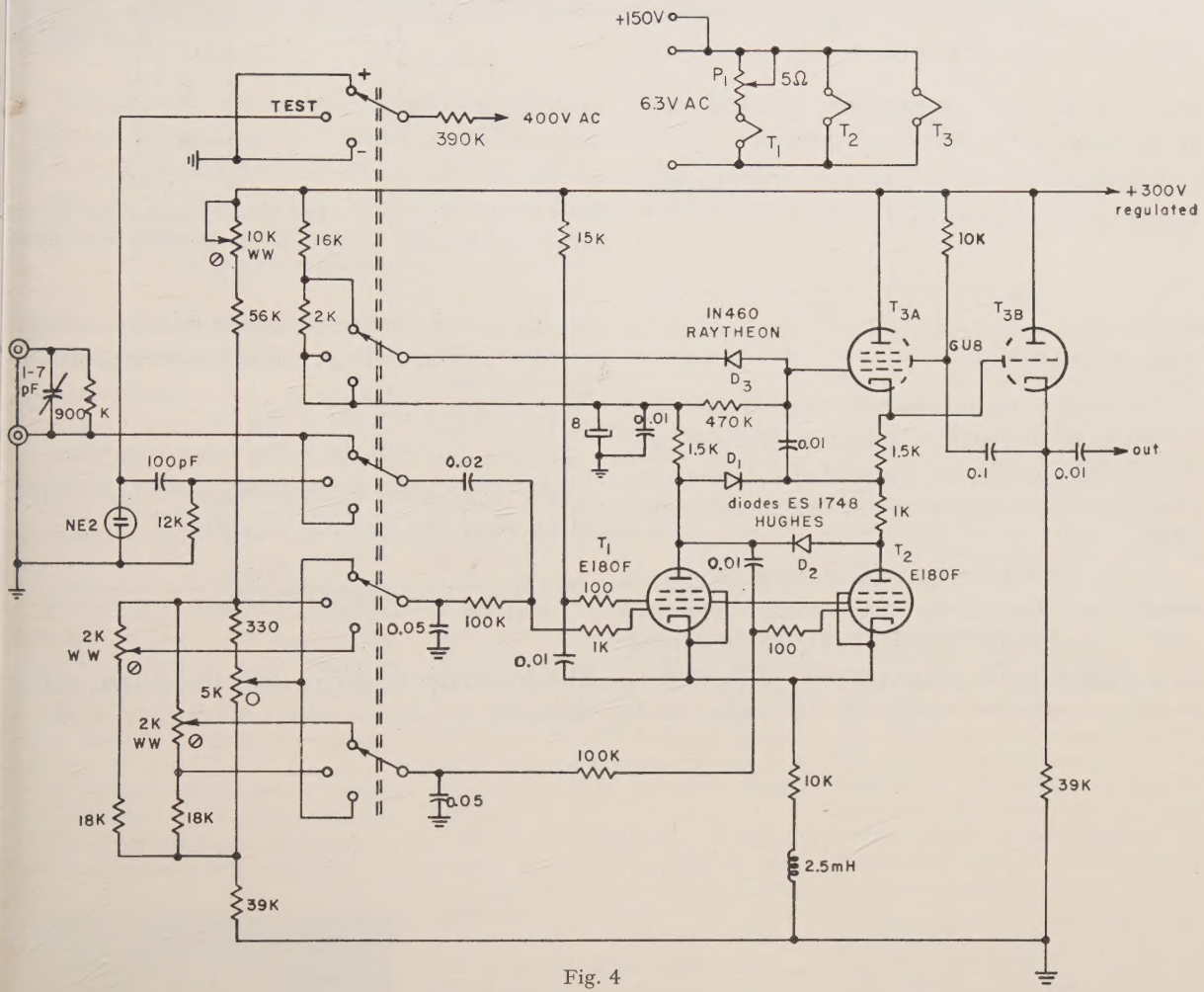

Fig. 4

having carried out the experimental work. This investigation was carried out under the auspices of the Scientific Department, Ministry of Defense, Israel, and is published with its permission.

P_1 is properly adjusted. With negative input pulses, some additional drift owing to changes in temperature will be experienced, because now D_3 has no temperature compensating effect.

The hysteresis is 30 mV. The output pulse has an amplitude of 5 Volts, and a rise-and-fall time of 40 nanoseconds.

Acknowledgement

The author wishes to thank Mr. Solomon Rozenstein for helpful suggestions, and for

Appendix

Computation of the critical value of R_{L1}, which will make the loop gain in a Schmitt Trigger equal to one.

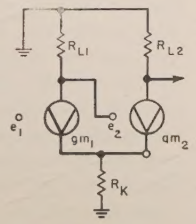

Fig. 5a

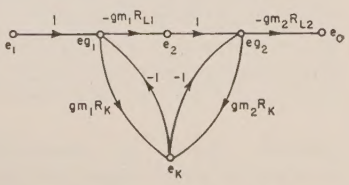

Fig. 5b.

Fig. 5a shows the equivalent circuit diagram for fig. 1, and fig. 5b its flow diagram. From this,

$$\frac{e_0}{e_1} = \frac{gm_1 R_{L1} gm_2 R_{L2} + gm_1 R_k gm_2 R_{L2}}{1 + R_k (gm_1 + gm_2) - gm_1 R_{L1} gm_2 R_k} .$$

Assuming R_k to be very large compared with the other circuit constants, we obtain

$$\frac{e_0}{e_1} = \frac{gm_1 gm_2 R_{L2}}{gm_1 + gm_2 - gm_1 gm_2 R_{L1}} .$$

The condition for regenerativity is obtained, equalling the denominator to zero:

$$R_{L1}\,\text{crit.} = \frac{1}{gm_1} + \frac{1}{gm_2} . \qquad (9)$$

The circuit of fig. 3.

The static conditions of this circuit are shown in fig. 6a, and its dynamic behavior may be derived from fig. 6b. The grid of T_1 is assumed to be initially negative with respect to the grid of T_2.

Static conditions prevail as long as D_1 is conducting. During the regenerative action, a shift of conduction from D_1 to D_2 will be caused by a change in the plate currents of T_1 and T_2 by Δi, as indicated in fig. 6b. The value of Δi may be found by equalling the increase of the voltage across R_{L1}, owing to the increase of i_1,

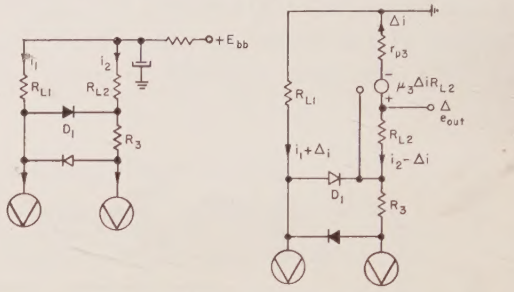

Fig. 6. (a) Static equivalent circuit diagram for fig. 3, neglecting the grid bias of T_3. (b) Dynamic equivalent circuit diagram for fig. 3.

to the corresponding decrease of the voltage across R_3, R_{L2}, and r_{p3}, owing to the decrease of i_2:

$$(i_1 + \Delta i)R_{L1} = i_2 (R_3 + R_{L2}) - \\ - \Delta i (R_3 + R_{L2} + r_{p3}) - \mu_3 \Delta i R_{L2} .$$

Using (2) in order to express i_1 and i_2 in terms of I_k, R_{L1}, R_{L2}, and R_3, we obtain

$$\Delta i = I_k \frac{R_{L1} R_3}{(R_{L1} + R_{L2}) [R_{L1} + R_{L2} (\mu_3 + 1) + R_3 + r_{p3}]} . \qquad (10)$$

The hysteresis is $\Delta i R_{L1}$, and the output pulse $\Delta i(\mu_3 R_{L2} + r_{p3})$.

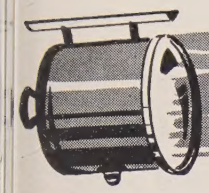

Spotlight on Industry

This section appears each month and features various happenings of interest in the nuclear industrial world and objective information on products of the nuclear manufacturers. It is offered entirely as a service and all nuclear manufacturers are cordially invited to submit clearly objective and descriptive material on their endeavours and product developments for consideration for use in this section.

CONTINUOUS READING METER-RELAY

Assembly Products, Inc., Chesterland, Ohio, U.S.A.

Meter-relays with a new design principle, retaining the reliability of locking contacts but providing instantaneous reset, have been developed.

With the new CR (Continuous Reading) design, the moving pointer shows the signal level at all times, even when the set point has been passed and control circuits have been energized. The circuits remain operative until reset calls for opposite action.

A separate coil increases control dependability by boosting contact torque at set point and thus insuring positive actuation of a load relay.

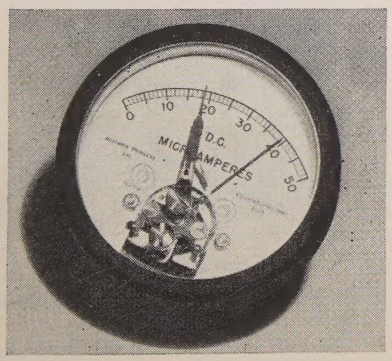

The indicating pointer has passed the set point but control circuits remain energized. Other features are a booster coil to insure positive operation bij increasing contact torque, and instantaneous reset when the indicating pointer returns to set point.

In applications using the new CR meter-relay, control action is directly linked to the signal.

Meter-relays with the new design may be used in virtually any application requiring only one set point. Sensitivities are the same as those of existing API meter-relays, beginning with full scale ranges of 0 to 5 microamperes.

Key to the new design is a V-shaped toggle, with contacts on each of its arms. The toggle is pivoted on the under side of the adjustable pointer that marks the set point. Both the toggle and the adjustable pointer are made of layers of isolated metal that are parts of separate circuits from the respective toggle contacts.

When the indicating, or signal, pointer reaches set point, a two-stage action occurs, almost instantaneously:

1. A contact on the pointer touches a contact on the toggle and a circuit is closed through both the booster coil and the coil of a multi-pole load relay. The booster coil assures firm meter-relay contact action.

2. As the load relay initiates the desired control action through one set of contacts, another set closes and pulls a surge of current through the meter-relay movement. Enough torque is thus added to the indicating pointer to cause it to snap the toggle and move past it. The meter-relay contacts are then separated and the booster circuit is opened. This sequence of action may begin at either high or low limit.

The load relay remains energized as long as the signal is higher (or lower) than set point. The indicating pointer moves freely with fluctuating signal strength.

When the indicating pointer returns to set point, its contact again touches a contact on the toggle. A circuit including the booster coil is closed and the load relay is dropped out. The indicating pointer snaps the toggle the other way and again pushes past, opening the booster circuit once more.

The design and positioning of the toggle are such that a contact on the indicating pointer always passes by the toggle arm closer to it and strikes the contact on the further arm. The indicating pointer has two isolated contacts, one touching a toggle contact while moving upscale, the other being operative when the pointer moves downscale.

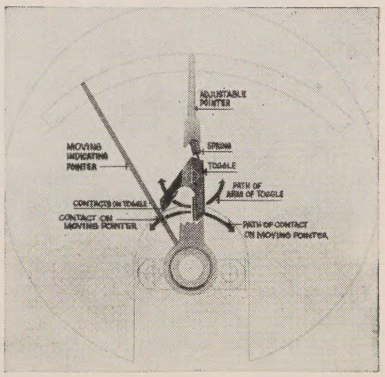

Movement of pointer contacts across the toggle contacts exerts a wiping action that keeps contacts clean and makes for more positive action and longer contact life.

MINIATURE A. C. CHOPPER RELAY

Electromechanical Division, Ericsson Telephones Ltd., Beeston, Nottingham

General

The nucleus of the design is a special magnetic circuit which has been developed as a result of intensive research over a considerable period.

The general principle is such that susceptibility to electromagnetic pick-up between contacts and the driving magnetic flux is low, and it also enables a geometrically and mass balanced armature system to be used. This balanced system is mounted on a torsional suspension and is therefore immune from pivoting trouble.

Two changeover contacts can be provided, each of which is isolated from the other electrically, and the contact output can be arranged to give make-before-break or break-before-make action on both contact units. Precise operation of contact pairs is made possible by the specially designed spring buffering system which regulates the spring compliance through-out the armature stroke, so that symmetrical contact output is obtained with no contact bounce.

This chopper is available with several adjustments and various contact efficiencies.

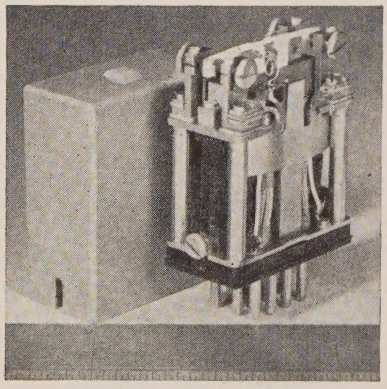

SPECIFICATION

Dimensions

Height above chassis:

2.0 × 1.562 × 0.844 in. (51 × 40 × 21 mm).

Weight

Approx. 4.22 oz. (120 g).

Coils

The standard winding is for 6.3 volt working (with a d.c. resistance of 500 ohms). Coils to suit other voltages can be supplied to order.

Contacts

Single c/o action, platinum-iridium alloy is standard, but a special gold-silver-copper alloy is now available and will eventually supersede the platinum-irridium alloy. A two-changeover unit is also available.

Frequency

1. The standard working frequency is 50 c/s with choice of contact sequence as follows, but these choppers can also be made available for operation in the range 10–100 c/s with consequent change in contact output.

a. Make-before-break.

b. Break-before-make.

c. Differential between two contactunits. (Break-before-make only.) Where rectification is required.

2. Choppers for operation at 250 c/s and 400 c/s are under development.

Driving Power

This is related to the driving frequency and varies from 20 m/V amps to 600 m/V amps.

Contact Efficiency

As required from 35% to 55% closure of each contact per cycle, with bias drift within ± 2% on both contact units, and the two contact unit outputs within ± 4% of each other. Where required, such as for rectification, the two contact unit outputs can be arranged to give a differential of 10%.

Noise Level

By virtue of the very low driving power and the special screening of the coils and contacts, the noise level is reduced to practically negligible proportions. In the case of the 50 c/s 6.3 volt single c/o chopper the level is 100 μV Peak to Peak measured across a 1 megohm load.

Phase Displacement

The output of the 50 c/s 6.3 volt chopper lags the applied voltage by approx. 90°, with good phase stability.

Life

Extensive tests have shown that maintenance-free running periods appreciably in excess of 100 h are consistently obtained with the 50 c/s 6.3 volt chopper. Further extension of life is usually possible with a re-trim of the contacts.

PENCIL SIZE BF_3 COUNTER

Radiation Counter Laboratories, Inc., Nucleonic Park, Skokie, Ill.

RCL's pencil size BF_3 Counter measures distribution of neutron flux in critical assemblies. Counter is 6″ long with $\frac{1}{2}$″ diameter; has $2\frac{1}{8}$″ active anode and 0.032″ brass walls. Counter has approximate operating region of 900 V; typical plateau length of 150 V; and an average plateau slope of 3% per 100 V.

NEW DEHYDRATOR

Kahn and Company, Inc., 541 Windsor Street, Hartford 1, Connecticut, U.S.A.

A new concept in dehydrator design and operation has been developed and effectively utilized in a dehydrating air supply unit. This dehydrator, Model KC-1114, is particularly suited for such applications as pressurizing transmission lines and radar wave guides and purging electronic components.

Dry air output is continuous. Desiccant reactivation is accomplished by a dry air purge. No heater is necessary. Controls are automatic.

Small, compact units are available (19″ high × 20″ wide × 12″ deep) capable of drying 100° F saturated input air to —44 degrees C dewpoint with an oil-free output flow of 50 cubic in./min at 2 psig pressure. Units can

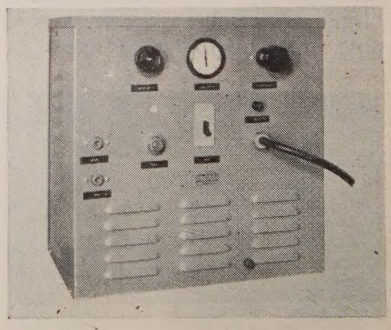

also be furnished for delivery of up to 3000 cu. in./min of dry air at up to 30 psig.

The unit is engineered for dependable performance within an ambient temperature range of —40° F to + 140° F, at altitudes between sea level and 7000 feet, and is unaffected by exposure to salt laden air as encountered in coastal U.S. The unit is also drip-proof.